

# **DEVELOPMENT AND EVALUATION OF DAMPING CHARACTERISTICS AND SHEAR PROPERTIES OF MAGNETORHEOLOGICAL ELASTOMERS**

Thesis

Submitted in partial fulfilment of the requirements for the degree of

**DOCTOR OF PHILOSOPHY**

by

**SRIHARSHA HEGDE**



DEPARTMENT OF MECHANICAL ENGINEERING  
NATIONAL INSTITUTE OF TECHNOLOGY KARNATAKA,  
SURATHKAL, MANGALORE-575025

October- 2017

# **D E C L A R A T I O N**

I hereby declare that the Research Thesis entitled “**DEVELOPMENT AND EVALUATION OF DAMPING CHARACTERISTICS AND SHEAR PROPERTIES OF MAGNETORHEOLOGICAL ELASTOMERS**” which is being submitted to the **National Institute of Technology Karnataka, Surathkal** in partial fulfilment of the requirements for the award of the Degree of Doctor of Philosophy in Mechanical Engineering is a *bonafide report of the research work carried out by me*. The material contained in this Research Synopsis has not been submitted to any University or Institution for the award of any degree.

Register Number : **1100474ME10F08**

Name of the Research Scholar : **Sriharsha Hegde**

Signature of the Research Scholar :

**Department of Mechanical Engineering**

**Place: NITK-Surathkal**

**Date:**

# CERTIFICATE

This is to certify that the Research Thesis entitled “**Development and Evaluation of Damping characteristics and Shear properties of Magnetorheological elastomers**” submitted by **Mr. Sriharsha Hegde (Register Number:100474ME10F08)** as record of the research work carried out by him, is *accepted as the Research Thesis submission* in partial fulfilment of the requirements for the award of degree of **Doctor of Philosophy**.

**Research Guide**

**Dr. K.V. Gangadharan**

Date:

Chairman-DRPC

Date:

## ACKNOWLEDGEMENTS

It has been a wonderful experience indeed to have worked under the guidance of Dr.K.V. Gangadharan Professor, Mechanical Engineering Department for my PhD at NITK, Surathkal. I would like to take this opportunity to humbly and sincerely thank his continuous support and guidance during the duration of the work. I also would like to thank him for providing the financial as well as technical support required for the smooth running of the research. I am indebted to him for the patience and the composure he showed even when I was slow at times and for standing by me throughout. He has been a great motivator who stood by his statement “Let us find an excuse to work” which he has proved by his actions and the way in which he has established the CSD-SOLVE Lab which is the best place to work at NITK, Surathkal. I am also very thankful to The Director NITK, Surathkal and the Head of the Mechanical Engineering Department for allowing me to conduct my research work.

I would also like to thank my Research Progress Assessment Committee members Dr. Anandhan Srinivasan (Associate Professor, Department of Metallurgical Materials and Science) and Dr. Ajith K.M (Assistant Professor, Physics Department) for their valuable comments and critical inputs which helped in shaping up my Research work.

My sincere thanks to Kiran Katari who helped me during my initial experimental works who also happen to be a very good friend of mine. Special thanks to my dear friend Umanath R Poojary who has continuously helped me during my work with his timely suggestions and also in correcting the thesis. He has been a true inspiration all along the research work. I would also like to extend my gratitude to Avinash B Pai and Gururaja Udupa who have been a constant source of inspiration who also happen to be my very good friends. I also would like to extend my gratitude to my SOLVE lab mates Shyam Sundar, Praahas Amin, Arun Parameswaran, Ashwin, Girish , Riessom Weldegiorgis, Jayaram Thumbe and Praveen Shenoy for their continuous support. I would like to thank Ms.Jyothi who helped in many documentation related activities. I also thank Mr.Harishchandra, Mr.Jaya Devadiga, and Mr.Pradeep from Machine shop, Mechanical Engineering, for their support in conducting the experiments.

I am indebted to my parents Sarveshwar Hegde and Nagaveni Hegde for having extended their support and faith in me for doing the PhD work. I also would like to thank my brother Srichaithra Hegde for the moral support. A special thanks to my dear wife Vibhavathi for her patience and constant support throughout the course of my Research. I also would like to thank all my extended my family members especially my in-laws for their moral support.

Finally I extend my heart felt gratitude to Dr. Navin Karanth, Assistant Professor, Mechanical Engineering Department-NITK for inspiring me to do PhD under Dr.K.V Gangadharan without which this work would never have been realized.

(Sriharsha Hegde)

## ABSTRACT

Elastomers are widely used to reduce vibrations and noise in structures, machines, and instruments. The passive nature of elastomers inhibits its use over a wider range of frequencies. Incorporating ferromagnetic ingredients in the non-magnetic elastomer matrix makes these structures smart when exposed to a magnetic field. These elastomers are better than conventional elastomers and can be applied in a wide frequency range. They belong to a class of smart material called Magnetorheological materials whose rheological properties can be reversibly controlled by a magnetic field.

This research is focused on preparation and damping characterization isotropic magnetorheological elastomers using different matrices by varying the volume percentage of carbonyl iron powder. Natural rubber, Nitrile rubber, RTV and HTV silicone and a new type of MRE by mixing RTV silicone and polyurethane was prepared and tested at various magnetic fields and input conditions. Experimental studies were conducted to understand the influence of matrix material, percentage concentration of carbonyl iron powder and magnetic field on the mechanical properties of the MREs i.e. shear modulus ( $G$ ) and dynamic damping (loss factor  $\eta$ ). Force vibration tests were performed to understand the enhancement of damping property of MRE samples. Experimentally it was proved that nitrile rubber and silicone-polyurethane hybrid MREs showed better damping performance than other matrix materials. The performance was also dependent upon the input strain rate and weakly on the operating frequency. The influence of size of the particle ingredient was investigated on a small scale. The inherent damping property of the matrix plays a major role in the respective MRE sample. Magnetic field and percentage particle content was found to be the dominating parameters influencing the damping properties. The dimension of the test sample, input strain and frequency also influence the damping on a lesser scale. Linear viscoelastic model was fitted to the experimental data using the MATLAB optimization tools which closely matched with the experimental values. The application of MRE as damping material was investigated by following ASTM E756-05 standard in sandwich beam configuration. The loss factor and shear modulus modifications were investigated under non-homogeneous magnetic field by subjecting it to impulse excitation.

Key words: smart materials, magnetorheological elastomers, carbonyl iron powder, force vibration, isolation, vibration damping.

## TABLE OF CONTENTS

ACKNOWLEDGEMENTS .....	i
ABSTRACT.....	iii
LIST OF FIGURES .....	vii
LIST OF TABLES .....	x
NOMENCLATURE .....	xi
INTRODUCTION .....	1
1.1 MAGNETORHEOLOGICAL MATERIALS.....	2
1.1.1 MAGNETORHEOLOGICAL FLUIDS .....	2
1.1.2 MAGNETORHEOLOGICAL FOAMS .....	3
1.1.3 MAGNETORHEOLOGICAL ELASTOMERS.....	3
1.2 RELEVANCE OF MRE IN VIBRATION ISOLATION.....	3
1.3 MODES OF OPERATIONS OF MR ELASTOMERS .....	4
1.4 TYPES OF MR ELASTOMERS .....	5
1.5 FORMATION OF THE THESIS.....	5
2 LITERATURE SURVEY .....	7
2.1 MAGNETORHEOLOGY OF MR MATERIALS.....	7
2.2 MATERIALS AND THE EXPERIMENTAL CHARACTERIZATION METHODS OF MRE.....	8
2.3 MODELING TECHNIQUES AND METHODS OF MRE.....	12
2.4 APPLICATIONS OF MAGNETORHEOLOGICAL ELASTOMERS.....	15
2.5 CONCLUSIONS FROM THE LITERATURE SURVEY .....	16
2.6 RESEARCH GAP .....	18
2.7 MOTIVATION AND OBJECTIVES OF PROPOSED WORK .....	18

2.8	SCOPE OF THE RESEARCH WORK .....	19
3	DYNAMIC CHARACTERIZATION OF MRE .....	21
3.1	THEORETICAL BACKGROUND FOR FORCE TRANSMISSIBILITY TESTS .....	21
3.2	MATERIAL PROCESSING.....	24
3.3	EXPERIMENTAL SET UP FOR DYNAMIC CHARACTERIZATION.....	27
3.3.1	FORCE VIBRATION TESTS.....	28
3.3.2	RESULTS AND DISCUSSIONS.....	31
4	PARAMETRS INFLUENCING THE MAGNETORHEOLOGICAL EFFECT .....	49
4.1	INFLUENCE OF PERCENTAGE CONTENT OF CIP.....	49
4.2	INFLUENCE OF PARTICLE SIZE.....	51
4.3	INFLUENCE OF DIMENSIONS OF THE MRE .....	55
4.4	INVESTIGATION OF HYBRID MRE.....	61
4.4.1	MATERIAL PREPARATION .....	61
4.4.2	EXPERIMENTAL ANALYSIS .....	63
4.4.3	INFLUENCE OF STRAIN AND FREQUENCY .....	67
5	PARAMETER IDENTIFICATION BY VISCOELASTIC MODELING.....	75
5.1	FORMULATION OF THE MODEL.....	76
5.2	PARAMETER IDENTIFICATION.....	79
6	MRE AS A MATERIAL FOR CONSTRAINED LAYER DAMPING .....	81
6.1	MATERIAL PROCESSING.....	81
6.2	EXPERIMENTAL TECHNIQUE .....	81
6.2.1	SUMMARY OF THE METHOD.....	82
6.2.2	SANDWICH BEAM PREPARATION.....	83
6.3	RESULTS AND DISCUSSIONS .....	87
6.3.1	LOSS FACTOR VARIATION.....	87



6.3.2	SHEAR MODULUS VARIATION .....	92
7	CONCLUSIONS AND SCOPE FOR FUTURE WORK.....	99
7.1	SCOPE FOR FUTURE WORK.....	101
	REFERENCES .....	103
8	APPENDIX.....	113
	MATLAB Code for parameter Identification .....	113

## LIST OF FIGURES

<b>Figure 1.1:</b> Operating modes- (a) shear mode, (b) squeeze or compressive mode.....	4
<b>Figure 1.2:</b> Magnetorheological elastomer- (a) randomly distributed, (b) structured MRE...	5
<b>Figure 3.1.</b> Schematic of the set up .....	22
<b>Figure 3.2.</b> System modeled as SDOF with base excitation .....	22
<b>Figure 3.3</b> Vector representation of Forces (W.T Thomson) .....	23
<b>Figure 3.4.</b> Natural rubber samples .....	26
<b>Figure 3.5.</b> Microstructure of CIP and Natural rubber MRE samples. a) CIP, b) Pure NR, c) 10% MRE, d)15% MRE, e)20% MRE and f)25% MRE .....	27
<b>Figure 3.6</b> Test samples for forced-vibration transmissibility tests .....	28
<b>Figure 3.7</b> Photograph of the experimental set-up. 1 and 3 –Force transducers to measure output force and input force respectively,2- MRE test sample, 4- Stinger used to transmit linear force from shaker, 5-Electrodynamic shaker VTS-100, 6-Accelerometer, 7 and 8- Neodymium permanent magnets .....	29
<b>Figure 3.8</b> FEMM simulation with a gap of 40mm between the magnetic poles .....	30
<b>Figure 3.9</b> FEMM simulation with a gap of 30mm .....	31
<b>Figure 3.10.</b> Behaviour of Pure Natural Rubber .....	32
<b>Figure 3.11.</b> Behaviour of 10% NR MRE .....	32
<b>Figure 3.12.</b> Behaviour of 15% NR MRE .....	33
<b>Figure 3.13.</b> Behaviour of 20% NR MRE .....	33
<b>Figure 3.14.</b> Behaviour of 25% NR MRE .....	34
<b>Figure 3.15.</b> Structural Loss factor variation of NR MRE samples .....	34
<b>Figure 3.16.</b> Behaviour of Pure Si-HTV MRE .....	35
<b>Figure 3.17</b> Behaviour of 10% Si-HTV MRE .....	36
<b>Figure 3.18</b> Behaviour of 15% Si-HTV MRE .....	36
<b>Figure 3.19</b> Behaviour of 20% Si-HTV MRE .....	37
<b>Figure 3.20.</b> Behaviour of 25% Si-HTV MRE .....	37
<b>Figure 3.21</b> Structural Loss factor variation of Si-HTV MRE samples .....	38
<b>Figure 3.22.</b> Behaviour of Pure NBR sample .....	39
<b>Figure 3.23.</b> Behaviour of 10% NBR sample .....	39
<b>Figure 3.24.</b> Behaviour of 15% NBR sample .....	40

<b>Figure 3.25.</b> Behaviour of 20% NBR sample .....	40
<b>Figure 3.26.</b> Behaviour of 25% NBR sample .....	41
<b>Figure 3.27.</b> Structural Loss factor variation of NBR MRE samples .....	41
<b>Figure 3.28.</b> Behaviour of Pure Si-RTV sample .....	42
<b>Figure 3.29.</b> Behaviour of 10% Si-RTV MRE .....	43
<b>Figure 3.30.</b> Behaviour of 15% Si-RTV MRE .....	43
<b>Figure 3.31.</b> Behaviour of 20% Si-RTV MRE .....	44
<b>Figure 3.32.</b> Behaviour of 25% Si-RTV MRE .....	44
<b>Figure 3.33.</b> Structural Loss factor variation of Si-RTV MRE samples .....	45
<b>Figure 4.1.</b> FEMM Simulation of force between CIP particles at 20 $\mu$ m .....	50
<b>Figure 4.2.</b> FEMM Simulation of force between CIP particles at 10 $\mu$ m .....	50
<b>Figure 4.3</b> Microstructure of (a) 6.25 $\mu$ m MRE and (b) 3.15 $\mu$ m MRE. ....	51
<b>Figure 4.4.</b> Transmissibility Ratio V/s Input frequency comparison of 3.15 $\mu$ m MRE .....	52
<b>Figure 4.5.</b> Transmissibility Ratio V/s Input frequency comparison 6.25 $\mu$ m MRE .....	53
<b>Figure 4.6.</b> Loss factor variation with magnetic field .....	54
<b>Figure 4.7.</b> Increase in effective diameter due to agglomeration .....	55
<b>Figure 4.8.</b> MRE Test samples .....	56
<b>Figure 4.9.</b> Transmissibility plot of Pure Silicone .....	57
<b>Figure 4.10.</b> Transmissibility plot of 15% MRE .....	57
<b>Figure 4.11.</b> Transmissibility plot 25% MRE .....	58
<b>Figure 4.12.</b> Loss factor variation of 15% MRE .....	59
<b>Figure 4.13.</b> Loss factor variation of 25% MRE .....	59
<b>Figure 4.14.</b> Magnetic field variation across the thickness .....	60
<b>Figure 4.15.</b> Pure silicone and Silicone MRE .....	62
<b>Figure 4.16.</b> Pure 80-20 and 80-20+Fe MRE .....	62
<b>Figure 4.17.</b> Pure 70-30 and 70-30+Fe MRE .....	62
<b>Figure 4.18.</b> Pure 60-40 and 60-40+Fe MRE .....	63
<b>Figure 4.19.</b> Transmissibility Silicone MRE samples .....	63
<b>Figure 4.20.</b> Transmissibility 80-20 (Si+PU) MRE samples .....	64
<b>Figure 4.21.</b> Transmissibility 70-30 (Si+PU) MRE samples .....	65
<b>Figure 4.22.</b> Transmissibility 60-40 (Si+PU) MRE samples .....	65

<b>Figure 4.23.</b> Loss factor variation of the MRE samples .....	67
<b>Figure 4.24.</b> Experimental setup .....	69
<b>Figure 4.25.</b> Force v/s Displacement plots at 5 Hz .....	70
<b>Figure 4.26.</b> Stiffness variation of Si-MRE with frequency .....	71
<b>Figure 4.27.</b> Stiffness variation of 80-20-MRE with frequency .....	72
<b>Figure 4.28.</b> Stiffness variation of 70-30-MRE with frequency .....	72
<b>Figure 4.29.</b> Stiffness variation of 60-40-MRE with frequency .....	73
<b>Figure 5.1.</b> Maxwell Model .....	76
<b>Figure 5.2.</b> Zener Model .....	77
<b>Figure 5.3.</b> Modified Model .....	78
<b>Figure 5.4.</b> Silicone MRE sample behavior at 0.15mm strain .....	80
<b>Figure 5.5.</b> Silicone MRE sample behavior at 0.075mm strain .....	80
<b>Figure 6.1.</b> Configuration for test specimens (ASTM-E756-05) .....	82
<b>Figure 6.2.</b> A sandwich beam used in experiment .....	83
<b>Figure 6.3.</b> Schematic top view of the experimental setup .....	84
<b>Figure 6.4.</b> Snapshot of the impact test .....	85
<b>Figure 6.5.</b> Loss factor variation of Natural rubber samples .....	87
<b>Figure 6.6.</b> Loss factor variation of Silicone-HTV rubber samples .....	88
<b>Figure 6.7.</b> Loss factor variation of Nitrile rubber samples .....	88
<b>Figure 6.8.</b> Loss factor variation of Silicone-RTV rubber samples .....	89
<b>Figure 6.9.</b> Shear modulus variation of Natural rubber samples .....	93
<b>Figure 6.10.</b> Shear modulus variation of Silicone-HTV rubber samples .....	93
<b>Figure 6.11.</b> Shear modulus variation of Silicone-RTV rubber samples .....	94
<b>Figure 6.12.</b> Shear modulus variation of Nitrile rubber samples .....	94
<b>Figure 6.13.</b> Modulus values of pure samples .....	98

## LIST OF TABLES

Table 3.1	Ingredients for vulcanization.....	25
Table 3.2	Types of samples prepared.....	26
Table 3.3	Comparison of structural loss factors of Natural rubber samples.....	35
Table 3.4	Comparison of structural loss factors of Si-HTV samples.....	28
Table 3.5	Comparison of structural loss factors of NBR samples.....	42
Table 3.6	Comparison of structural loss factors of Si-RTV samples.....	45
Table 4.1	Loss factor values calculated from the transmissibility plot.....	53
Table 5.1	Parameters Identified for Silicone samples at 15Hz.....	77
Table 6.1a	Loss factor values of the MRE samples.....	88
Table 6.1b	Loss factor values of the MRE samples.....	89
Table 6.2a	Shear modulus values.....	93
Table 6.2b	Shear modulus values.....	94

## NOMENCLATURE

MRF	Magnetorheological fluid
MRE	Magnetorheological elastomer
HTV	High temperature vulcanization
RTV	Room temperatures vulcanization
ATVA	Adaptive tuned vibration absorbers
NVH	Noise vibration and harshness
DMA	Dynamic mechanical analyzer
CIP	Carbonyl iron powder
PU	Poly-urethane
PDMS	Poly-dimethyl-siloxane
LVE	Linear viscoelastic
SEBS	Styrene-b-ethyleneco- butylene-b-styrene
ACN	Acrylonitrile
UTM	Universal testing machine
SEM	Scanning electron microscope
SDOF	Single degree of freedom
RV	Radiation vulcanizing
FFT	Fast Fourier transforms
FEM	Finite element method
TVA	Tuned vibration absorbers
AVA	Active vibration absorber
SA	Semi-active absorber
HVA	Hybrid vibration absorber
PID	Proportional integral derivative
RMS	Root mean square
$\text{NH}_4\text{HCO}_3$	Ammonium bicarbonate
ASTM	American standard testing methods
NI-PXI	National Instruments-PCI extensions for instrumentation
LabVIEW	Laboratory Virtual Instrumentation Engineering Workbench
$G$	Shear modulus

$E$	Young's modulus
$\eta$	Loss factor
$F_{tr}$	Transmitted force
$F_o$	Input force
TR	Transmissibility ratio
$\zeta$	Damping ratio
$\varepsilon$	Strain
$\sigma$	Stress
$\lambda$	Frequency ratio
$\omega$	Operating frequency
$\omega_n$	Natural frequency
$\mu_o$	Permeability of free space
$\mu_p$	Relative permeability of particles
$\mu_r$	Relative permeability
$H$	Magnetic field intensity
$B$	Flux density

## CHAPTER 1

### INTRODUCTION

Excessive vibrations transmitted from a machine to the foundation of a structure are detrimental to the structural integrity. The isolation of these unwanted vibrations poses a challenging task to the researchers. One of the most popular and economical methods is to employ viscoelastic materials, which isolate the structures from the source of vibrations (Lakes, 2009). The passive nature of these isolators does not meet the isolation criteria for varying levels of frequency inputs. To provide effective isolation for a wider range of frequencies, attempts have been made to employ active as well as semi-active isolators. The bulky nature and the high-energy requirements of active isolators make semi-active isolators a better choice among the available isolators (George Luca et al. 2005). The semi active vibration isolators based on smart materials makes the wide range of isolation very practical since the smart material in it imparts the ability to adjust to variable levels of vibrations.

‘Smart’ materials can sense and respond to their ambient conditions. The applications include areas as diverse as health, defense, packaging and even structural and vehicle damping. Piezoelectric materials, shape memory alloys, thermo-chromic materials, photo-chromic materials and magnetorheological (MR) are some of the examples of smart materials (Goddard et al.1997 and, Pagel, et al. 2015). Electrostrictive polymers and magnetostrictive materials are also employed in active vibration control; however the small actuation limits them. The electrostrictive materials are also sensitive to temperature which limits its applications (Giurgiutiu et al. 2000). Magnetostrictive materials are limited by their weight which tends to be heavier (Claeysen and Lhermet 2002). Shape memory alloys can remember the shape and transform from low temperature martensite to high temperature austenite shape when heated to a higher temperature. This is one-way shape memory effect which allows for 100% strain recovery of up to a maximum of 8% extensional pre-strain. Two-way shape memory allows for transformation between two preset shapes above and below certain transformation temperatures. Its use as noise and vibration reduction applications is limited because of slower response due to heating and cooling (Chung 2001, Monner 2005). Other limitations of shape memory alloys include higher cost and the difficulty in machining (Alam et al. 2007a and Alam et al. 2008b).Piezoelectric ceramics are one of the best choices for active noise and vibration reduction applications. The application



includes their integration into structural components by means of fibers, patches, and stacks (Monner 2005). The MR damper can produce at least 3 to 4 times the maximum force than a similar size piezoelectric damper and it is also more economical. The voltage requirement is also lower for MR dampers (Unsal et al. 2004). MR materials are found to be insensitive to contaminants and impurities. The magnetic polarization of MR materials is also independent of the chemistry of the matrix (Carlson and Jolly 2000). MR materials can also be employed at extreme conditions without compromising on the integrity of its properties (Bellan and Bossis 2002). These reasons along with ease of preparation make MR materials one of the better suited materials for semi-active isolation applications (Goddard et.al.1997).

## **1.1 MAGNETORHEOLOGICAL MATERIALS**

Magnetorheological materials are smart materials in which magnetically-polarizable particles are distributed in a non-magnetic medium (Carlson and Jolly 2000), and their rheological properties can be controlled rapidly and reversibly by an externally applied magnetic field. MR materials are considered as the most sorted materials for vibration isolation applications due to the unique field-induced behavior. Depending on the type of matrix material, MR materials are classified as MR fluids, MR foams and MR elastomers. The following section briefs about three types of MR materials.

### **1.1.1 MAGNETORHEOLOGICAL FLUIDS**

MR fluids consist of a fluid base like silicone oil, mineral oils, polyesters, synthetic hydrocarbons, water, and other types of oils (Carlson and Jolly 2000) that are filled with ferromagnetic particles which are typically spherical in shape. Agents are added to treat the iron particles to prevent them from settling down and to avoid agglomeration of particles. The size of the iron particles usually varies from 3 to 10  $\mu\text{m}$  in diameter (Li 2008a). These fluids, when subjected to a magnetic field becomes thicker i.e. the viscosity of the fluid increases tremendously. It becomes liquid again when the field is removed i.e. the process is reversible. Their ability to change the form from liquids to semisolids almost instantly makes them useful for dampening of impacts and vibrations. MR fluids are also used in power transmission devices such as clutches and brakes (Carlson and Jolly 2000; Ruddy et al. 2007). MR fluids are used as dampers and mounts in semi active or adaptive vibration control devices and are also used in aircraft landing gears and helicopter rotor damping augmentation (Shixing et al. 2011; Hu Wei 2005).

Though MR fluids possess superior properties i.e. the rheological property enhancements under the influence of magnetic field, the sedimentation problems often pose a limitation to its usage (Ruddy et al. 2007; Rich and Doyle et al. 2012 and Vicente et al. 2010).

### **1.1.2 MAGNETORHEOLOGICAL FOAMS**

MR fluid foam consists of fluids constrained in an absorbent medium or open-cell foam, felt or fabric. The absorbent medium acts as a container to hold the fluid medium between the magnetic poles. The open structure of MR foams overcomes the constraint and can easily accommodate multiple degrees of freedom. Fluids in these foam devices do not settle because of the wicking action of the matrix. MR foams are more suitable only for low to medium force applications where a high dynamic range is desired and MR fluid foam can be used as vibration dampers and brakes (Carlson and Jolly 2000).

### **1.1.3 MAGNETORHEOLOGICAL ELASTOMERS**

MR elastomers are solid analogous of MR fluids, where, an elastic matrix material is used instead of liquid medium. This has an obvious advantage as the iron particles in MR elastomers do not settle down over a period of time as in the case of MR fluids. Storage is also easy since there is no leakage (Ruddy et al. 2007). The most noteworthy difference between MR fluid and elastomers is the mode of operation i.e. in case of MR fluids, they are operated in post-yield regime and MR elastomers are operated in pre-yield regime (Carlson and Jolly 2000). The strength of MR fluids is characterized by field dependent yield stress and the strength of MR elastomers is characterized by field dependent modulus (Weihua Li 2008a).

MR elastomers are employed in many variable stiffness devices like adaptive tuned vibration absorbers (ATVA), stiffness tunable mounts and suspensions (Gong and Deng 2007m, Xiao-Min et al. 2009). Ford Motor Company has patented an automotive bushing made with MR elastomer. They can also be used in fluid controlling valves (Li 2003), in space applications (Kim et al. 2010) and as sensors and actuators also (Bose Holger et al. 2012).

## **1.2 RELEVANCE OF MRE IN VIBRATION ISOLATION**

The semi active vibration isolators are better suited for isolator applications since the energy requirements are very little when compared with active vibration control techniques, and a minute energy source like batteries is enough to power them. The semi-

active systems do not add energy, but they can control the parameters of the systems such as spring stiffness or viscous damping present in the system (Luca et al. 2005). This will give enough stability to the system by keeping the vibration amplitude to acceptable levels. MREs can be effectively used as semi active devices due to the ferromagnetic particle ingredients in it, which imparts the flexibility to change their stiffness or dynamic damping when exposed to an external magnetic field of particular intensity. This makes MRE an excellent vibration suppressing element, which needs to be addressed in detail.

### 1.3 MODES OF OPERATIONS OF MR ELASTOMERS

Based on the direction of application of magnetic field and the stress, the operational modes of MR materials are classified into two main categories- shear mode and squeeze mode or compressive mode of operation (Carlson and Jolly 2000). In shear mode of operation, the direction of magnetic flux line and the direction of input excitation are perpendicular to each other and in squeeze mode; the direction of input excitation to the MRE is along the flux lines. The schematic of both types is displayed in figure 1.1 below.

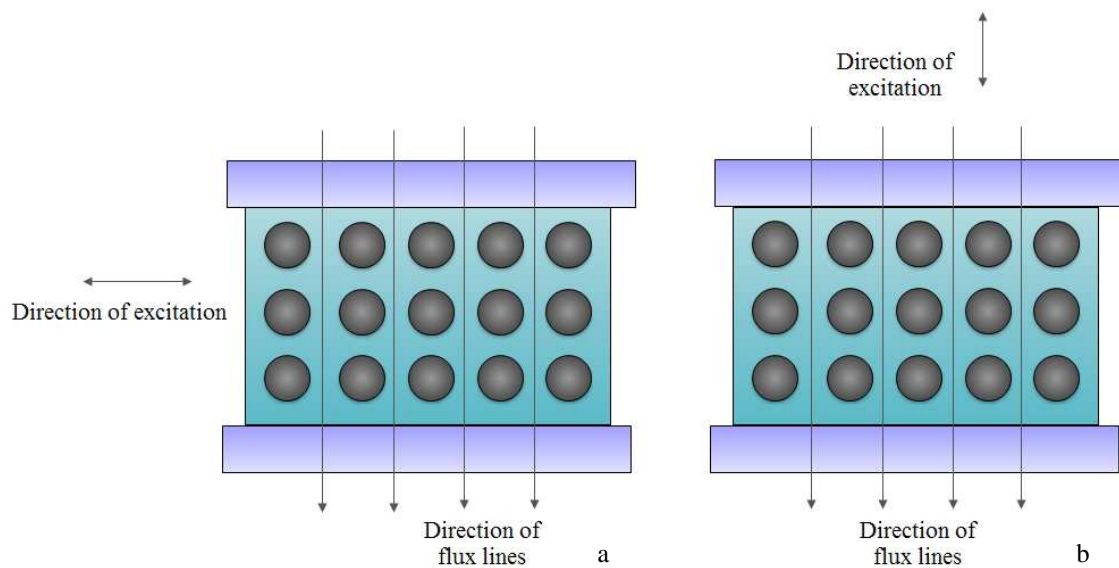


**Figure 1.1:** Operating modes- (a) shear mode, (b) squeeze or compressive mode

Generally conventional isolators which are elastomeric in nature are operated in both shear and squeeze modes. These operating modes are preferred depending on the application (Lakes 2009; Jones 2001). Like conventional elastomer isolator, MRE also is elastomeric by nature and it is also preferred in shear mode and squeeze mode of operation.

## 1.4 TYPES OF MR ELASTOMERS

Based on the curing process, there are two types of MR elastomers. If the MR elastomer is cured under a magnetic field, the iron particles form a chain like structure in the direction of flux path thereby imparting directional properties. These may be assumed as weakly anisotropic in nature. They are also referred to as structured MR elastomers (Jolly et al. 1996a). If no magnetic field is applied during curing, the particles are uniformly distributed in the matrix making them isotropic in nature (Gong et al 2005f; Ruddy et al 2007). The arrangements are shown in the figure 1.2 below.

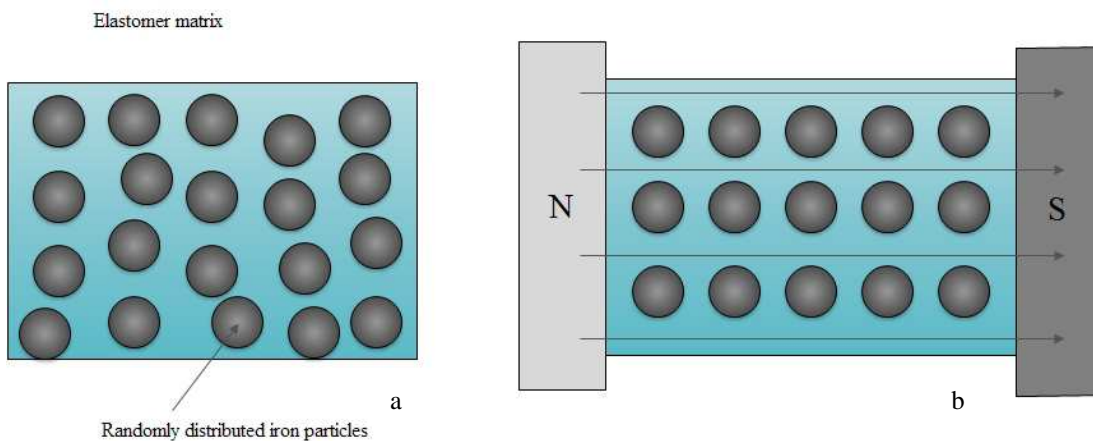


**Figure 1.2:** Magnetorheological elastomer- (a) randomly distributed, (b) structured MRE

MREs can also be classified based on the way the elastomer matrix is processed or vulcanized i.e. high temperature vulcanizing (HTV) and room temperature vulcanizing (RTV) (Gong et al., 2008a and 2009l). Both these types of MR elastomers have created lot of interest in the last decade and their field dependent properties are being explored by many researchers all over the world to utilize them in isolation applications.

## 1.5 FORMATION OF THE THESIS

The introduction about vibration isolation and its need is discussed along with different types of smart materials are presented in chapter 1. The relevance of MRE as a semi-active vibration isolator and its advantages over other types of MR materials are also discussed in brief. In order to understand the preparation methods and testing techniques employed to characterize MRE, the research works reported on MRE in the last few decades is studied extensively. Literatures related to different types of modeling techniques are also studied in the second chapter. The research gap is identified to set the objectives. The scope of the research work is defined in chapter 2 along with the problem statement. Different types of matrix materials were used to prepare MRE samples by

varying percentage content of carbonyl iron powder. The types of matrix materials used, their preparation methods and the microstructure of the samples are discussed in chapter 3. The experimental set up, the hardware and the software required for characterization of the samples are also briefed. Chapter 4 discusses about the influence of parameters on the dynamic performance of MRE. The influence of parameters like geometry of MRE samples, particle ingredient size, operating frequency and strain amplitude on dynamic performance of MRE samples are discussed in detail. The phenomenological model developed for the MRE is discussed in chapter 5. A four-parameter linear viscoelastic model is proposed. The parameter identification was done by fitting the experimental results to the proposed model using MATLAB optimization toolbox. Chapter 6 discusses an application to enhance the damping property of bare beam by subjecting it to MRE treatment in sandwich beam configuration. The conclusions from various experiments and the parameter identification modeling are done in the chapter 7. The most important factors which influence the performance of the MRE samples are also discussed in this chapter. The improvements and the scope for future studies related to MRE are also proposed. References and the appendix along with a brief Resume of the author are given at the end of the theses.

## CHAPTER 2

### LITERATURE SURVEY

The research work on MRE has gained great importance in the past decades due to its field induced property enhancements and the advantages it has over other MR materials. To investigate MRE as a potential isolator material, the preparation method and the type of testing characterization needs to be understood. The current research is focused on preparing and conducting dynamic characterization of magneto rheological elastomers. This chapter deals with the literature study mainly focusing on following important aspects.

- ❖ Magnetorheology of MR materials.
- ❖ Different types of matrix materials used to prepare the MRE samples.
- ❖ Size and percentage content of ferromagnetic ingredients used.
- ❖ Type of characterization methods employed to understand the field dependent behavior of MRE.
- ❖ Different mathematical modeling techniques like parametric, non-parametric and finite element studies on MRE.

The literature study is carried out to understand electro and magnetorheology and to understand the behaviour of viscoelastic materials. A summary of the literature study along with the research gap is given in the end of this chapter. The problem statement and the scope of the work along with the objectives of the current research are also stated at the end of this chapter.

#### 2.1 MAGNETORHEOLOGY OF MR MATERIALS

Focus on wide frequency vibration attenuation has always been the focus of many researchers in the past few decades. Smart materials have been found to be an alternative to conventional ones over a wide range of frequencies as well as variable levels of strain inputs. Electro and magnetorheological materials are such smart materials whose rheological properties can be controlled by an appropriate level of electric and magnetic field respectively. Suspensions with ferromagnetic fillers in oil like medium are potential stress transfer devices. Magnetorheological fluids were found to be better at field-induced behaviour than electrorheological fluids. (Ginder et al. 1998a). The degree of enhancements of properties under the influence of magnetic field is called MR effect. MR fluids, foams and elastomers are the three types of magnetorheological materials. They

are potential vibration attenuation devices in shear, squeeze and compression mode. Field dependent behaviour of MR fluids result from the polarization of the ferromagnetic particles during the chain formation (Ginder et al. 1998a, Carlson and Jolly 2000b). Theoretical studies of MR fluid involve chain formation of fillers along the magnetic flux lines. The studies on magnetic saturation on shear stress of MR fluids revealed that the maximum stress was proportional to the square of the magnetization of particles. Shear properties are independent of average magnetic induction at saturation (Ginder & Davis 1994).

Effect of magnetic field on the deformation of particle chains within the elastomers is modeled using a quasi-static dipole model. The gap between the iron particles, maximum field saturation of particles and pre-cured viscosity of composites has a bearing on the field-induced response of the elastomer (Jolly et al. 1996a). Theoretical analysis of field dependency of static response of magneto-sensitive elastomer is carried out by considering mechanical equilibrium equations. Axial and circumferential magnetic-field effect is investigated by considering an extension of a cylindrical specimen subjected to internal pressure and axial load. Non-linear isotropic magneto-elasticity comparison with experiments is necessary to understand the field-induced changes due to deformations (Ogden 2005).

Field-induced plasticity of MRE subject to cyclic reversal of strains under magnetic-field results in a temporary anisotropy due to dipole-dipole attractions along the flux lines (Melenev et al. 2011). The field-induced rheological enhancement is called MR effect. The addition of graphite along with ferromagnetic particles increases the zero-field storage and loss modulus, but reduces the MR effect (Li 2012).

## **2.2 MATERIALS AND THE EXPERIMENTAL CHARACTERIZATION METHODS OF MRE**

The choice of matrix materials is plenty for the preparation of MR test samples. Reviews done on MRE discuss about different matrices like thermoplastic, natural rubber, silicone, butyl, acrylonitrile, vinyl PVA glutaraldehyde, polyurethane etc. The type of filler includes iron, nickel, cobalt and alloys in powdered form ranging from 3 $\mu$ m to 10 $\mu$ m in size (Li and Zhang 2008).

The silicone RTV is the most widely used matrix for most research works due to availability and ease of processing in the laboratory. Many researchers have extensively worked on silicone based MRE samples (Gong et al. 2005e to 2005g, 2008a and b, 2010i;

Li et al. 2009 and 2010e; Demuch and Kuzum 2002; Possinger et al. 2013; Melenev 2013; Elejebareta et al. 2014 and Jian Quin 2015). Natural rubber has good mechanical properties, and it is easily available in nature has also been experimentally investigated by researchers (Gong et al. 2007i, 2008a; Li et al. 2010). Few works have been reported on matrices like chloroprene (Gong et al. 2008a), polydimethylsiloxane (PDMS) (Li et al 2005c), cis-polybutadiene (Gong et al. 2008), nitrile (Stenberg and Lokander 2003) and polyurethane (Wu Jinkui et.al. 2007).

Few literatures of MRE samples with matrices comprising of two different polymers in different proportions also have been reported. These hybrids consisting of silicone-polyurethane resulted in better MR effect (Gong et al. 2005g). Mixture of cis-polybutadiene and natural rubber in different proportions (Stenberg and Lokander 2003 and Gong et al. 2010d) proved that higher natural rubber content results in better MR effect.

The preparation of MRE involves high-temperature vulcanization (HTV) and room temperature vulcanization (RTV) methods of curing. RTV MRE samples have been tested extensively due to ease of preparation. Based on whether the magnetic field is applied during curing, MRE samples are called isotropic if cured without the field and anisotropic if cured under the field. This type of curing influences the properties of MRE under zero fields and with magnetic field also. Very few comparisons between isotropic and anisotropic MRE samples under similar testing conditions have been reported. Experimental works have proven that damping property of structured cis-polybutadiene MRE is less than the isotropic sample if the percentage concentration of CIP is kept equal (Sun et al, 2008 and Gong et al. 2010d). Studies conducted by Lu et al. (2011) on isotropic and anisotropic SEBS (polystyrene-b-ethyleneco- butylene-b-styrene) samples prove that isotropic MRE prepared at a higher temperature showed better storage modulus values than the sample prepared at room temperature. Anisotropic samples were prepared at a very high magnetic field of about 1.2 Tesla. The anisotropic samples at zero fields showed better characteristics than an isotropic sample at same percentage content of ferromagnetic particles. The mechanical properties of anisotropic MRE samples are a function of the magnetic field applied during curing (Gong et al. 2007j). The characterization of these samples was conducted by applying a homogeneous magnetic field where the whole sample dimension was uniformly subjected to a uniform field. Li et.al. (2011b) investigated MRE sandwich beam exposed to non-homogeneous magnetic-field strengths of lower intensity below 0. 1 Tesla. Characterization was carried out by



sine sweep test on the sandwich beam by varying frequency from 0 to 30 Hz. The magnetic field was applied only for a length of 50 mm during sweeping tests. Field was applied at distance of 130 mm from the fixed end of the cantilever and then moved till 255 mm. The tests revealed that with the increase in the magnetic field, the first natural frequency of the beam shifted leftwards, and the amplitude reduced. In addition, as the field was shifted away from the fixed end, the first natural frequency goes on reducing.

The inclusion of different type of additives during curing greatly affects the MR effect. The addition of silane coupling agents does not improve the absolute MR effect. However, the distribution of particles within the matrix was more uniform resulting in a better relative MR effect (Gong et al. 2006e). Studies conducted by Kaleta et.al. (2011) proved that the addition of plasticizers alters the properties of MRE samples. Studies conducted by Tian et al. (2011) revealed that graphite as an additive improves the dispersion of iron particles within the matrix. Addition of graphite was found to affect the linear viscoelastic range. The zero-field modulus improved but at the cost of MR effect. Artificially inducing porosity by changing the percentage content of  $\text{NH}_4\text{HCO}_3$  within the polymer matrix revealed that the storage modulus reduced with an increase of  $\text{NH}_4\text{HCO}_3$ . This resulted in improved loss factor as well as MR effect (Yu et al. 2012).

The MR effect is a function of the percentage concentration and the size of the particle ingredient in the elastomer matrix. The influence of carbonyl iron powder is investigated by varying the percentage content up to 90% by weight. Gong et al. (2008a) prepared MRE sample with natural rubber by varying the percentage CIP from 60% to 90% by weight, and the tests showed that damping properties was found to increase with weight percentage. Similar studies have (Gong et al. 2011h and 2001i) shown that loss factor has increased up to 80% weight fraction and then reduced with a further increase CIP content. The shear modulus of MRE with smaller-sized particle was found to be better than the sample with bigger sized particle for the same weight fraction. The relative MR effect which is the field-induced modulus improvement increased with the field up to a particle content of 70% by weight, and then it reduced. Loss factor decreased with an increase in operating frequency but increased with strain amplitude (Sun et al. 2008). Jian Quin et al. (2015) investigated the influence of particle size on the rheological properties of silicone based magnetorheological elastomers. Silicone-based MRE samples were prepared by using different size of iron particles ranging from five  $\mu\text{m}$  to 150  $\mu\text{m}$  in diameter. The zero-field shear modulus was observed to be decreasing with the increase

in diameter. The MR effect increased with the diameter of particle, and it reached a maximum value for 74  $\mu\text{m}$  particle, and enhancements were not reported for CIP size more than. Experiments conducted by Li and Zhang (2009g) by employing two different-sized particles 50  $\mu\text{m}$  and the other with 5  $\mu\text{m}$ . It was observed that for the same percentage content, the MRE with larger-sized particles has higher MR effect and lower zero-field modulus. When these two CIP samples were mixed in different proportions, the zero-field property was not affected, but the MR effect was enhanced.

The characterization of MRE is required to understand the behaviour of the samples and its potential as a vibration damper/isolator. Rheometer equipped with an electromagnet is very effective in experimental characterization of MRE. Many researchers have used parallel plate rheometer in oscillatory mode (Li et al. 2005c; Gong and Jian 2008b; Li and Zhang 2009g; Zhou and Tian, 2010e; Tian et al. 2011; Li 2012 and Li 2012h; Gong et al. 2012k) to investigate the influence of strain amplitude, frequency, and magnetic field on the storage modulus and loss factor. Rheometer is also used in tensional oscillation test (Kramarenko et al. 2011b), squeeze mode (Farjoud et al. 2011) and stress controlled mode (Lu et al. 2011). The creep and recovery behaviour (Li et al. 2010d) and Payne effect (Gong et al. 2012k) investigations are also done on MRE. Dynamic mechanical analyzer (DMA) is another effective method of experimental characterization. MR effect is analyzed using modified DMA (Wu Jinkui (2007); Gong et al. 2007i, 2007j, 2007m, 2008n, 2009i and 2011h; Gong and Sun (2008); Xiao-Min (2009); Opie and Yim (2010) and Lu. (2011)) to investigate the damping characteristics. The dynamic characteristics of MRE can also be carried out using forced-vibration test approach by employing electrodynamic shakers. Storage modulus variation with percentage concentration and magnetic field is evaluated using an electrodynamic shaker to conduct the dynamic tests (Gong et al. 2005f). Zhou and Li (2003) investigated the dynamic response of MRE subjected to uniaxial deformation by analyzing the acceleration response of the system under harmonic loading of different frequency using an electrodynamic shaker. Hysteresis plot obtained by plotting two accelerometer data acquired from the mass, and the base is analyzed to understand the behaviour of MRE. Stress-strain behaviour of MR samples was conducted using shakers to evaluate the MR effect (Yu et al. 2012).

Impulse excitation technique using an impact hammer is a quick way of characterizing the damping properties. Pan Jie et al. (2005) evaluated the frequency-

dependent stiffness and damping property of a rubber mount by making use of an impact hammer. The results were matching closely with the test results done by electrodynamic shaker Ripin and Ooi (2010) determined the loss factor of an engine mount by driving point stiffness and blocked transfer stiffness method using an electrodynamic shaker and compared it with an impact hammer. The results obtained from both the methods were in close agreement. Impact hammer was used to find out the natural frequency and damping ratio dependency on the magnetic field by Zhou (2002). Impact hammers have been used for evaluating the frequency-dependent modulus of 15 human levers extracted from patients at different levels of fibrosis (Basdogan Cagatay et al. 2010).

The characterization of MR elastomers can be conducted using sandwich beam configuration in different boundary conditions. Investigation of variation of storage modulus and loss factor with magnetic field was conducted using sandwich beam configuration under fixed-free conditions (Demchuk and Kuz'min 2002) Experimental work on magnetic-field dependent natural frequencies of MRE samples in fixed-free sandwich beam configuration is done using sine sweep technique (Ke-Xiang et al. 2008). Li et.al. (2011b) investigated MRE sandwich beam exposed to non-homogeneous magnetic-field strengths of lower intensity below 0.1 Tesla. They conducted a sine sweep test on the sandwich beam by varying frequency from 0 to 30Hz. As the field was shifted away from the fixed end, the first natural frequency goes on reducing.

### **2.3 MODELING TECHNIQUES AND METHODS OF MRE**

MRE consist of a matrix which is viscoelastic in nature. Many modeling techniques have been employed to predict the behaviour of MRE under zero field as well as under the influence of magnetic field. Different modeling methods are briefly review in this section.

The most basic study involves the modeling of the dipole interactions between the particles during the chain formation. The effect of magnetic saturation on the zero field and at saturation on the shear property of the MRE is modeled (Jolly et al.1996 and Davis 1999). The interaction between the adjacent particles along the carbonyl-iron powder chain formation was modeled. These studies have proven that maximum change in modulus is observed for a carbonyl iron percentage concentration of around 27 to 30% by volume.

Reitich and Jolly et.al. (1999) developed a mathematical theory based on homogenization. They derived the relations which could predict the response of the ferromagnetic particle chains in the fluid medium by magnetic saturation. This model

proposed could predict the effective permeability of magnetorheological fluids and numerical simulations were performed, which was then compared with the experimental results and was found to be effective in predicting the behaviour. Li., Zhang, and Gong (2008f) proposed an effective permeability model to predict the influence of magnetic-field dependent modulus change of MREs. They made use of Maxwell-Garnet's mixing rule of predicting the effective permeability of chains and modified it to derive the equation of field-induced shear modulus of MREs. Similar modeling studies conducted by Li and Zhang (2009g) also made use of effective permeability of the MRE to find the MR effect agreed with the experimental results. Dong et al. (2013) conducted theoretical studies on MREs subjected to normal pressure, and a model was developed based on the effective permeability rule. In this study, the chain structure in the matrix was assumed to be anisotropic in nature. By fitting the experimental results, an empirical relation for effective permeability formula was developed which in turn was applied to develop a relation for field-induced shear modulus. The studies showed that the modulus was a function of magnetic field as well as the normal pressure. Effective permeability theory has also been used to derive the stiffness matrix (Sun et al. 2013) for chain structure of iron particles in MREs. They derived the equation to find the magnetic field induced shear modulus of anisotropic MREs. A numerical simulation was carried out using ANSYS coupled magnetic-structural analysis to validate the analytical method. It was assumed that the particle volume concentration was 27%. The differences among the values calculated from analytical and experimental were within the acceptable range. Maxwell-Garnet's mixing rule was employed to compute the effective permeability. Bohdana Marvalova (2008) made use of equations developed by Dorfmann and Ogden (2004) to account for non-linear magneto-elastic deformation to implement magneto-static problem in finite-element code using Comsol Multiphysics coupled-field analysis. A simple simulation of the shear deformation of a finite sized block of MRE subjected to a magnetic field. They considered edge effects resulting from finite geometry of the body as well as huge displacements of the boundaries.

FEM studies have also been conducted on MRE samples in sandwich configurations in beam and plate geometries. The field-induced shear modulus enhancements of an MRE core sandwich beam in multilayered configuration have been studied (Zhou et al. 2006c and Zhou et al. 2006d) which is an extension of the work from the same author (Zhou et al. 2005c) in which Hamilton's principle was used to develop the dynamic model. FEM and Guyan reduction methods were employed to derive the

governing differential equations of a sandwich beam with normal and MRE cores (Dwivedy et al. 2011b). Bolotin method was used to determine the dynamic stability. They concluded that the proposed method can be used to predict the natural frequencies and loss factor of sandwich structures. Apart from sandwich beam, sandwich plate configuration (Yeh 2013) with MRE cores is also considered for modeling. Governing equations of the plate were developed by Hamilton's principle and the magnetic-field influence on the natural frequencies and the damping behaviour was analyzed.

Lin Chen et al. (2011) modeled the MRE as a standard linear spring with two springs and a dashpot, a third spring element to compensate for field-induced modulus change and a fourth Spring-Coulomb friction slider element to account for interfacial action. Jung et al (2012) developed a model to predict the behaviour of MRE by combining Ramberg-Osgood and the Maxwell model in shear mode of operation. Validation of the developed model was verified by comparing with the experimental results which showed that the fit was good (about 90% match). Kramarenko et.al. (2011b) fitted rheological models for the experimental results in Poyting-Thomson model which has an extra element of shear modulus than Kelvin model. Influence of resonance on the dynamic modulus of elastomer was also taken into consideration. The dynamic modulus in the presence of magnetic field was derived. It was observed that in the tested frequency range, there were errors resulting from inertial effects. The model developed could describe the frequency and field dependent rheology to good effect. Melenev et.al. (2011) modeled the plasticity induced in MREs due to the influence of magnetic field i.e., magnetic shape memory. A phenomenological model was developed using a spring-mass and a slider spring element to account for friction between the particle and the matrix arising due to dipole attraction resulting from the magnetic field. The model reproduced the experimental results effectively.

Mooney-Rivlin hyper-elastic model was fitted to experimental data, and stress-strain relationship was studied (Bossis et al. 2006). An analytical model was also developed to describe the behaviour of structured material. This model predicts that the particles are not in contact in the matrix, and the distance between them is 5.6% of the radius. Microstructure study confirmed this hypothesis. They concluded that the performance of the MRE to high strains will depend on the bonding between the particles and the matrix.

Bossis et.al. (2006) investigated the effect of structuring of particles within the matrix on the quasi-static behaviour in tension. Anisotropic MRE samples were prepared

and in second stage, the CIP was treated with a coupling agent to investigate the effect it has on the interface between the particle and the elastomer matrix. Mooney-Rivlin hyper-elastic model was chosen for parameter curve fitting. Stress-strain relationship was also studied, and Mooney-Rivlin and Christensen's isotropic models were fitted to the experimental results. An analytical model was developed to describe the behaviour of structured material. They concluded that the performance of the MRE to high strains will depend on the bonding between the particles and the matrix.

## **2.4 APPLICATIONS OF MAGNETORHEOLOGICAL ELASTOMERS**

Magnetorheological elastomers have many potential applications in vibration damping applications. Many researchers have attempted to explore its capabilities as vibration attenuation devices. Adaptive tuned vibration absorber by employing natural rubber in shear mode was tested in the range of magnetic field up to 0.4 Tesla (Gong and Deng 2007m). The advantage of this ATVA was also discussed, and it was experimentally observed that 145% increase in natural frequency was possible at 0.5 A current or 0.9 Tesla magnetic field (Gong and Deng 2008n).

MRE as field-dependent spring in three different vibration absorber configurations was explored by Cunefare and Lerner (2007). MRE samples were prepared using silicone gels incorporated with iron particles, and they were implemented as tunable springs and operated three modes- shear mode, compressive mode, and squeeze mode. In this research, the absorber designs were like the TVAs of ATR42 and ATR72 aircraft fuselages. Experimental results conclude that for vibration absorber with flexible design constraints, squeeze mode of operation yields the best results as variable stiffness devices. MRE damper in shear mode configuration resulted in effective vibration absorption over a wide frequency range (Xiao-min et al. 2009).

MRE is also explored as MR fluid-elastomer based mount and its controllability were discussed assuming SDOF system (Gordaninejad et al. 2011b). Farjoud et al. (2011) tested MR fluid damper in squeeze mode by incorporating MRF in a polyurethane elastomer. They experimentally concluded that the mount was capable of large range of controllable force for short stroke length. PID controlled MR devices were also explored under real-time conditions to investigate its feasibility as a vibration isolator (Opie and Yim 2010). Both structured and isotropic MRE showed good enhancements in modulus.

Apart from above-mentioned cases, microgripper in which jaws made of MRE were experimentally tested (Naimzad et al. 2011). MRE as a possible vibration

suppression device for miniature cryogenic devices used for cooling of actuators in sensors in surveillance satellites were explored by Kim et al. (2010). The tests led towards the conclusion that MRE gives wider frequency range control than the passive absorber. Sandwich beam with MRE core as a smart system for micro-vibration control of equipments was experimentally investigated by Ni., Ying and Chen (2011). It was concluded that this type of MRE core sandwich beam has vibration suppressing abilities for different types of stochastic motion excitations. Experimental evaluation of actuation behaviour of MREs in ring shaped specimen revealed the potential of MRE as flow control devices (Bose Holger, Rabindranath, and Ehrlich 2012). Li., Zhang and Du (2012h) explored MRE isolator as a potential seat isolation system which would reduce the vibrations experienced by the driver while in transit. Dynamic tests were conducted on isolator by subjecting it to harmonic input of 5Hz frequency at different magnetic fields, and force-displacement behaviour was plotted. The plots indicated that stiffness at 3A current increased to about three times when compared with the stiffness at 0A current. They concluded that for practical implementation of a full-scale isolator, optimization and control strategy development is required.

## **2.5 CONCLUSIONS FROM THE LITERATURE SURVEY**

Literature survey MREs was done based on the magnetorheology, materials used and preparation methods, experiments conducted and on the Mathematical modeling of MREs. The following conclusions are made from the literature survey.

- (i) The matrix of MR elastomers has lots of choice, like thermoplastic rubber, silicone rubber, plastic, natural rubber, and synthetic rubber, and so on. Natural rubber has very good mechanical properties, flexibility, and processing performance. It is very suitable for the practical MR elastomer. Butyl rubber has an excellent chemical stability, insulation, and high damping factor, which makes it suitable for developing MR elastomer based shock absorber. In addition, the silicone rubber and thermoplastic rubber has been widely used to prepare MR elastomer in a lab because they are easy to be processed. The other matrices include acrylonitrile rubber, vinyl PVA glutaraldehyde synthetic polymers, polyurethane - oxygen fluorine polymer, polyurethane and formaldehyde plastic. The availability and ease of processing parameters make room temperature vulcanizing silicone the most popular choice of most of the researchers. Apart from these, combining two

different elastomer matrices also shows good properties, which combine the advantages of both the polymers.

- (ii) There are different materials available for the particle to be incorporated within the elastomer matrix which is ferromagnetic, i.e., iron, cobalt and nickel powders with average diameters ranging from  $5\mu\text{m}$  to  $100\mu\text{m}$ . All the above materials can be used as particle ingredients. Carbonyl iron powder of diameters ranging from  $5\mu\text{m}$  to  $10\mu\text{m}$  which has low coercivity is the most effective (i.e., little, or no residual magnetism when the external magnetic field is removed).
- (iii) There are many methods to characterize the field dependent viscoelastic properties of MREs. Most effective methods being the use of DMA, rheometer and custom-made experimental set ups using an electrodynamic shaker. The use of an impact hammer to give impulse excitation and taking the response also serve as a means of characterizing by replacing the expensive and bulky set ups. Impact hammers are as effective as other methods in characterizing the viscoelastic behaviour of MRE.
- (iv) Influence of various parameters such as the matrix materials, the types of curing i.e. isotropic or anisotropic, operating conditions like input frequency, strain amplitude and magnetic field have been explored in detail. It was found that most important factor deciding the MR effect is percentage concentration of ferromagnetic ingredient and the magnetic field. A volume concentration between 25 to 30% and a magnetic field of around 0.3 Tesla produces the best results.
- (v) The frequency shift of MRE under the influence of magnetic field is up to 150%. The storage modulus and loss factors show a good amount of enhancements proving its damping capabilities. Many experimental results have shown that the property enhancements were pronounced up to a field of 0.3 Tesla and after that it saturates or decreases. To produce the magnetic field, both electromagnets as well as neodymium rare earth magnets have been used.
- (vi) Several models have been developed to describe MRE behaviour. The theoretical models use Maxwell's equations to couple structural and magnetic-field dependent modifications. To determine the field-induced changes in MRE, Gold-Guth equation has been used to derive the relations. Maxwell-



Garnet mixing rule of finding the effective permeability of mixtures to derive the modulus change in structured MREs. Many of the existing rheological models are modified to account for the magnetic-field induced changes and the experimental values are fitted to these models, and parameter identification is done. Many FEM studies are also conducted to simulate the field-induced behaviour with good efficiency.

- (vii) Many potential applications have been experimentally explored, and the results have been backed up with the simulations. Most explored application of MRE is ATVA, which has been discussed by several researchers. Along with this, MRE is also had been explored in valves to control fluid flow. MRE as vibration isolator for reducing the fatigue of drivers in vehicles and in aircraft fuselages for vibration isolation applications have been discussed. It is also considered for space applications to reduce vibrations in satellites arising due to compressors. MRE can be used as miniature grippers and sensors also. However, MRE is very effective as a semi active vibration isolation/absorber element.

## **2.6 RESEARCH GAP**

There have been many attempts to prepare and characterize the MRE for potential use as vibration isolation and many other applications. But there are very few instances of investigating the influence of MRE dimensions and the size of MRE particles. The comparative studies of influence of matrix materials on the damping properties are also not extensively done. There are few investigations in which more than two types of matrices were used in a single study to prepare MR elastomers. The current research work attempts to address these issues and an attempt will be made to fill these gaps by characterizing the MRE prepared by various matrix materials and the influence of various parameters will be experimentally investigated.

## **2.7 MOTIVATION AND OBJECTIVES OF PROPOSED WORK**

Minimizing the vibrations in structures, machines or vehicles has always been a challenging task which would not only improve the efficiency but also reduces the maintenance cost. The properties of conventional vibration dampers cannot be controlled unlike Magnetorheological Elastomers whose rheological properties can be controlled by the application of external magnetic field. The field dependent properties of these MREs

can be employed to reduce vibration of structures, machines or even vehicles. Due to the field dependent properties, MREs can be used over wider range of frequencies compared to conventional dampers. But the challenge here is to find a way to control the properties by varying the magnetic field. These factors have led us to investigate the different parameters involved with MREs like types of matrix materials used, percentage of ferromagnetic particle ingredients and the different methods of preparation of MRE. These things have motivated the current research to explore the smart material MRE as a potential material for vibration attenuation devices.

Keeping these in view, the following objectives are set for the current research work.

- 1) To prepare magnetorheological elastomers using different matrix materials by varying the carbonyl iron percentage volume concentration.
- 2) To develop suitable experimental set up and investigate the influence of magnetic field, operating frequency, and strain amplitude on the dynamic behaviour of MRE.
- 3) To investigate the influence of geometry of samples and the size of the ferromagnetic particle ingredients on the damping.
- 4) To develop a phenomenological model to simulate the dynamic viscoelastic properties of MRE.
- 5) To investigate the application of MRE in constrained layer damping approach.

## **2.8 SCOPE OF THE RESEARCH WORK**

In this research, the high temperature vulcanizing samples studied are natural rubber, silicone rubber and nitrile rubber elastomers and room temperature vulcanizing silicone rubber is also studied. Along with these matrices, a new type of matrix material prepared by mixing RTV silicone, and polyurethane in different proportions is also investigated. Dynamic characterization is done using forced-vibration tests using electrodynamic shaker and using impact hammer techniques. Experimental studies will be conducted on isotropic MRE samples by varying the carbonyl iron powder content up to 25% volume concentration. Four parameters mathematical modeling technique will be employed for parameter identification. Modified linear viscoelastic model would be used to fit experimental data for parameter identification purpose. The influence of the geometry is studied by using four different thickness samples of Silicone MRE and keeping the particle content equal. The influence of particle size is not done extensively, and only two

different-sized particles are used for the study. The application of MRE as a damping material is investigated by constrained layer damping approach making use of ASTM standard E756-05 in sandwich beam configuration.

## CHAPTER 3

### DYNAMIC CHARACTERIZATION OF MRE

The dynamic characterization of MR elastomers is carried using rheometer, dynamic mechanical analyzer or using force vibration approach. Force vibration tests are carried out either by force transmissibility approach or displacement transmissibility. This chapter discusses about the force transmissibility test approach for the dynamic characterization of MRE. A comparative study of experimental response of all the samples is carried out to understand the influence of above-mentioned factors on the properties. Different types of matrix materials and preparation methods employed for fabricating MRE samples are discussed in detail. The microstructure images of the MRE samples are also discussed to understand the distribution of CIP within the elastomer matrix. The theoretical backgrounds of the force transmissibility tests carried are discussed briefly. This chapter deals with the force transmissibility measurement approach to investigate the effect of matrix material, percentage concentration of iron particles and the magnetic field on the loss factor variation of different samples.

#### 3.1 THEORETICAL BACKGROUND FOR FORCE TRANSMISSIBILITY TESTS

The schematic of the experimental set-up is shown in figure 3.1. The force vibration tests can reveal the damping properties of the different elastomer samples by plotting the transmissibility ratio verses the operating frequency graph. The system can be considered as a SDOF system with base excitation and can be modeled as a spring and a dashpot element as shown in figure 3.2.

The force generated by the shaker is impressed upon the MRE sample through the stinger. The transmitted force is the force measured by the force transducer at the top as depicted in the figure 3.1. This set-up is approximated to single degree of freedom system subjected to harmonic excitation force. The setup is modeled as a spring mass dashpot system. By employing force transmissibility approach, the transmissibility ratio can be calculated by the vector approach. Under steady-state conditions, the forces acting upon the system can be represented by the vector diagram (figure 3.3).

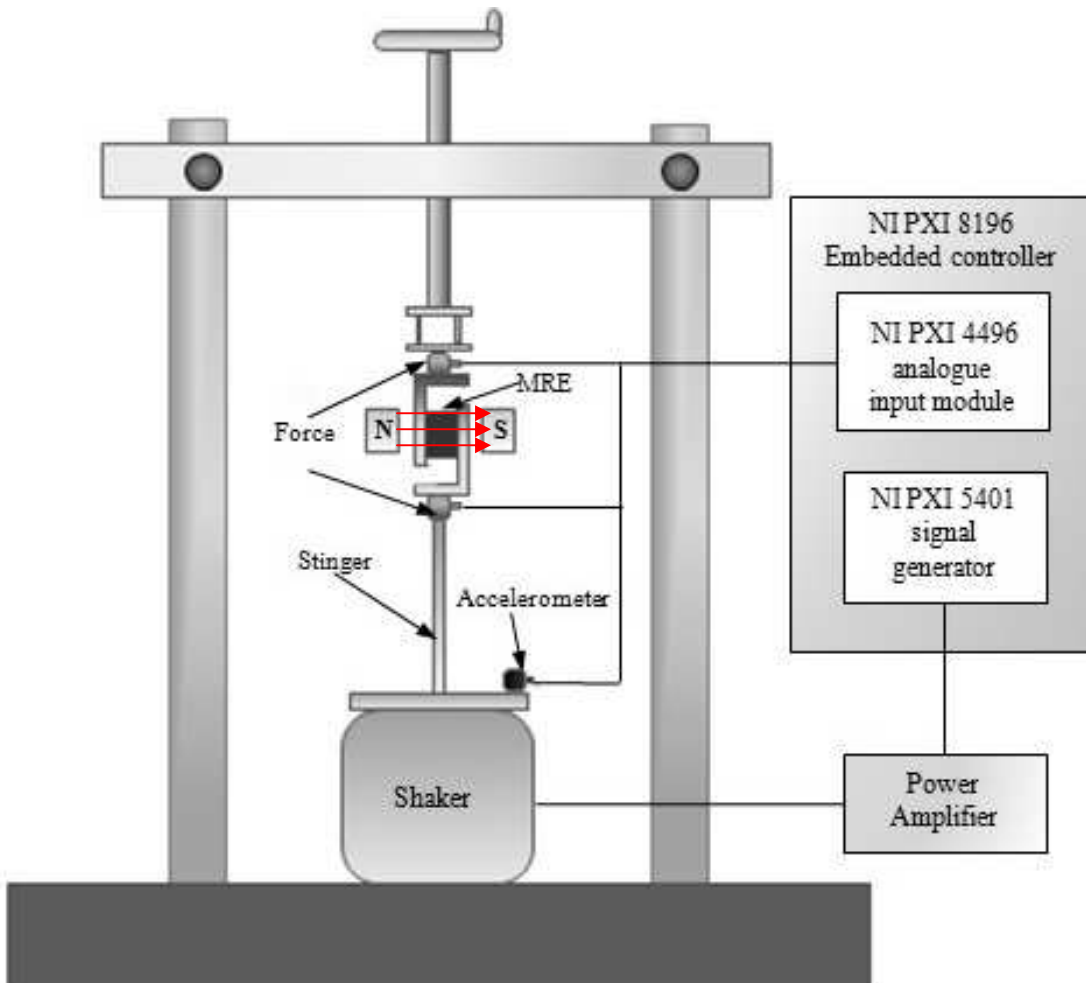


**Figure 3.1.** Schematic of the set up

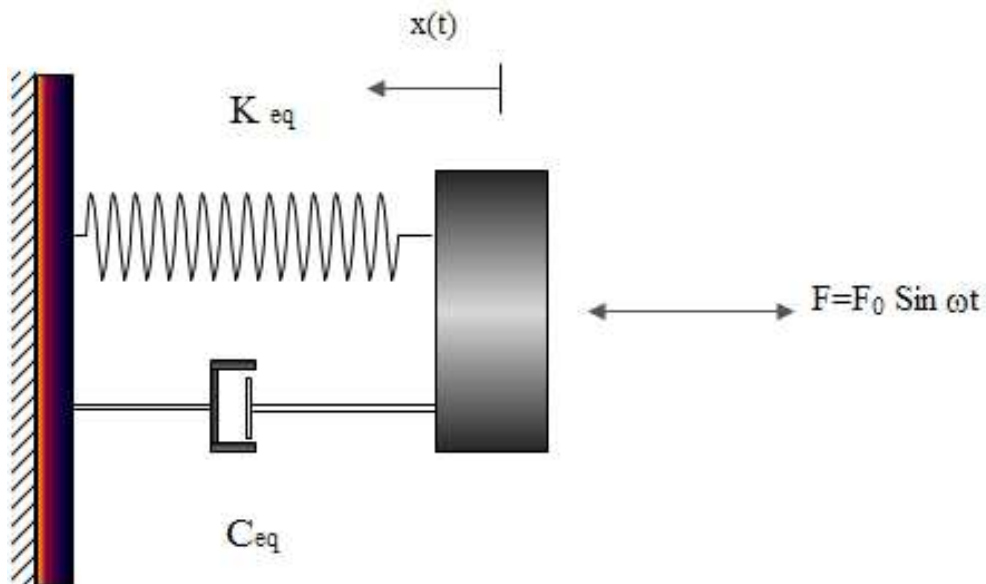


**Figure 3.2.** System modeled as SDOF with base excitation

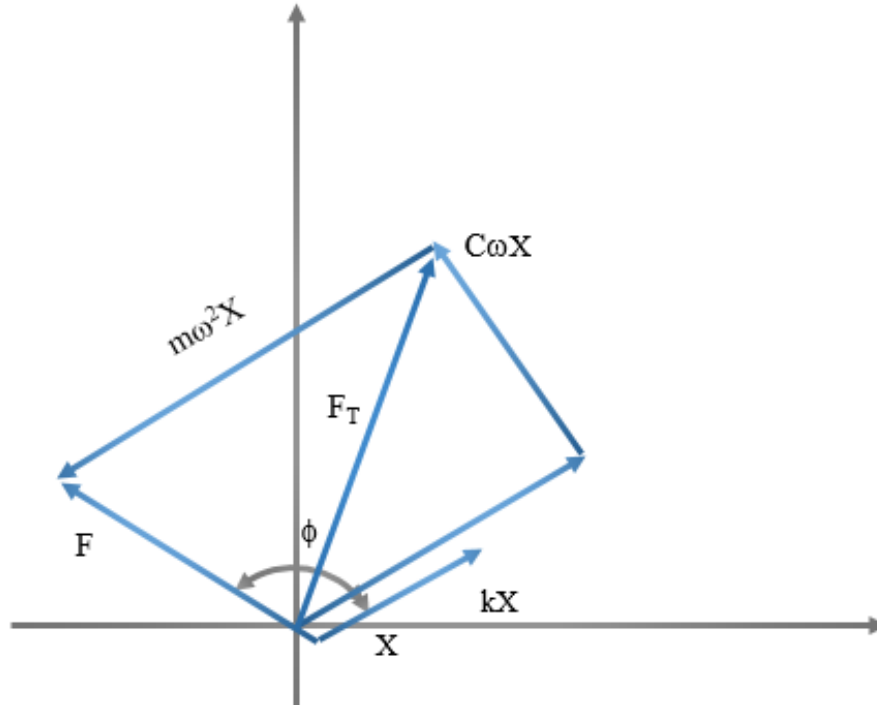


**Figure 3.3** Vector representation of Forces (W.T Thomson)

The spring force is represented by  $kX$  and damping force is represented by  $C\omega X$ .

The transmitted force  $F_{tr}$  is the vector sum of the two forces acting in opposite directions

$$F_{tr} = \sqrt{(kX)^2 + (c\omega X)^2} \quad (3.1)$$

$$F_{tr} = X\sqrt{k^2 + (c\omega)^2} \quad (3.2)$$

The input force  $F_o$  can be calculated from the vector diagram,

$$F_o = \sqrt{(c\omega X)^2 + (kX - m\omega^2 X)^2} \quad (3.3)$$

$$F_o = X\sqrt{(c\omega)^2 + (k - m\omega^2)^2} \quad (3.4)$$

The ratio of transmitted force to the input force gives the Transmissibility ratio.

$$TR = \frac{F_{tr}}{F_o} = \frac{\sqrt{(kX)^2 + (c\omega X)^2}}{\sqrt{(c\omega)^2 + (k - m\omega^2)^2}} \quad (3.5)$$

By writing equation 3.5 in dimensionless form, we get,

$$TR = \frac{F_{TR}}{F_o} = \frac{\sqrt{1 + \left(2\zeta \frac{\omega}{\omega_n}\right)^2}}{\sqrt{\left(1 - \left(\frac{\omega}{\omega_n}\right)^2\right)^2 + \left(2\zeta \frac{\omega}{\omega_n}\right)^2}} \quad (3.6)$$

Where,  $F_{Tr}$  and  $F_o$  are the transmitted force and the input force respectively in Newton.  $\zeta$  is the damping ratio and  $\omega/\omega_n$  is the frequency ratio. Where  $\omega$  is the operating frequency and  $\omega_n$  is the natural frequency of the system configuration in Rad/sec.

At resonance, the operating frequency  $\omega$  is equal to the natural frequency  $\omega_n$ . By incorporating these changes, the equation (3.6) can be so written that, loss factor can be expressed in terms of transmissibility ratio as shown below,

$$\zeta = \frac{1}{2} \sqrt{\frac{1}{(TR^2 - 1)}} \quad (3.7)$$

For materials with relatively small damping ratios, loss factor  $\eta$  can be approximated to be twice that of damping ratio i.e.

$$\eta = 2\zeta = \sqrt{\frac{1}{(TR^2 - 1)}} \quad (3.8)$$

Using of equation 3.8, the loss factor values of all the samples can be calculated from the response curves which would be used for analyzing the performance of the MRE samples.

### 3.2 MATERIAL PROCESSING

The magnetorheological elastomer consists of an elastomer matrix and a ferromagnetic ingredient which imparts field dependent properties. In the current research work, MRE samples were prepared by employing different types of elastomer samples and varying the percentage content of the particle ingredients. Natural rubber (CIS-polyisoprene), Silicone and Nitrile (NBR) were the HTV samples prepared for analysis. One RTV type of MRE was also prepared using silicone elastomer from Dow Corning. The main reason for selecting natural rubber is the ease of availability, and it is very economical. The damping property of the natural rubber is relatively lower, which enables to understand the influence of ferromagnetic particles and magnetic field on the loss factor enhancement. Silicone elastomer has excellent chemical resistance and high operating temperature range compared to other matrices, and NBR has excellent damping properties. By preparing MRE samples using these different types of elastomers with different damping properties, the influence of the ferromagnetic ingredients can be effectively investigated. The latex for the preparation of MRE was obtained from rubber trees (*Hevea brasiliensis*) in Sullia, Mangalore. The Nitrile and silicone HTV samples were obtained from S.K Rubber industries, Mangalore. The ferromagnetic particle ingredient selected for the MRE is the Carbonyl iron powders (CIP) form BASF-

Germany (Grade CC) which is of about 5  $\mu\text{m}$  in diameter. The preparation method of HTV samples is explained below.

The ingredients for the vulcanization of HTV MRE samples are listed in table 3.1 below. Mixing of the ingredients and molding was done at S.K Rubber industries, Baikampady Industrial estate, Mangalore. The vulcanization process of HTV rubber involves a process called mastication, which is done by passing uncured rubber sample between two rollers rotating in opposite direction. The rollers will be heated to around 120<sup>0</sup>C, by passing continuously between the rollers, the fluidity of rubber increases, and it reaches a mushy state. Once this state is reached, the ingredients mentioned in the table are added one by one and thoroughly mixed, and once it is mixed, the sample is kept for curing for about 24 hours.

**Table 3.1**Ingredients for vulcanization

<b>Ingredients</b>	<b>Amount (grams)</b>	<b>Type</b>
Rubber	1000	
ZnO	50	Activators
Stearic acid	20	
MBTS*	5	
Sulfur	20	Curing agents
TMT**	2	
Silicone oil	50	
TDQ***	5	Plasticizers

\*MBTS- Dibenzothiazole disulphide; \*\*TMT- Tetramethyl thiuram disulphide; \*\*\*TDQ- Trimethyl-1,2-Dihydroquioline

After 24 hours, it is passed through the rollers and once mushy state is reached, carbonyl iron powder is mixed. Silicone oil is added during the addition of iron powder to enhance mixing. After the mixing is done, it is kept in the mold and cured at 140<sup>0</sup>C and around 1000 N for 15 minutes. The prepared samples were blocks of size 34mm x 34mm x 16mm. Five samples of these two shapes were produced by varying the percentage by volume of Carbonyl iron powder. The prepared samples were of 0%, 10%, 15% and 20 and 25% CIP by volume. Strips of dimension 200mm x 20mm x 6mm were also prepared with the same percentage concentration and matrix materials. The photographs of some of the prepared samples (strips and the block) are shown in figure 3.4.



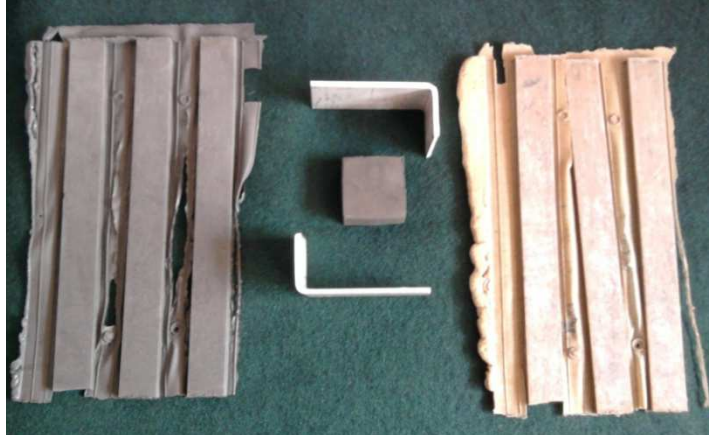


**Figure 3.4.** Natural rubber samples

The RTV silicone samples with similar dimensions as the HTV samples were prepared in the lab at NITK, Surathkal. The RTV silicone employed in the current work is a two-part system room temperature vulcanizing rubber from Dow Corning (SILASTIC® 3483). Appropriate quantity of carbonyl iron powder was mixed with resin and stirred thoroughly to maintain uniform distribution and then proper quantity of curing agent was added and properly mixed for about 15 minutes and poured into the mold and kept in a vacuum chamber to remove the air bubbles. It was kept under pressure in the mold for curing. Carbonyl iron powder sample from BASF Germany of average diameter of 5  $\mu\text{m}$  was used. Five samples prepared with 0%, 10%, 15%, 20% and 25% by volume of CIP in each type of matrix material, and in total 20 samples were employed for experiments. The samples and the type of matrices used are listed in table 3.2.

**Table 3.2**Types of samples prepared

Matrix Material	% of CIP by Volume	Type	Tests
Natural rubber		HTV	Force vibration and Impact tests
Silicone	0,10,15,20 and 25%	HTV and RTV	
Nitrile		HTV	

The microstructure of natural rubber samples is shown below (Figure 3.2b to 3.2f) which was observed using Jeol SEM facility at NITK, Surathkal. Figure 3.2a shows the microstructure of CIP and from 3.5 b to 3.5 f shows the microstructure of natural rubber and the MRE with 10%, 15%, 20% and 25% CIP concentration respectively. The microstructure studies were extended to different locations of the same sample to ensure uniform distribution. The microstructure study shows uniform distribution of ferromagnetic particles within the matrix.

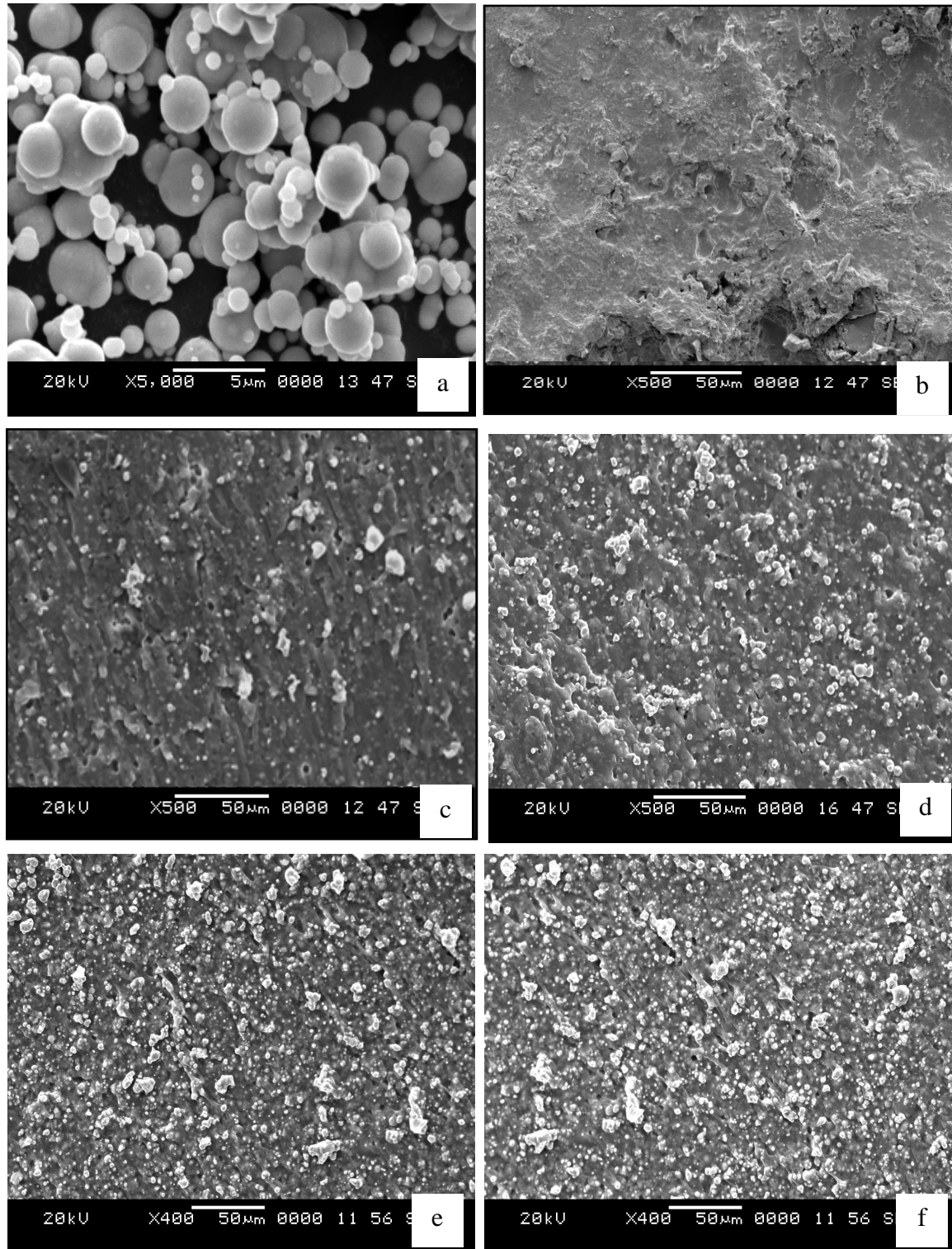


**Figure 3.5.** Microstructure of CIP and Natural rubber MRE samples. a) CIP, b) Pure NR, c) 10% MRE, d)15% MRE, e)20% MRE and f)25% MRE

### 3.3 EXPERIMENTAL SET UP FOR DYNAMIC CHARACTERIZATION

To realize the use of MRE as an effective isolator device, a proper understanding of the influence of various parameters on the property enhancements is essential. Different types of experimental approaches have been followed to assess the property enhancements. The

various methods adapted to characterizing the dynamic behaviour of MR elastomer have been presented in the previous chapter. In this chapter, a detailed analysis of the experimental results and discussions of the response curve of each sample is carried out to understand the magnetic field-induced enhancement of different samples. The absolute MR effect is referred to as the variation in field-induced enhancement with respect to the unfilled sample, and the relative MR effect is referred to as the field-induced changes under the influence of magnetic field. In other words, if the natural rubber is considered, the loss factor values of 15% or other samples would be compared with the pure natural rubber sample. The absolute and relative MR effect studies of all the MR samples are meticulously carried out.

### 3.3.1 FORCE VIBRATION TESTS

The photograph of the experimental set up is shown in Figure 3.7. The experimental samples were prepared by sandwiching the sample between 3 mm thick Aluminum strip which is 34 mm in width and bent in the form of an “L”. This is done to conduct single-lap shear dynamic tests on the samples. Cyanoacrylate based adhesive was used to bond the samples between two Aluminum strips. Photographs of some of the test samples are shown in Figure 3.6.



**Figure 3.6** Test samples for forced-vibration transmissibility tests

The MRE test sample was fixed to the top of the structure as shown in the photograph (Figure 3.6) and two Kistler force transducers (450 lbf and sensitivity 21.96 mV/g) were fixed at the top and bottom of the elastomer to measure the input and the transmitted force respectively. A sinusoidal signal generated by NI PXI-5401 was amplified and fed to the Electrodynamic shaker to generate the input force. Keeping the acceleration constant at 1 g throughout the experiment, the signal frequency was varied from 40 Hz to 400 Hz.

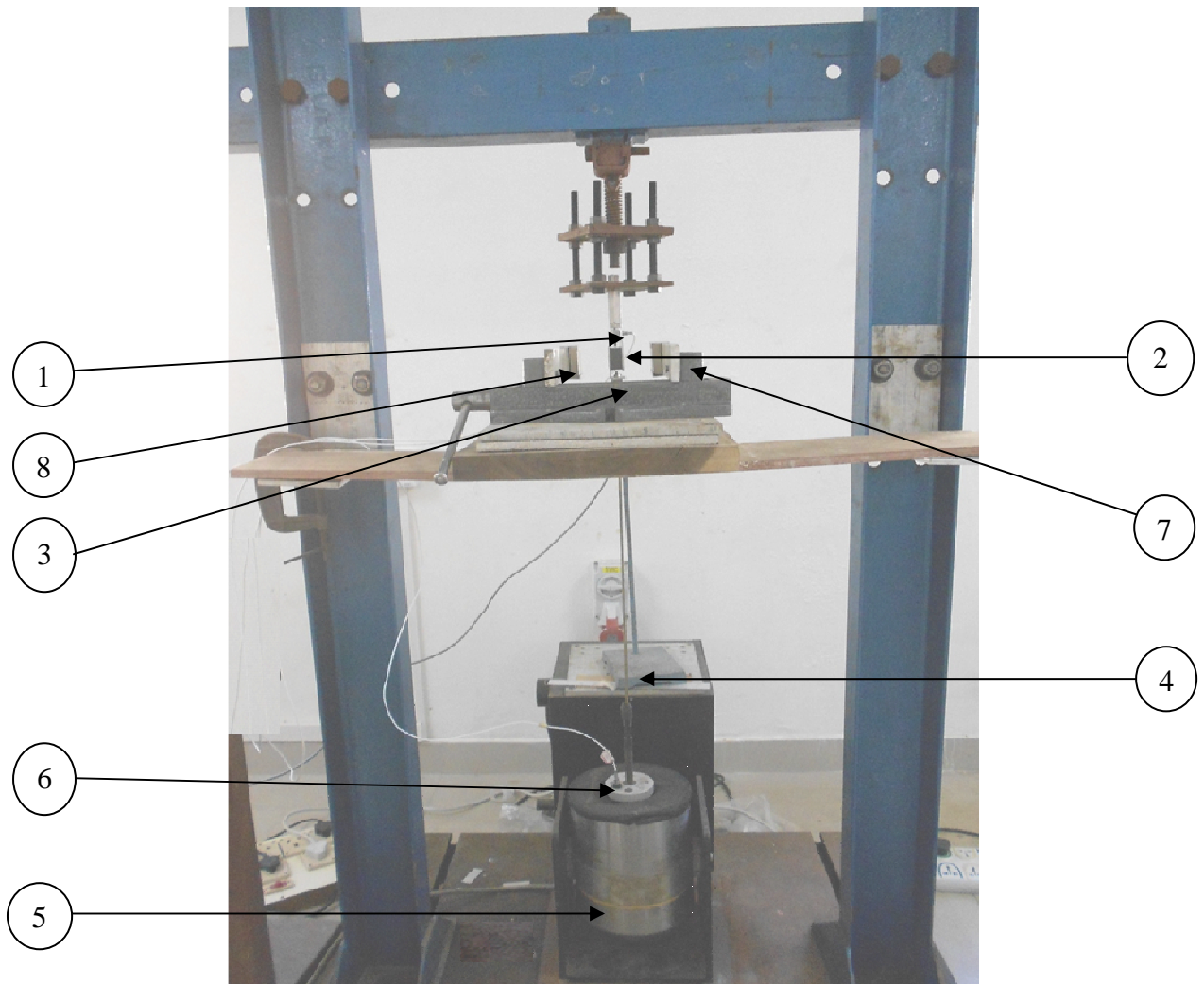


**Figure 3.7** Photograph of the experimental set-up. 1 and 3 –Force transducers to measure output force and input force respectively, 2- MRE test sample, 4- Stinger used to transmit linear force from shaker, 5-Electrodynamic shaker VTS-100, 6-Accelerometer, 7 and 8- Neodymium permanent magnets

The incremental frequency of 10 Hz in the stiffness and mass controlled region and 2 Hz in the damping controlled region. Data acquisition was made using LabVIEW 2010. The ratio of output force ( $F_{tr}$ ) and input force ( $F_o$ ) i.e. force transmissibility against the input frequency graph was plotted to analyze the system characteristics. The same experiments were repeated under the influence of magnetic field using Neodymium rare-earth permanent magnets (Grade 32) as a source of magnetic field. The magnetic field was increased from 0 Tesla to 0.3 Tesla in steps of 0.1 Tesla. All the set of experiments were repeated for 5 trials, and the average value was considered for the analysis to maintain the consistency and the repeatability of the experiments. The magnetic-field intensity was measured using Lakeshore Gauss meter. The magnetic-field intensity variation across the elastomer was achieved by varying the distance or air gap between

the magnets and elastomer using a modified self-centering vice. To observe the magnetic flux variation across the thickness of the test sample, a finite-element analysis with Finite-Element Method Magnetics (FEMM) was conducted. The analysis was done for two different air gaps between the poles of the magnet. The results (Figure 3.8 and 3.9) show the uniformity of magnetic field in the area where the test samples are kept. The field distribution along the vertical was also plotted to show the uniform distribution of the field. To understand the behaviour of the MRE, the transmissibility ratio versus operating frequency was plotted.

For the test sample preparation of RTV silicone same procedure was employed, but the adhesive used in this case was different. Silicone exhibits a unique property called abhesion which is the opposite of adhesion and because this, a special adhesive (Sil-poxy) had to be used to bond the samples with the aluminium. These samples were also tested for MR effect as mentioned above.

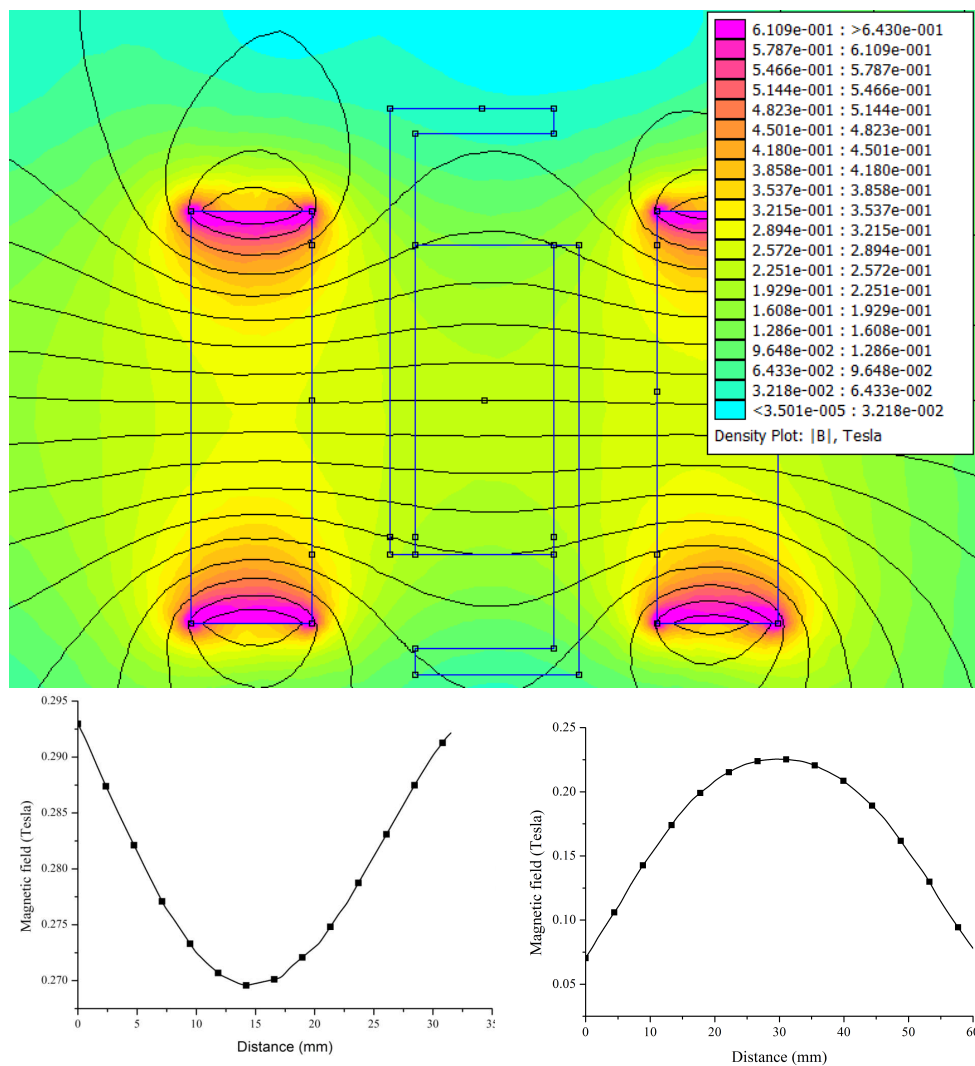


**Figure 3.8** FEMM simulation with a gap of 40mm between the magnetic poles

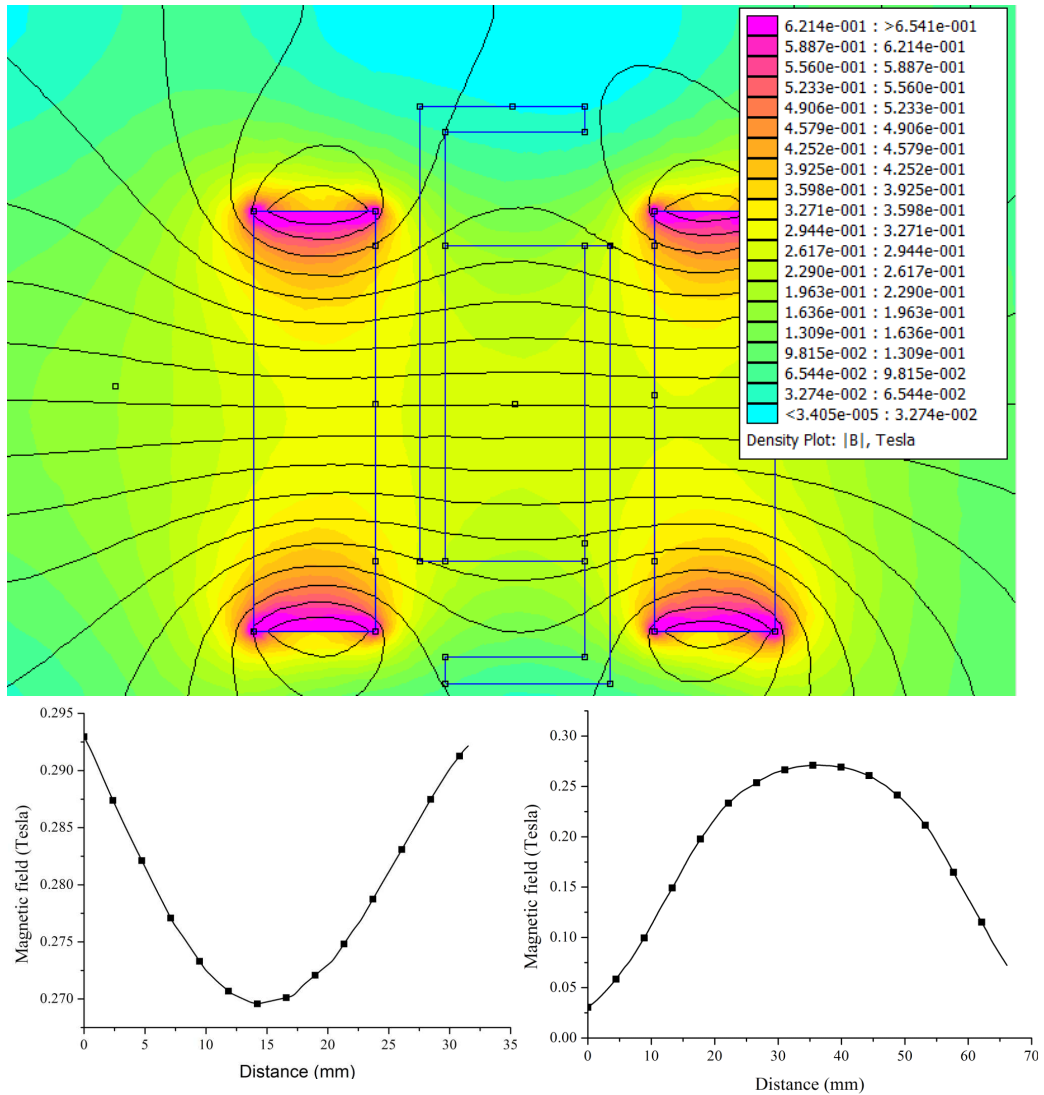


**Figure 3.9** FEMM simulation with a gap of 30mm

### 3.3.2 RESULTS AND DISCUSSIONS

The samples were tested under harmonic loading of different frequencies and magnetic field. The force transmissibility was assessed by measuring the input and transmitted force. The graph of the transmissibility ratio versus frequency was plotted, and loss factor values of each sample were calculated by the method described in section 3.1. By comparing the loss factor values of different samples under different magnetic fields, the extent of property enhancements is analyzed. The responses of the samples are shown in figure 3.10 to 3.33, and each graph is addressed for the analysis.

The figure 3.10 to 3.14 shows the force transmissibility of natural rubber samples. The increase in the damping ratio was observed with the increase in CIP concentration as well as the magnetic field. As observed from these plots, the transmissibility ratio of the pure natural rubber was the highest at 22 and as the percentage of iron powder was

increased, the transmissibility ratio was reducing. For 25% CIP sample at 0.3 Tesla, force transmissibility peak reduced to about 8 showing a 63% improvement in loss factor.

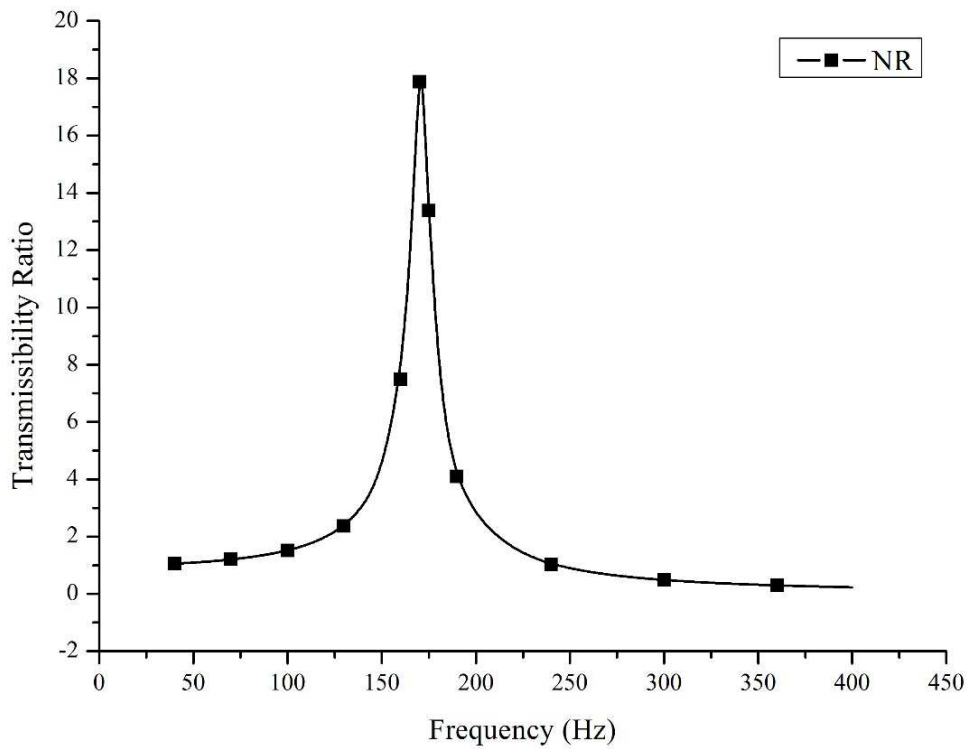


Figure 3.10. Behaviour of Pure Natural Rubber

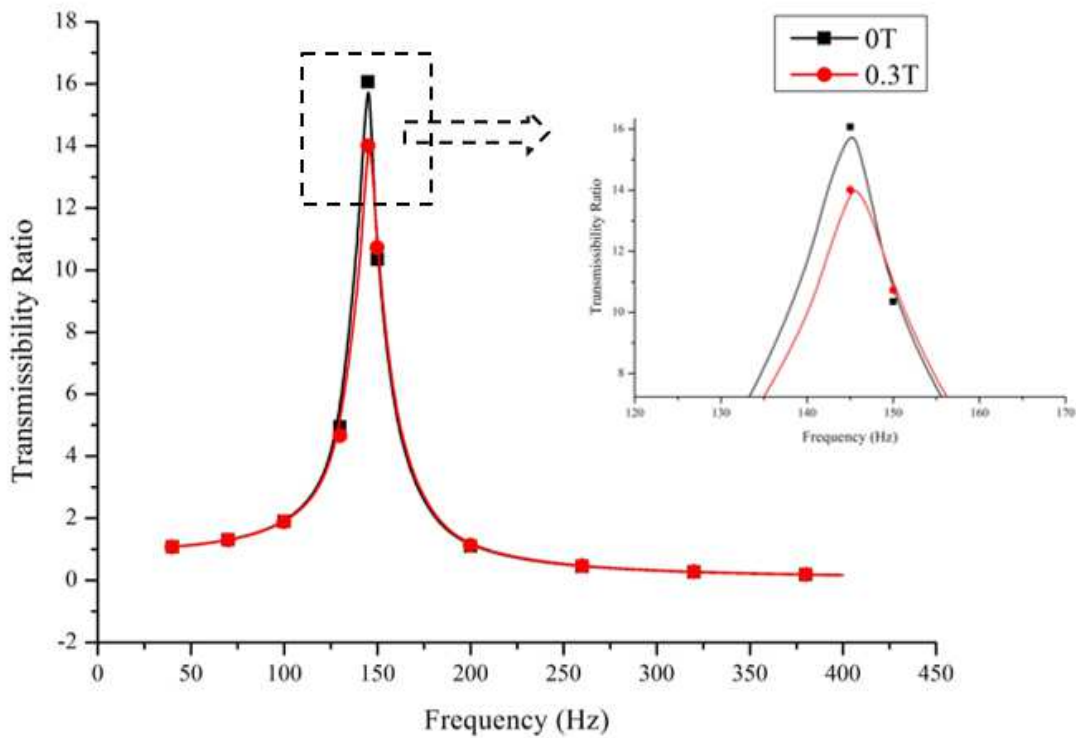
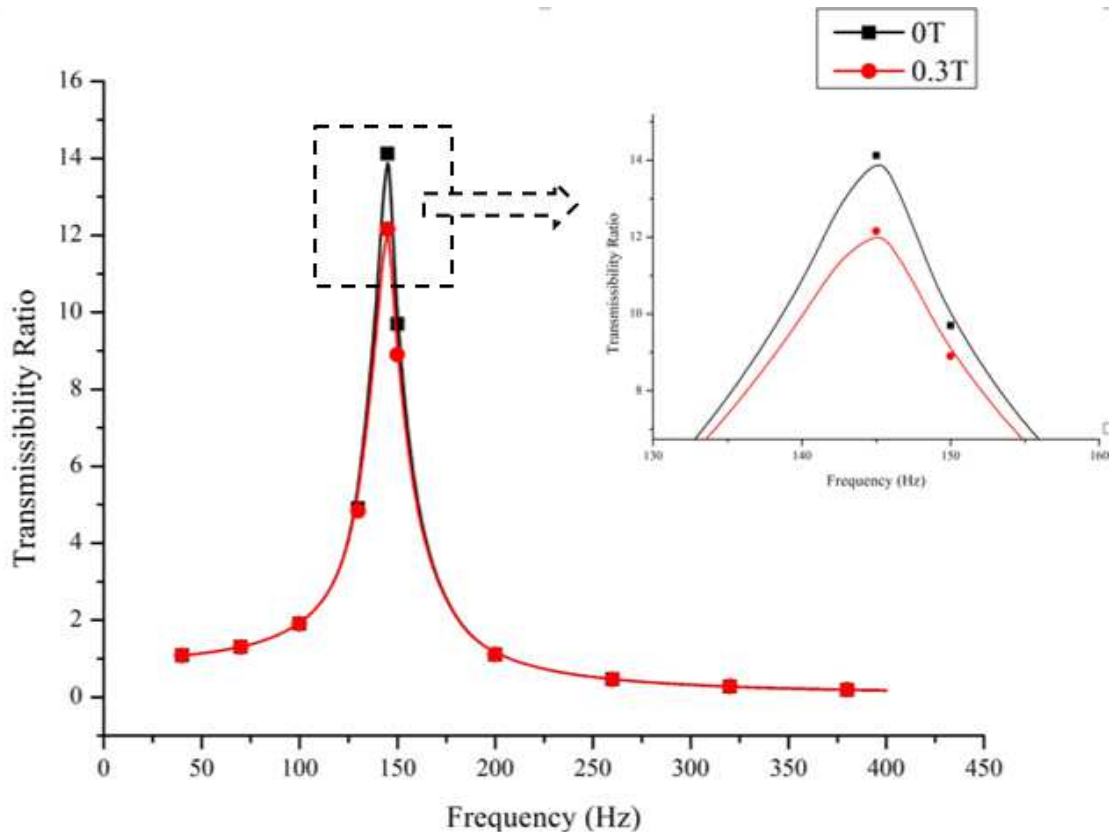
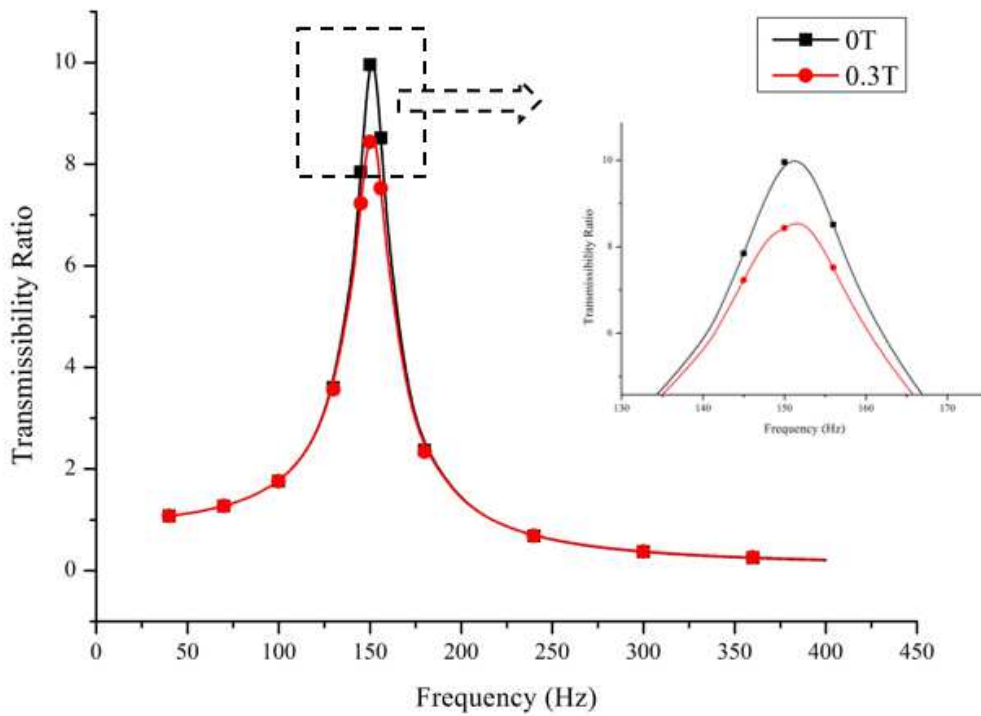


Figure 3.11. Behaviour of 10% NR MRE



**Figure 3.12.** Behaviour of 15% NR MRE



**Figure 3.13.** Behaviour of 20% NR MRE



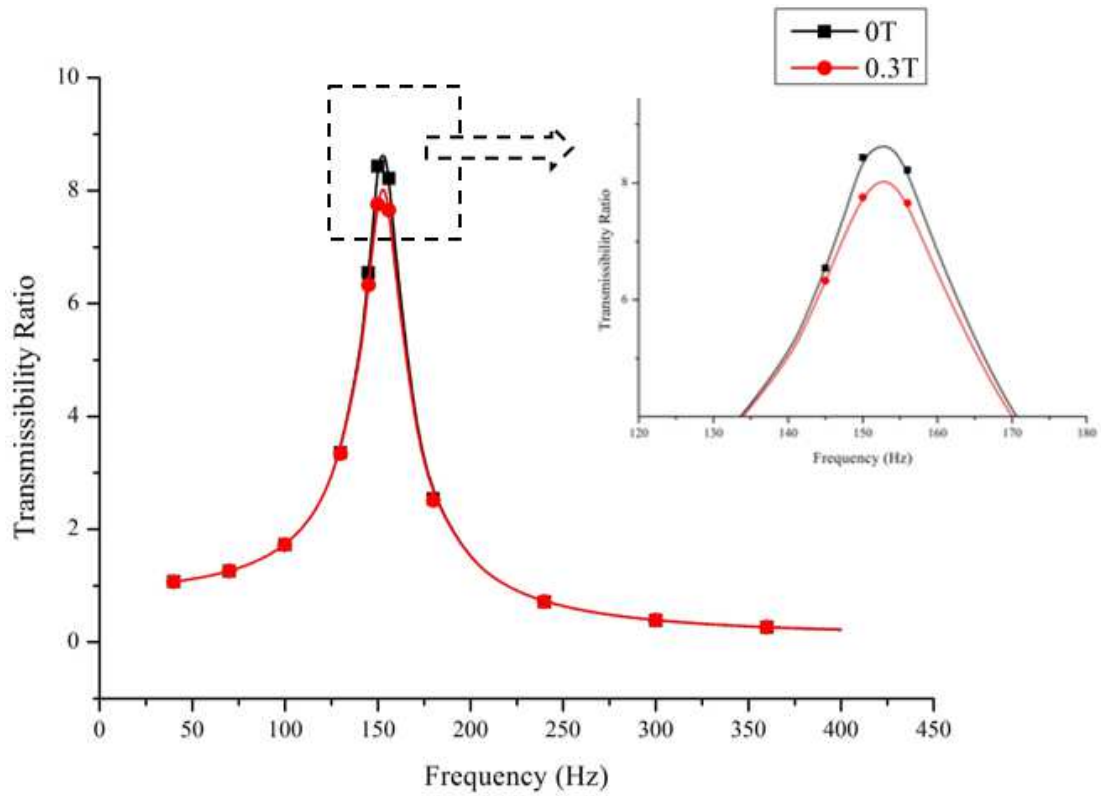


**Figure 3.14.** Behaviour of 25% NR MRE

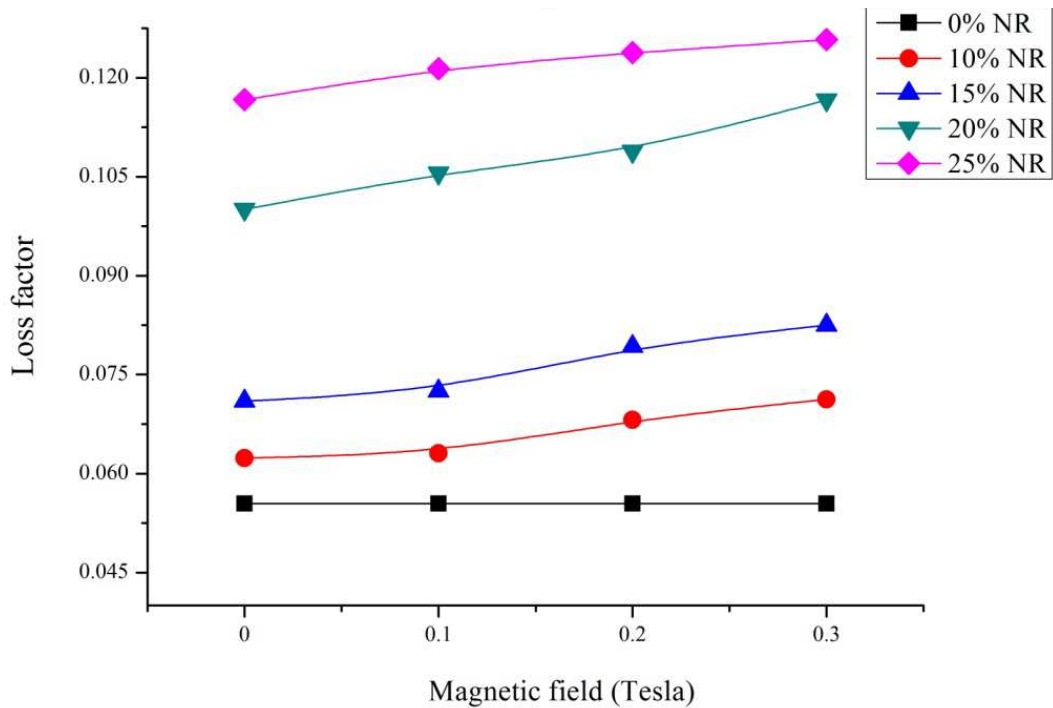


**Figure 3.15.** Structural Loss factor variation of NR MRE samples

The TR of 10% sample at 0 Tesla was about 16, and it reduced to about 14 at 0.3 Tesla showing enhancement in damping. Similar trend was noticed as the percentage content of CIP was increased though the percentage variation in loss factor enhancement was different.

The 25% sample showed the lowest transmissibility at about 8.6 at 0 Tesla and about 8 at 0.3 Tesla. However, the relative improvement was less. The variation of the loss factor with magnetic field and percentage of CIP is shown in figure 3.15. An absolute change of 110 % improvement (from 0.05543 for pure rubber to 0.1167 for 25% MRE at 0 Tesla) in loss factor was observed and a relative improvement of 127% (from 0.05543 for pure rubber to 0.1258 for 25% MRE at 0.3 Tesla). The variation in relative and absolute loss factor enhancements with magnetic field is shown in Table 3.3.

**Table 3.3:** Comparison of structural loss factors of Natural rubber samples

Field (Tesla)	CIP		% change		CIP	% change		CIP	% change		CIP	% change	
	0%	10%	Abs	Rel		15%	Abs		Rel	20%		Abs	Rel
0	0.055	0.062	12.466	N/A	0.071	28.053	N/A	0.100	80.516	N/A	0.117	110.500	N/A
0.1	0.055	0.063	13.765	1.155	0.073	30.796	2.141	0.106	90.402	5.477	0.121	118.979	4.028
0.2	0.055	0.068	22.966	9.336	0.079	43.027	11.693	0.109	96.356	8.775	0.124	123.345	6.102
0.3	0.055	0.071	28.522	14.277	0.083	48.872	16.258	0.117	110.428	16.570	0.126	126.917	7.799

From the table; it is observed that 15% and 20% CIP samples showed better relative improvement with the magnetic field. 25% sample showed least relative improvement in loss factor, but it registered the highest loss factor value among the natural rubber samples.

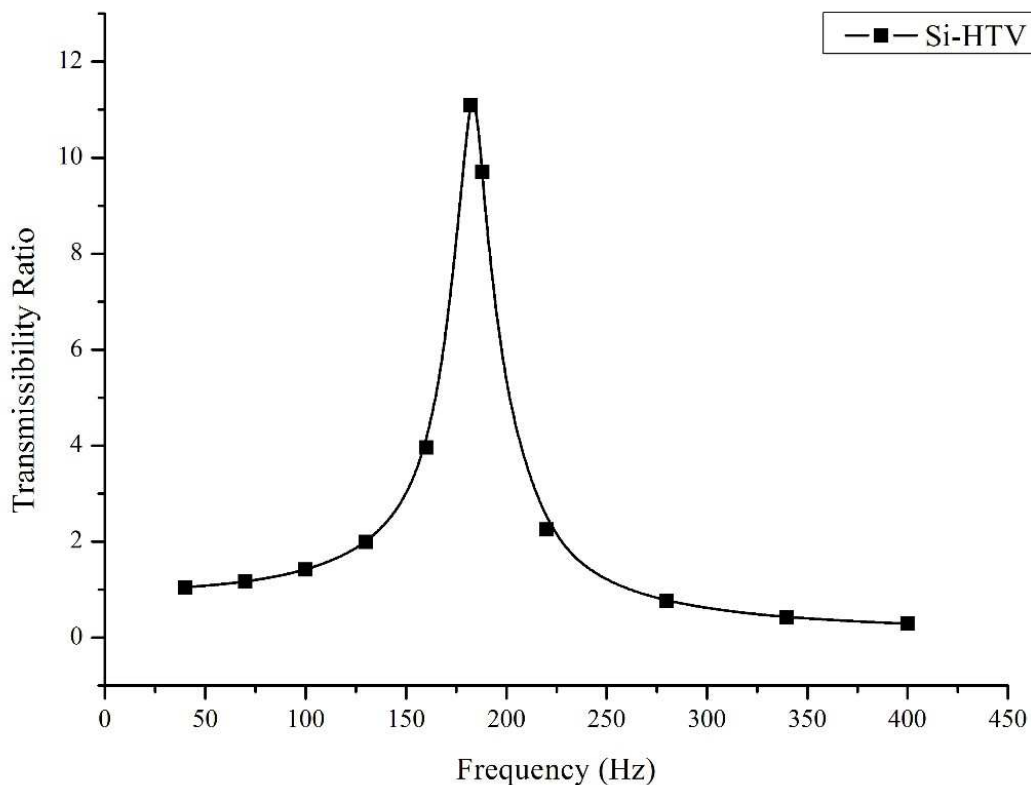


**Figure 3.16.** Behaviour of Pure Si-HTV MRE

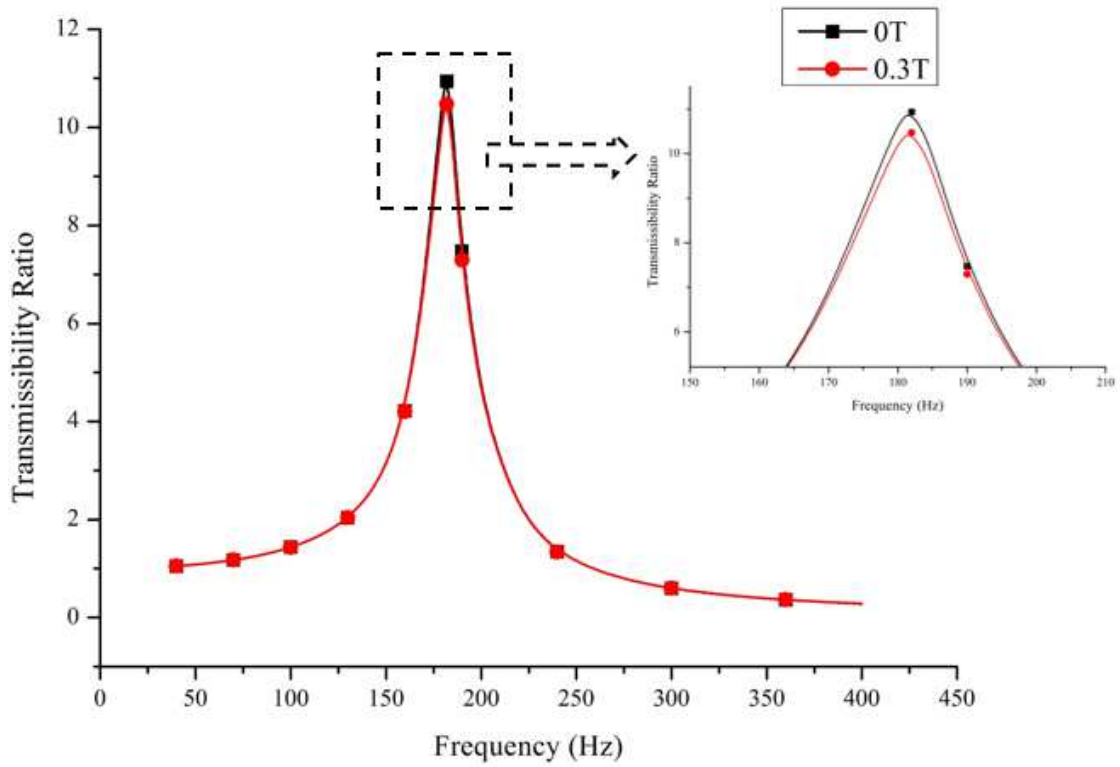


**Figure 3.17** Behaviour of 10% Si-HTV MRE

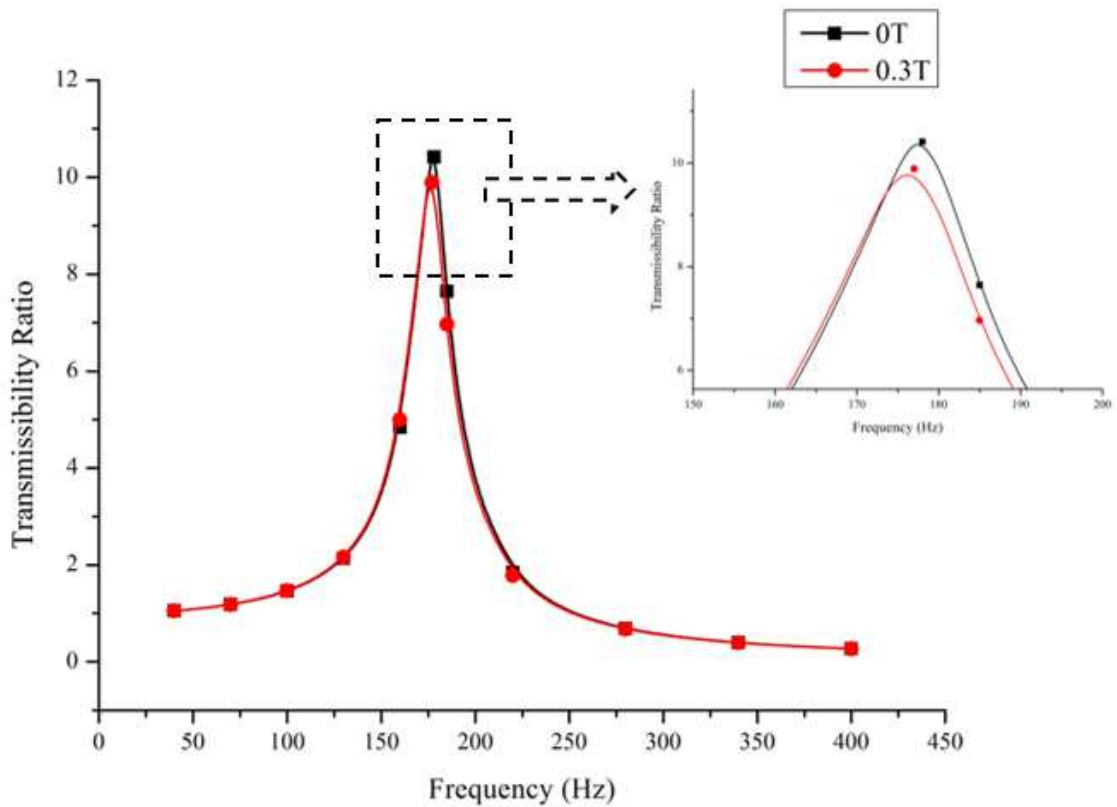


**Figure 3.18** Behaviour of 15% Si-HTV MRE

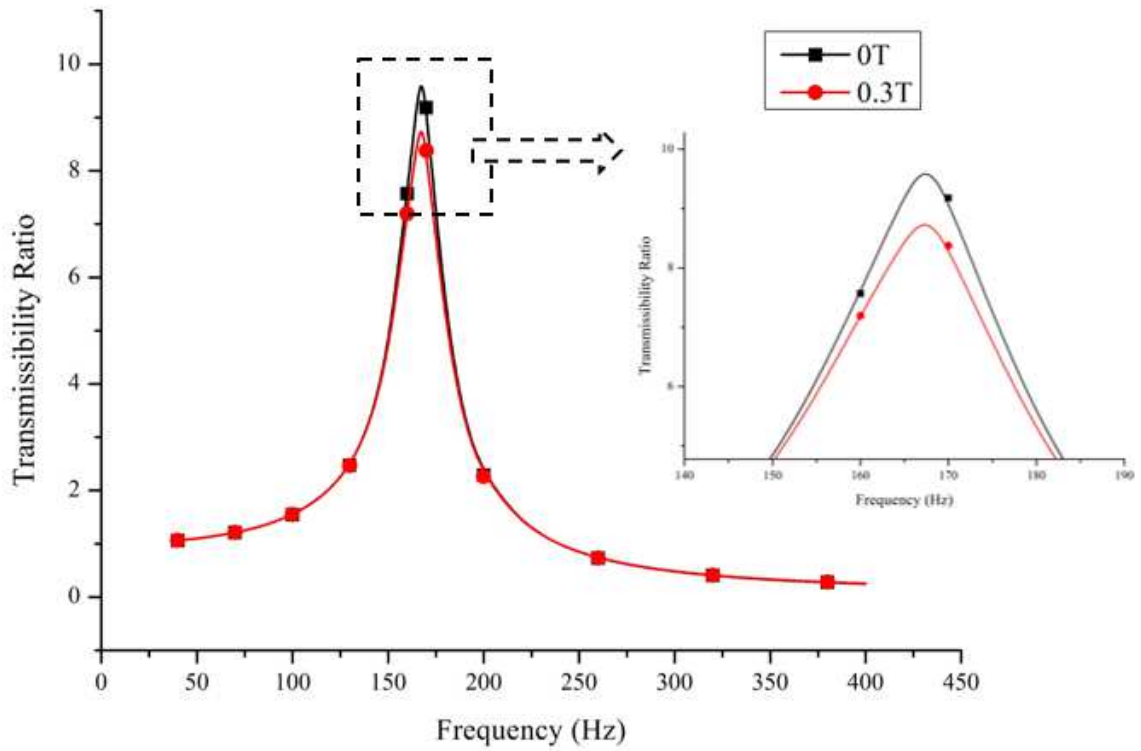


**Figure 3.19** Behaviour of 20% Si-HTV MRE

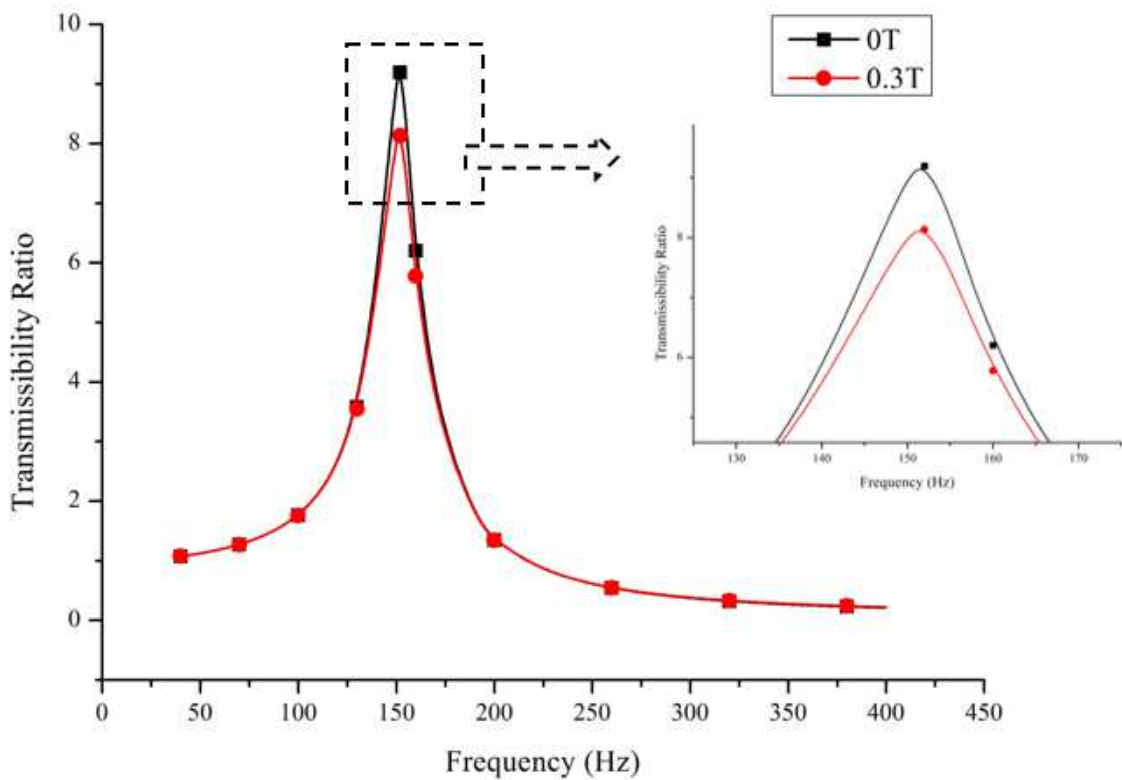


**Figure 3.20.** Behaviour of 25% Si-HTV MRE

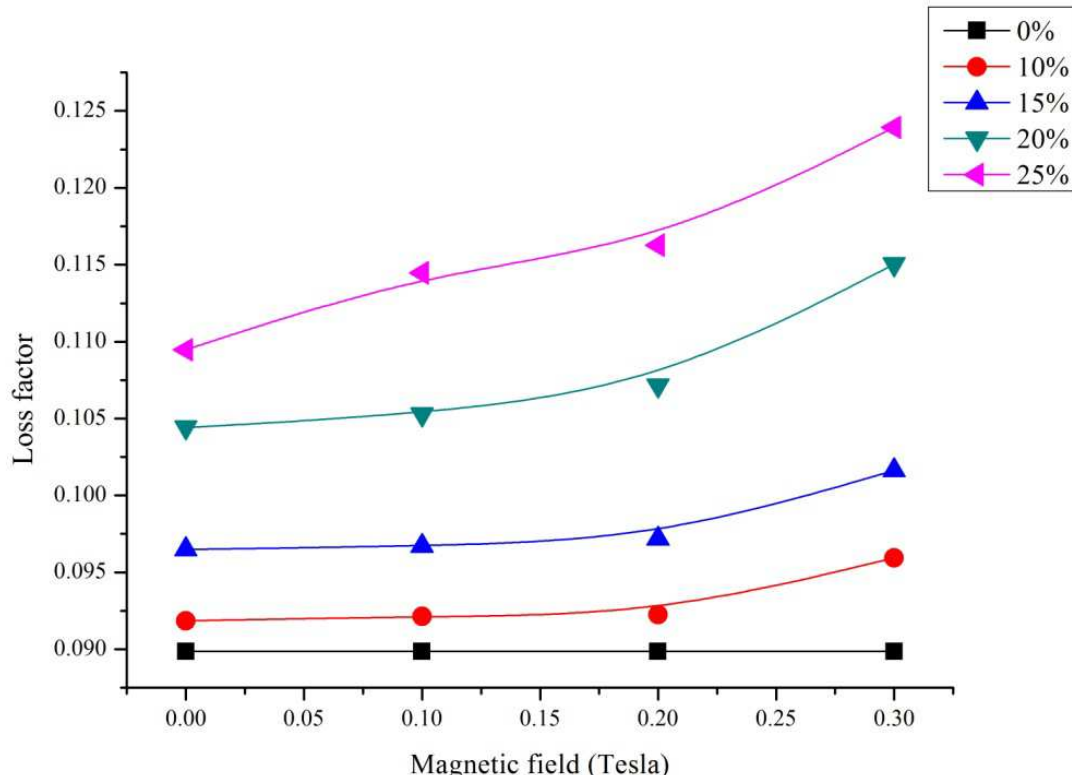


**Figure 3.21** Structural Loss factor variation of Si-HTV MRE samples

**Table 3.4:** Comparison of structural loss factors of Si-HTV samples

Field (Tesla)	CIP		% change		CIP		% change		CIP		% change		CIP		% change			
	0%	10%	Abs	Rel	15%	Abs	Rel	20%	Abs	Rel	25%	Abs	Rel	0%	10%	Abs	Rel	
0	0.090	0.092	2.215	N/A	0.096	7.378	N/A	0.104	16.203	N/A	0.109	21.823	N/A					
0.1	0.090	0.092	2.526	0.305	0.097	7.623	0.228	0.105	17.160	0.824	0.114	27.398	4.577					
0.2	0.090	0.092	2.660	0.435	0.097	8.146	0.715	0.107	19.252	2.624	0.116	29.390	6.212					
0.3	0.090	0.096	6.766	4.453	0.102	13.098	5.327	0.115	28.021	10.170	0.124	37.903	13.200					

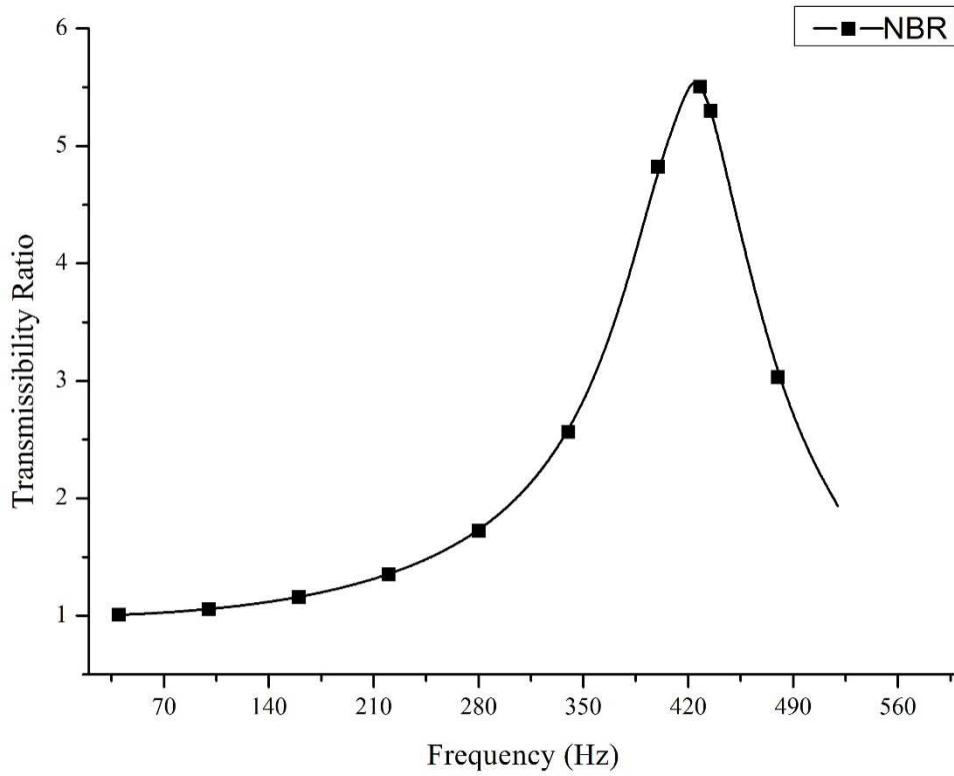


Figure 3.22. Behaviour of Pure NBR sample

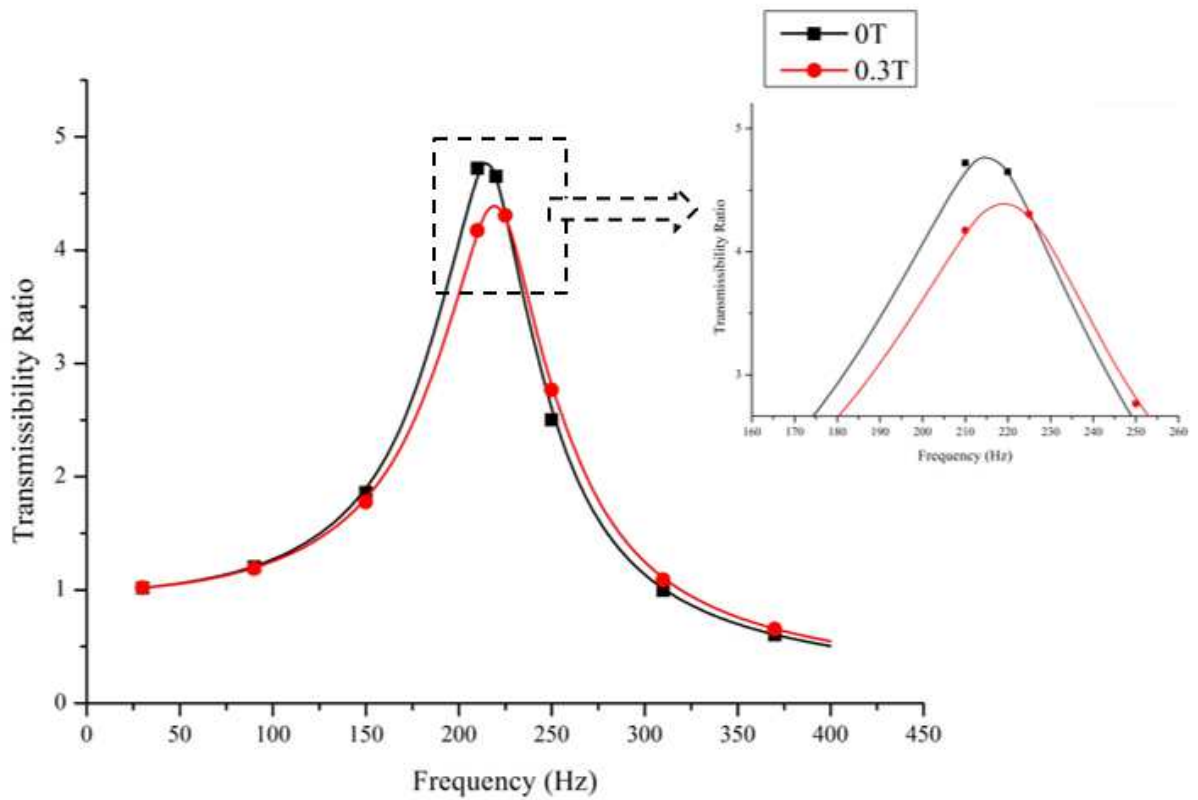


Figure 3.23. Behaviour of 10% NBR sample

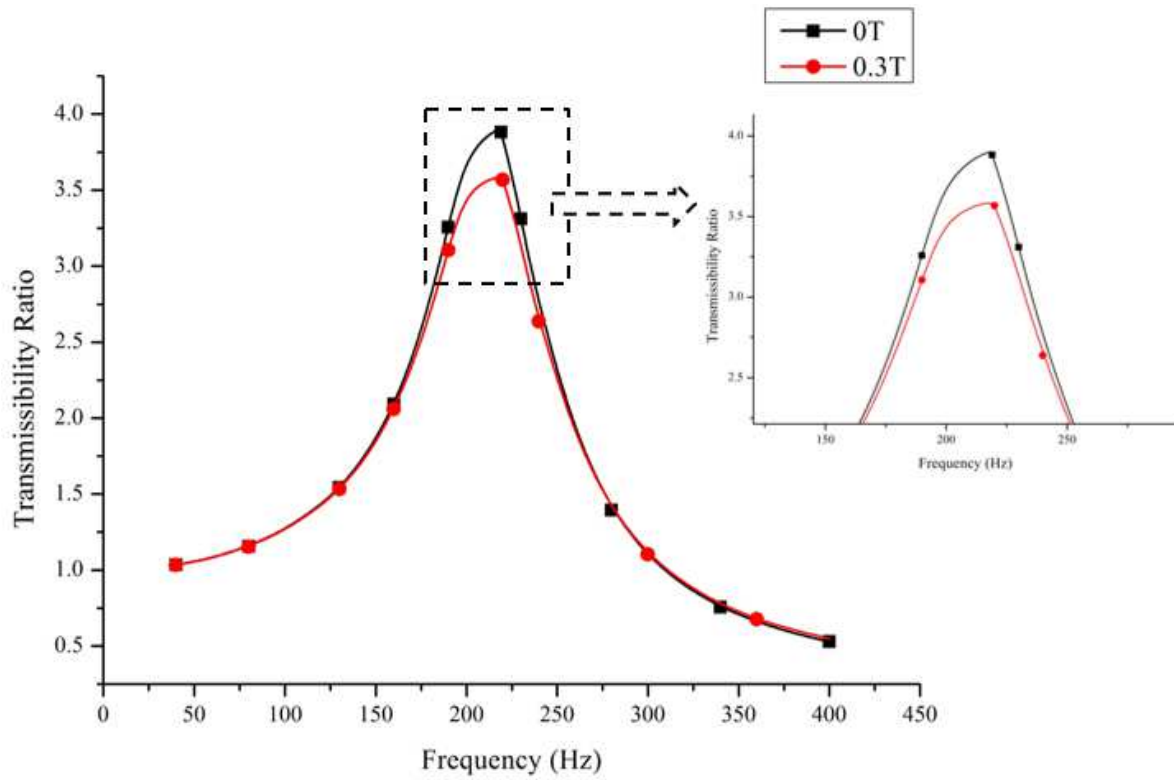


Figure 3.24. Behaviour of 15% NBR sample

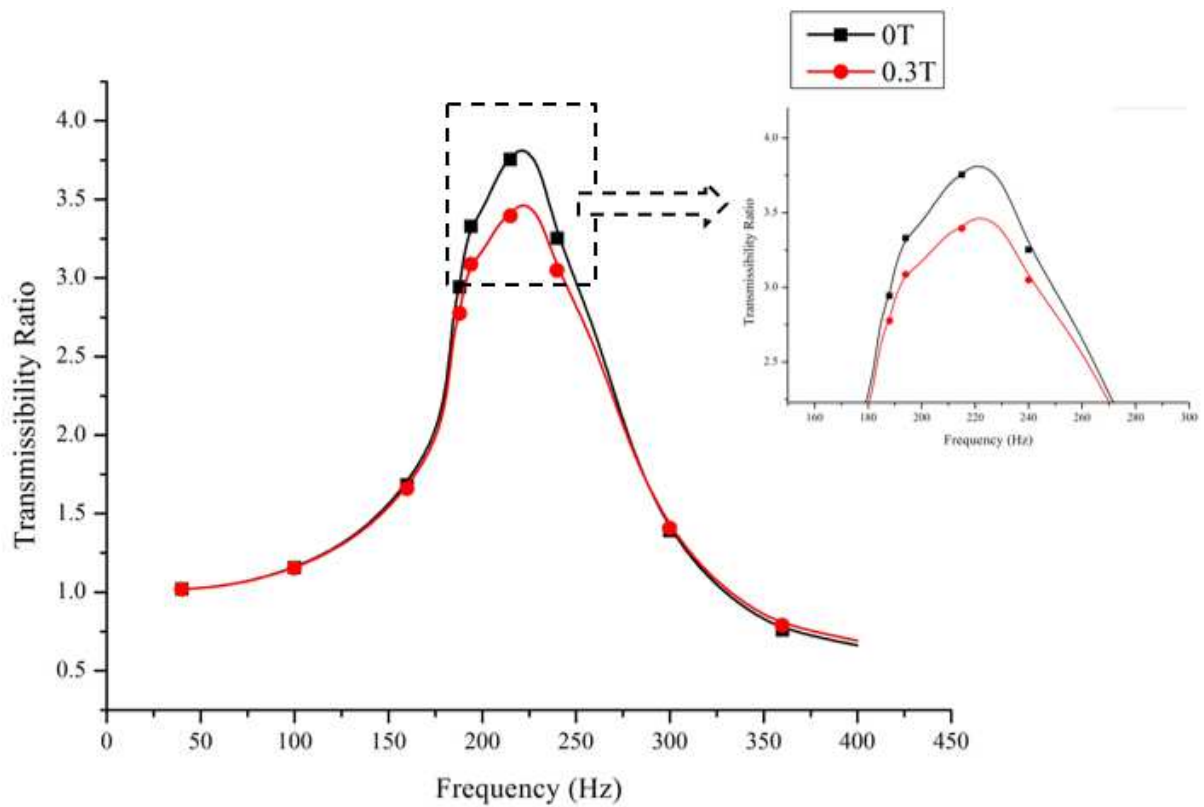
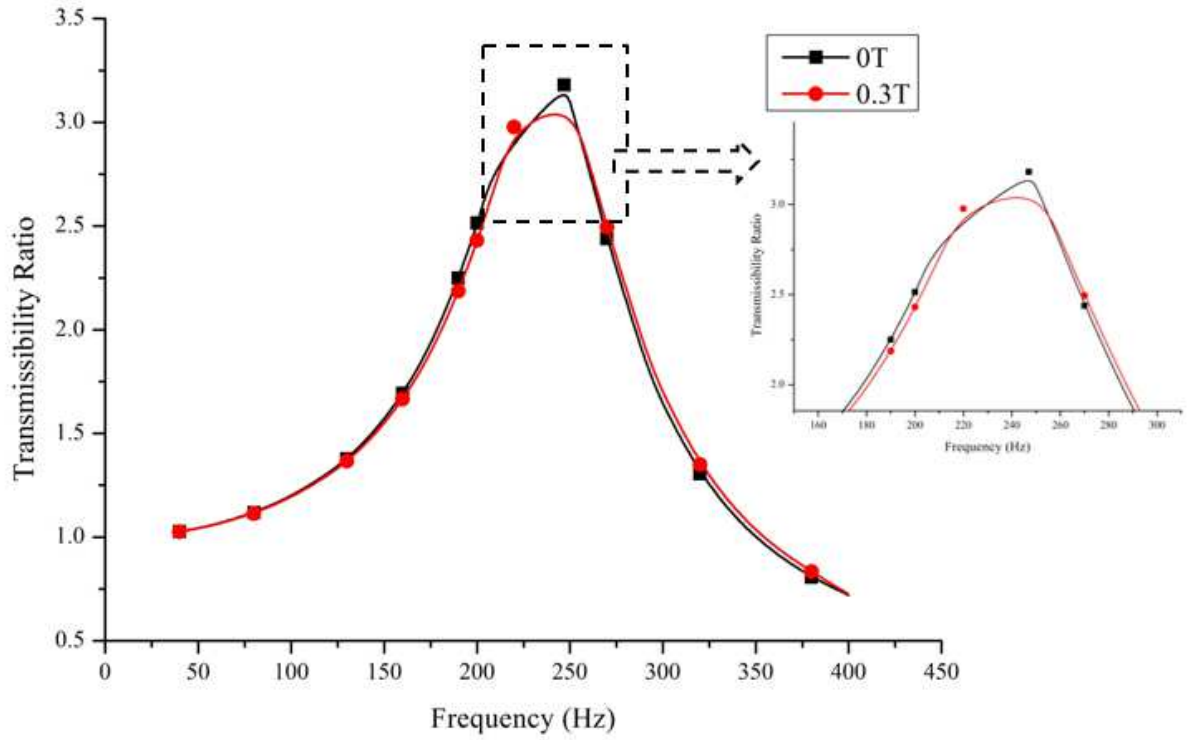
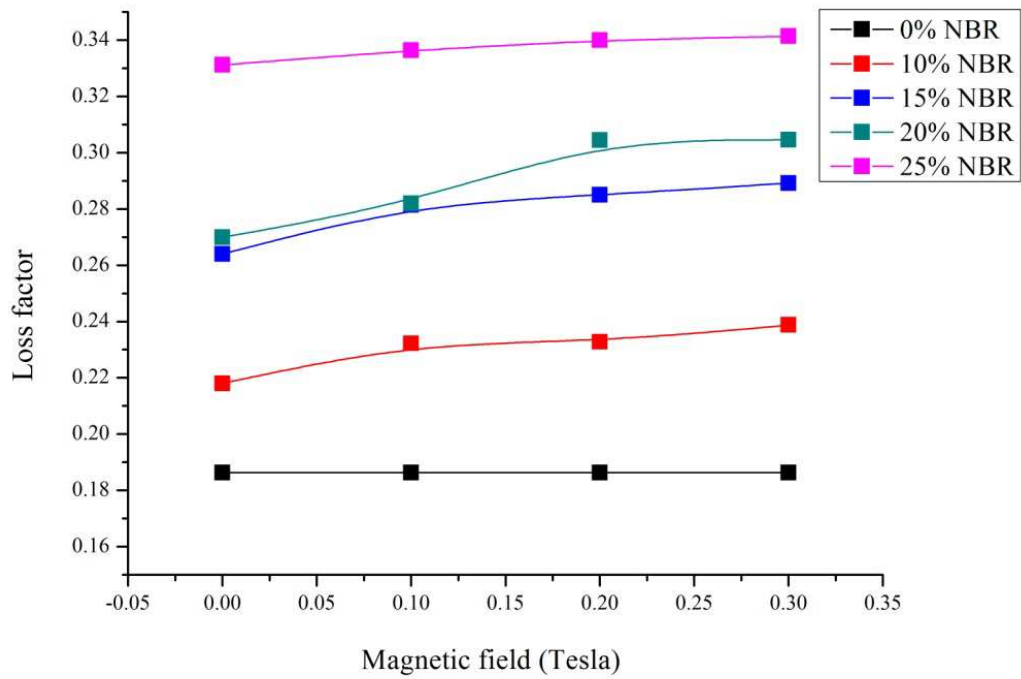


Figure 3.25. Behaviour of 20% NBR sample



**Figure 3.26.** Behaviour of 25% NBR sample



**Figure 3.27.** Structural Loss factor variation of NBR MRE samples



**Table 3.5** Comparison of structural loss factors of NBR samples

Field (Tesla)	CIP			% change			CIP			% change			CIP			% change		
	0%	10%	Abs	Rel	15%	Abs	Rel	20%	Abs	Rel	25%	Abs	Rel					
0	0.186	0.218	17.016	N/A	0.264	41.707	N/A	0.270	44.928	N/A	0.331	77.778	N/A					
0.1	0.186	0.232	24.638	6.514	0.281	51.047	6.591	0.282	51.369	4.444	0.336	80.569	1.570					
0.2	0.186	0.233	24.960	6.789	0.285	52.979	7.955	0.304	63.392	12.741	0.340	82.501	2.657					
0.3	0.186	0.239	28.180	9.541	0.289	55.233	9.545	0.305	63.500	12.815	0.341	83.253	3.080					

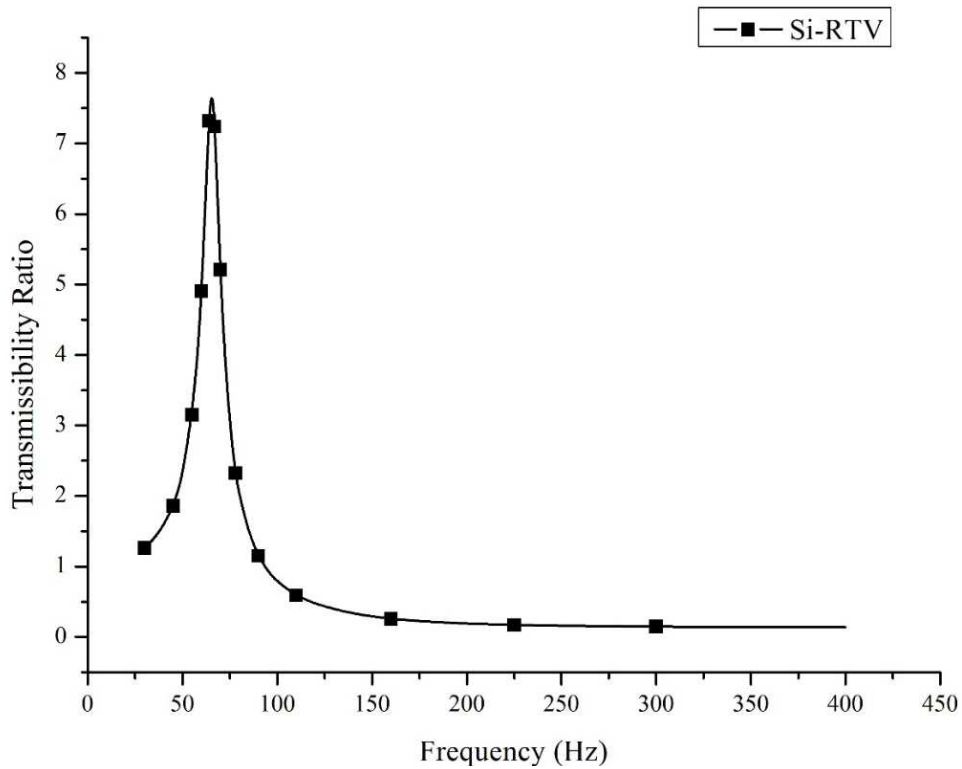


**Figure 3.28.** Behaviour of Pure Si-RTV sample

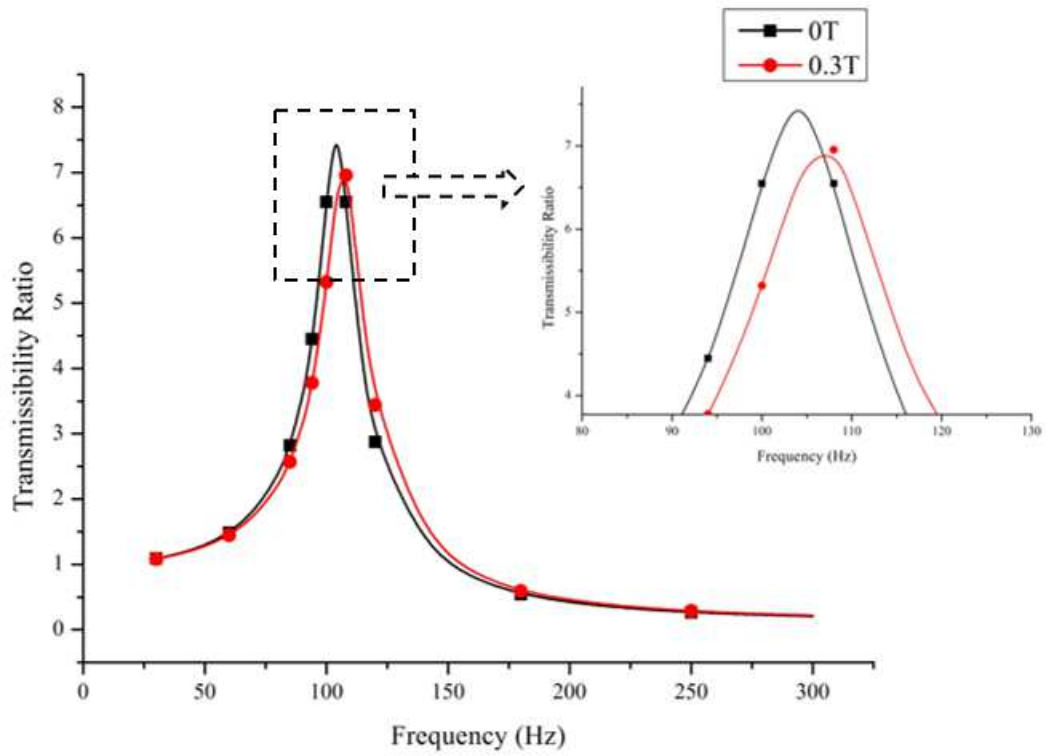


Figure 3.29. Behaviour of 10% Si-RTV MRE

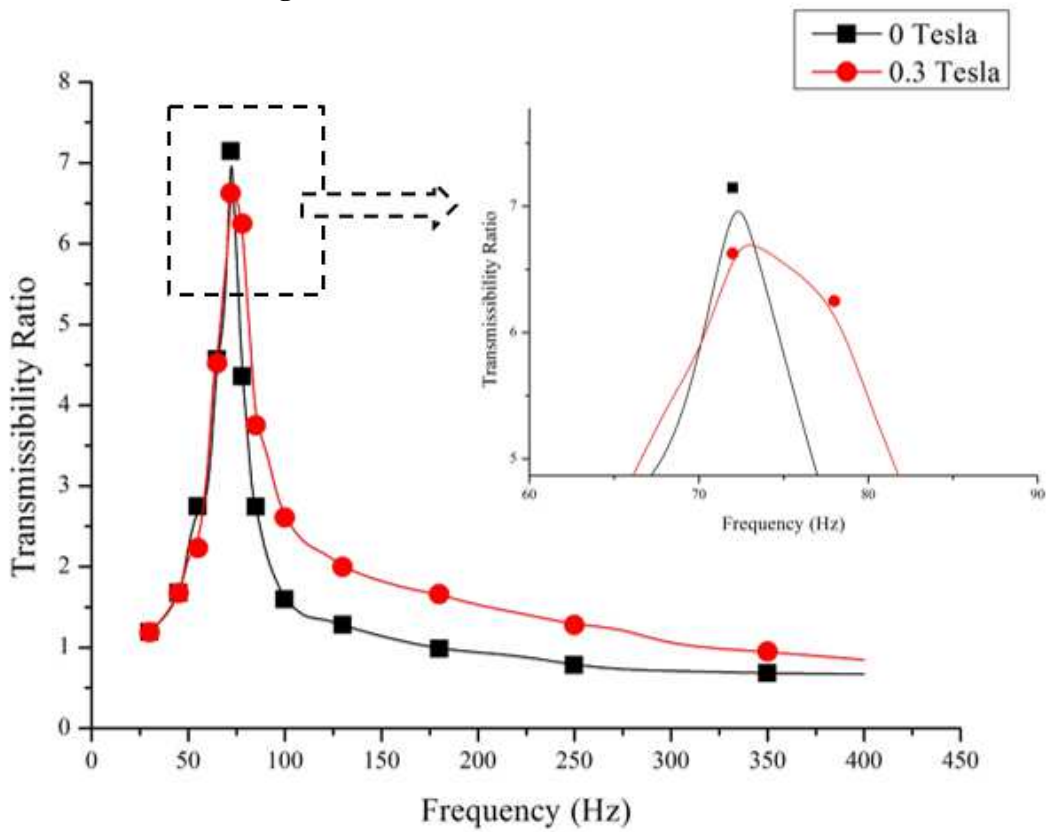
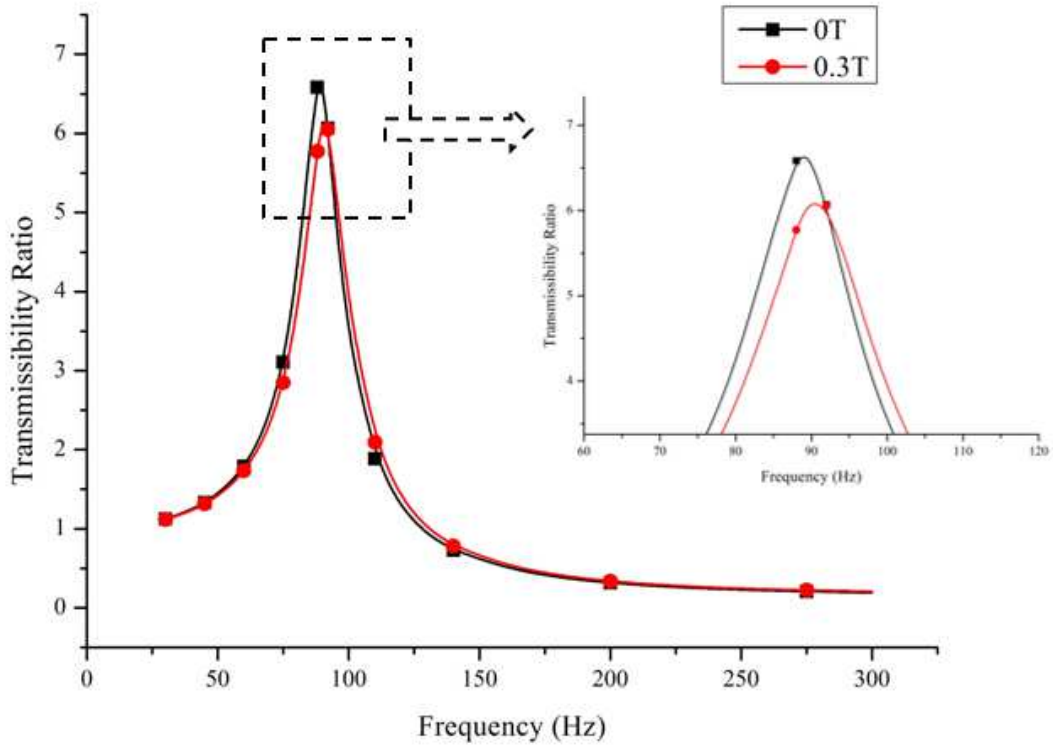
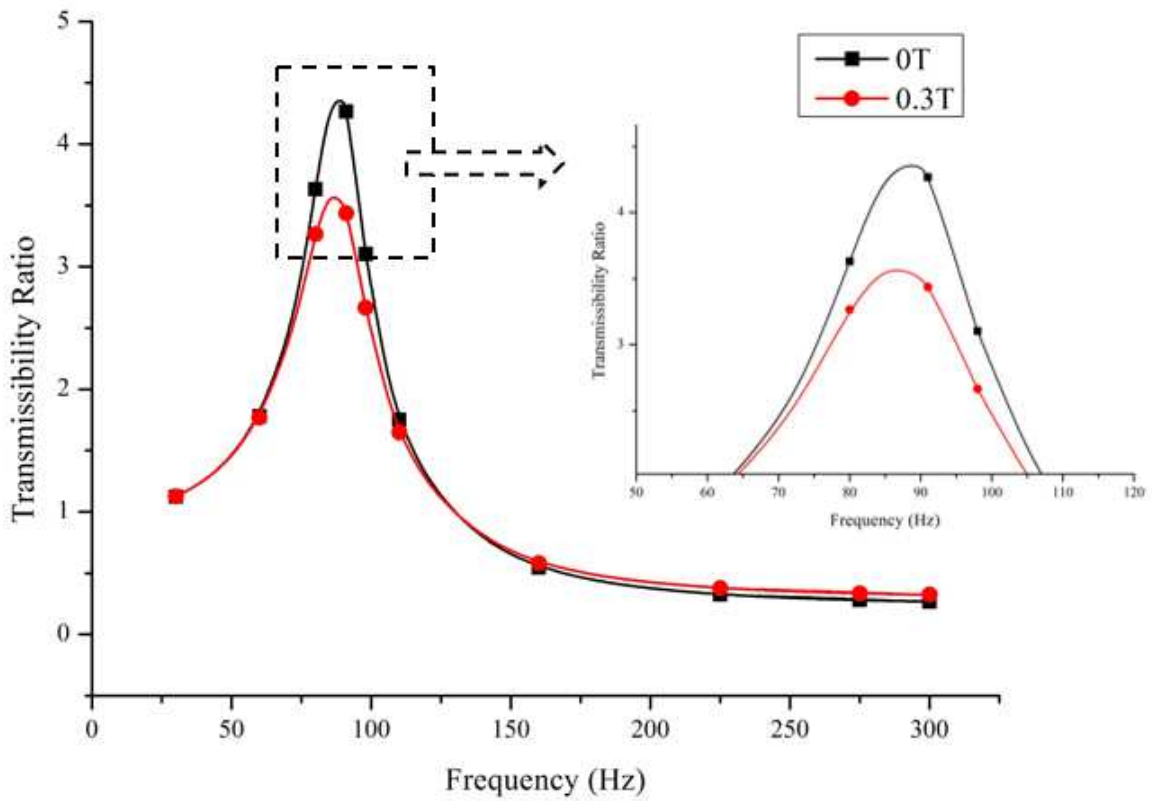


Figure 3.30. Behaviour of 15% Si-RTV MRE



**Figure 3.31.** Behaviour of 20% Si-RTV MRE



**Figure 3.32.** Behaviour of 25% Si-RTV MRE

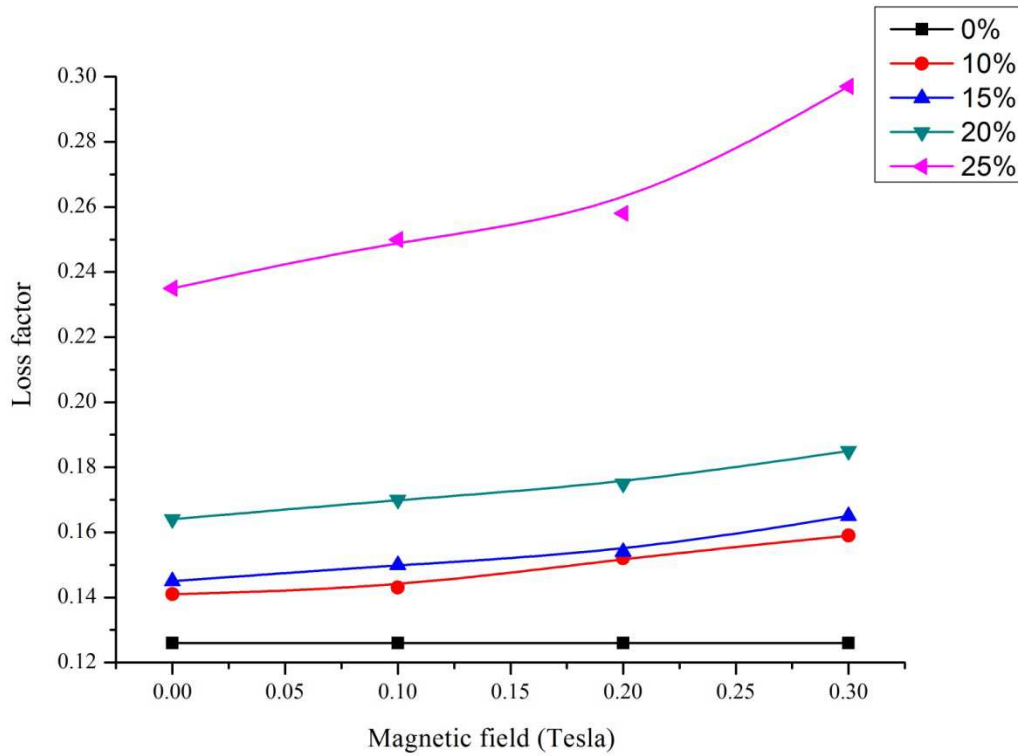


**Figure 3.33.** Structural Loss factor variation of Si-RTV MRE samples

**Table 3.6:** Comparison of structural loss factors of Si-RTV samples

Field (Tesla)	CIP		% change		CIP		% change		CIP		% change		
	0%	10%	Abs	Rel	15%	Abs	Rel	20%	Abs	Rel	25%	Abs	Rel
0	0.126	0.141	12.114	N/A	0.145	14.885	N/A	0.164	29.770	N/A	0.235	85.907	N/A
0.1	0.126	0.143	12.906	0.70615	0.150	18.369	3.032	0.170	34.204	3.417	0.250	97.862	6.431
0.2	0.126	0.152	20.506	7.486	0.154	21.774	5.996	0.175	38.717	6.894	0.258	104.592	10.051
0.3	0.126	0.159	25.736	12.147	0.165	30.879	13.921	0.185	46.081	12.569	0.297	134.917	26.363

The response of pure HTV silicone sample is shown in Figure 3.16. The peak transmissibility ratio was observed to be around 11 which is much better than natural rubber sample giving the indication that the matrix material plays an important role in controlling the loss factor of MREs.

The 10% sample shows very little improvement compared to pure sample (TR of 10.93) and the relative enhancement was also not pronounced (about 10.47 at 0.3 Tesla). The transmissibility decreased with the increase in magnetic field as well as with the CIP content. The force transmissibility registered for 25% sample was the least and unlike natural rubber sample, in Si-HTV samples, the samples with higher percentages namely 20% and 15% sample showed better relative improvement with magnetic field. The 25% sample depicted in Figure 3.20 showed the lowest value of TR at 0.3 Tesla (about 8.13).

Loss factor variation with magnetic field of Si-HTV samples is depicted in Figure 3.21. The Table 3.4 lists the values of the loss factor.

The relative change in loss factor showed an increasing trend with the increase in percentage of CIP. The overall relative change was lower than the natural rubber samples owing to high initial loss factor and the 25% sample showed better relative improvement than other samples. It was observed that by comparing the loss factor value of 25% sample at 0.3 Tesla (0.124) with pure sample (0.09), the total improvement was only about 38% which is lower than the natural rubber sample.

The Figure 3.22 shows the behaviour of Nitrile rubber sample without iron particles. The damping property of Nitrile rubber is quite high, which is evident from the very low peak TR which was observed to be about 5.45. This is much less than all the pure samples tested in the current research. The TR value of 10% sample reduced from about 4.69 at 0 Tesla to 4.3 at 0.3 Tesla showing about 8% reduction. Figure 3.24 shows that the 15% sample's TR at 0 tesla was about 3.91 and at 0.3 Tesla, it reduced to 3.6. The Figures 3.25 and 3.26 shows the TR plots of 20% and 25% sample respectively. It was observed that the relative change with the magnetic field was lesser than other matrix materials. The loss factor variation among the Nitrile samples is shown in Figure 3.27.

The loss factor values are much higher than all other matrix materials owing better damping properties of the Nitrile matrix material. The Table 3.5 lists the loss factor values of NBR samples.

The relative improvement of Nitrile samples was less than other matrix materials. Since the initial loss factor of Nitrile is quite high owing to inherent material damping, the magnetic field induced effects are not much. This also indicates that high initial loss factor may not be desirable for isolator applications owing to high damping factor.

Pure silicone RTV sample used for the study is a soft matrix, and the force transmissibility behaviour is shown in Figure 3.28. The peak TR is about 7.6, which is lower than natural rubber as well as Si-HTV pure samples. It reduced to 7.4 for 10% sample at 0 Tesla and to about 6.95 at 0.3 Tesla. The 15% sample showed further improvement damping property, which is evident from the reduction in TR shown in Figure 3.30. Further reduction in TR can be observed by 20% sample whose value is about 6.05 at 0.3 Tesla, which reduced from 6.57 at 0 Tesla. The TR of 25% MRE was about 4.34 at 0 Tesla, and it reduced to 3.51 showing about 19% reduction in TR with the magnetic field. The loss factor variation of Si-RTV samples is shown in Figure 3.33. The

loss factor values are listed in Table 3.6. The relative changes of these samples were higher than other samples and the 25% sample showed the best relative change of about 26% and an absolute increase of 135% when compared with pure Si-RTV sample.

The force transmissibility tests revealed interesting results of the performance of different samples. The samples with 15% and 20% concentrations showed better relative improvement in loss factor values. But the highest relative improvement was shown by 25% Si-RTV sample at 0.3 Tesla, which is softer than other samples used for the tests. This indicates that softer matrix makes the alignment of iron particles within the matrix easier which is reflected in higher relative improvement.



## CHAPTER 4

### PARAMETERS INFLUENCING THE MAGNETORHEOLOGICAL EFFECT

The performance enhancement of the MRE depends on percentage content of CIP, size of the particles, matrix material, the input strain and frequency and the dimensions of the test sample. This chapter deals with these aforementioned parameters and the analysis of each experiment is dealt with in detail. The experimental studies on the influence of the size of the particle ingredient and the strain amplitude are not extensively done.

#### 4.1 INFLUENCE OF PERCENTAGE CONTENT OF CIP

The force vibration tests and the sandwich beam tests have revealed that the loss factor and shear modulus of MRE samples increased with the percentage content as well as with the magnetic field. The effect of addition of CIP on the performance was analyzed by considering a unit cell of MRE comprising of only two CIP particles. Assuming a uniform CIP distribution, the distance between the adjacent particles will reduce if the percentage concentration is increased. As the separation distance reduces, the force of attraction increases between the adjacent particles. This increases the relative motion between the particles and the matrix at lower magnetic fields. The increase in force of attraction between adjacent particles can be verified by performing a simulation using FEMM software. Simulation was performed at two different separation distance between the particles, which is analogous to the condition of reduced distance between the fillers as the concentration is increased. The distribution of carbonyl iron powder in the matrix was assumed uniform, and the diameter of the powder is 5  $\mu\text{m}$ . The particle to particle magnetic force of attraction is responsible for the magnetic field induced property enhancement. The force between two magnetic dipoles is given by,

$$F = \frac{\mu q_1 q_2}{4\pi r^2} \quad (4.1)$$

Where,  $F$  is the force in Newtons,  $q_1$  and  $q_2$  are the intensities of poles 1 and 2 respectively in ampere-meter,  $\mu$  is the permeability of the medium in Henry/meter and  $r$  is the distance of separation of poles in meters. This force between dipoles is responsible for magnetic field induced enhancement in properties of MRE. This effect can be studied by computing the magnetic field energy stored in a particular area.



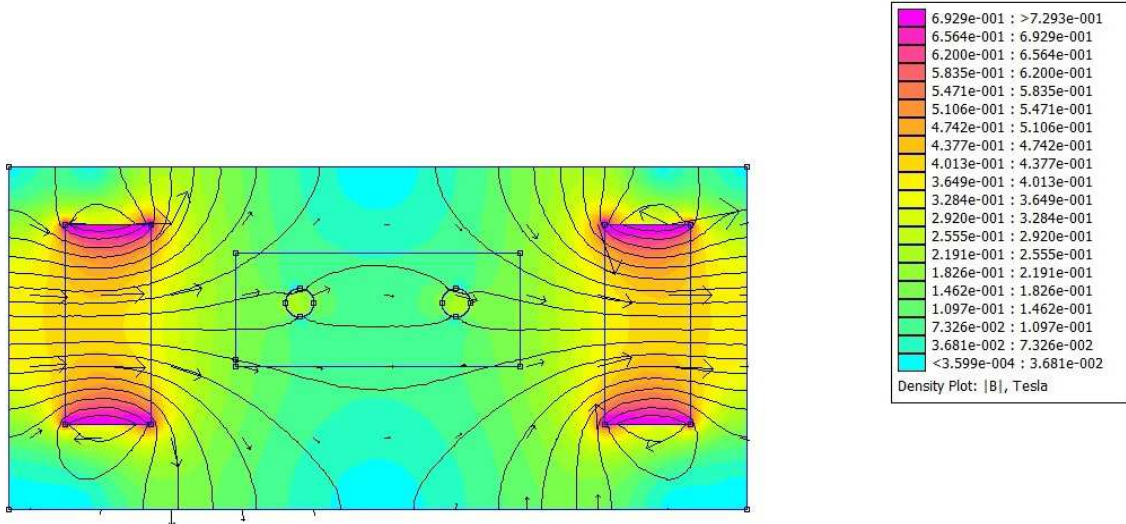


**Figure 4.1.** FEMM Simulation of force between CIP particles at 20µm

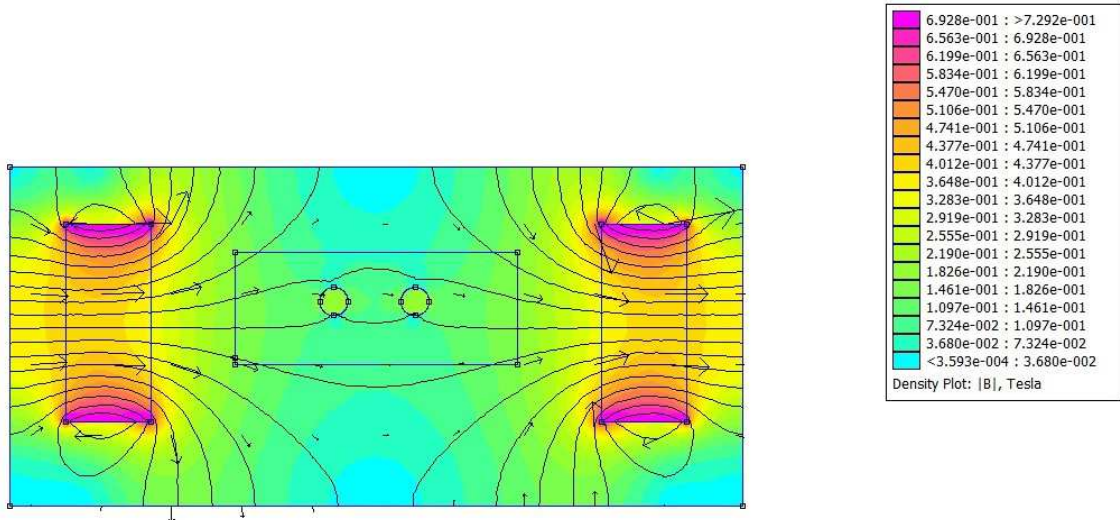


**Figure 4.2.** FEMM Simulation of force between CIP particles at 10µm

FEMM analysis package allows computing the magnetic field energy stored in the selected areas by making use of the following relation (M. David 2009 and J. Brauer, 2006).

$$W = \int \left( \int_0^B H(B') dB' \right) dV \quad (4.2)$$

Where  $H$  is the field intensity in Ampere turns/meter and  $B$  is the flux density in Tesla.  $V$  is the volume under consideration. The relation connects field intensity  $H$  and flux density  $B$  as,

$$H(B) = \frac{B}{\mu_0 \mu_r} = \frac{B}{\mu} \quad (4.3)$$

Where,  $\mu_0 = 4\pi \times 10^{-7}$  H/m is the permeability of free space,  $\mu_r$  is the relative permeability of the material. The equation (4.2) can be written as,

$$W = \int \frac{B^2}{2\mu} dV \quad (4.4)$$

From equation (4.4) it can be deduced that energy stored in a field is a function of the surface area of the CIP. Total surface area increases as the percentage concentration of iron is increased. Increased surface area increases the stored energy resulting in enhanced MR effect. The simulation results showed an increase in stored energy with the reduction in distance between the adjacent particles from 20 $\mu\text{m}$  to 10 $\mu\text{m}$  ( $2.75 \times 10^{-6}$  J at 20  $\mu\text{m}$  to  $3.86 \times 10^{-6}$  J at 10  $\mu\text{m}$ ).

## 4.2 INFLUENCE OF PARTICLE SIZE

The performance of the magnetorheological elastomers is dependent on several factors. The matrix material, the size of the carbonyl iron powder and the dimension of the MRE sample influence the characteristics of the test sample. The matrix material dependency was dealt in detail in the previous section. In this section, the influence of particle ingredient size on the damping capabilities are studied. Si -RTV based MREs were prepared using carbonyl iron powders of 2 different diameters with equal weight percentage and compared with the performance of pure silicone sample. The preparation methods are briefed in earlier chapters. The microstructure was observed using Confocal microscopy and the figures are shown below in figure 4.3.

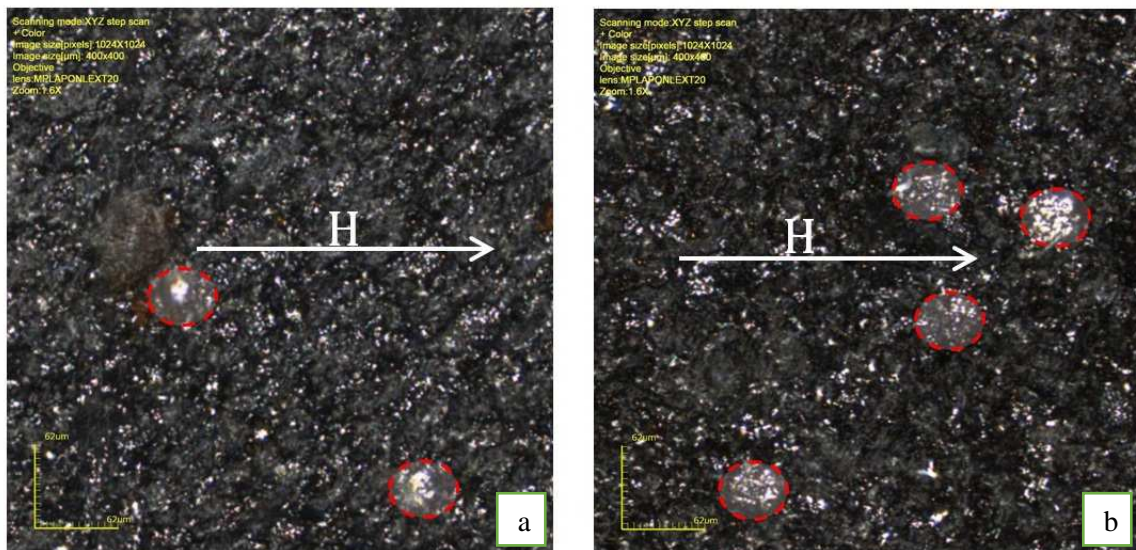


**Figure 4.3** Microstructure of (a) 6.25  $\mu\text{m}$  MRE and (b) 3.15  $\mu\text{m}$  MRE.

To compare the behavior of all the samples, the transmissibility ratio acquired from force transducers was plotted against input frequency. The plots of the two MRE samples at different magnetic fields were compared the behavior of Pure-Si sample,

which is shown in Figures 4.4 and 4.5 below respectively. The enhancement in loss factor is investigated to assess the effect of particle ingredient size on the field-induced behaviour of MRE. The method adapted for calculating the loss factor values from the transmissibility plots has been discussed in detail in chapter 3.

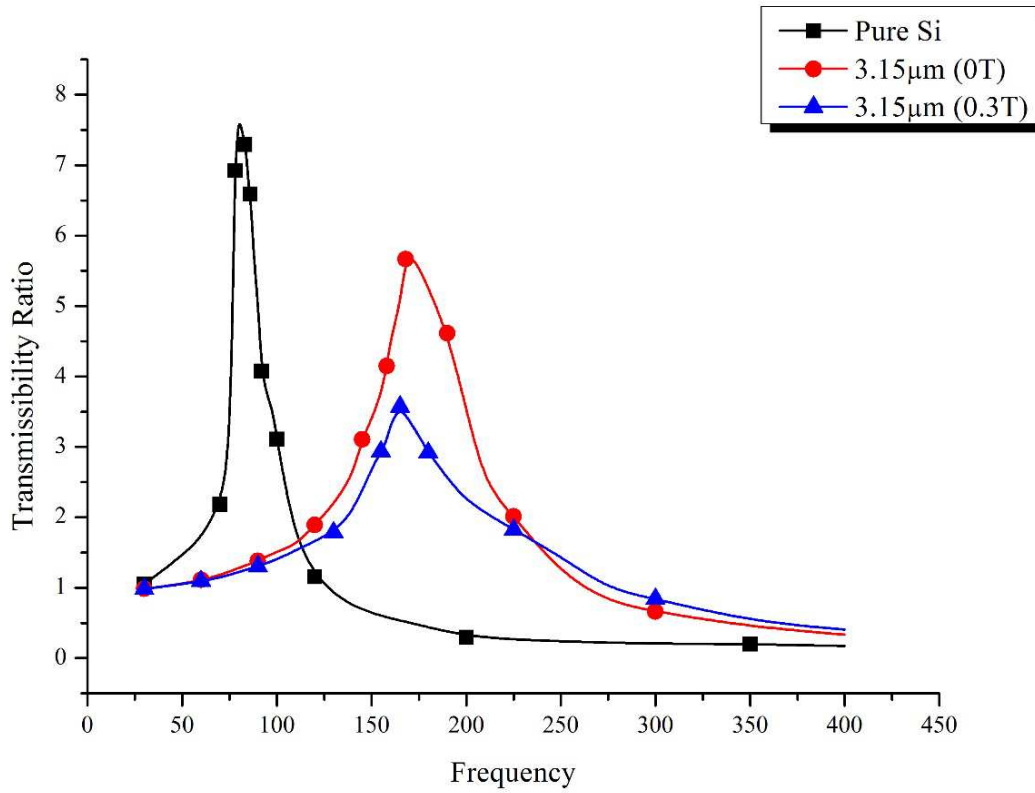


**Figure 4.4.** Transmissibility Ratio V/s Input frequency comparison of 3.15 µm MRE

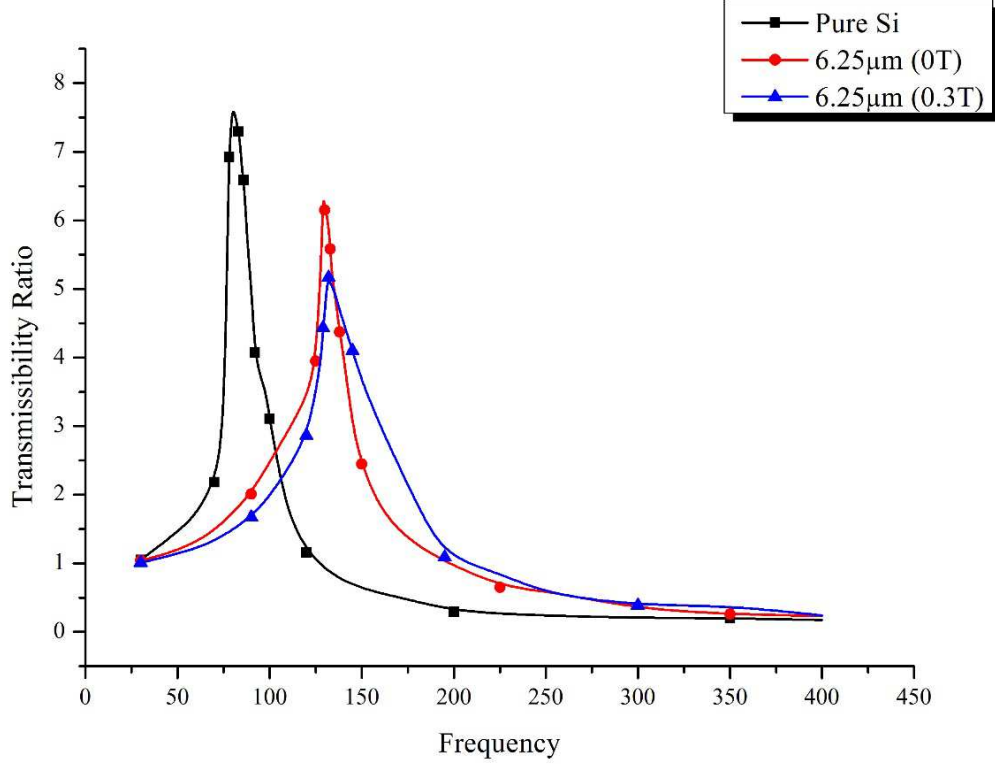


**Figure 4.5.** Transmissibility Ratio V/s Input frequency comparison 6.25  $\mu\text{m}$  MRE

Plots reveal that addition of iron powders has improved the damping characteristics of the Si which is evident from the reduction in the transmissibility ratio in the resonance region of the curves. The performance of MRE with different particle size is compared on the basis of MR effect. The MR effect is defined as the ratio change in loss factor to the loss factor of Pure-Si.

$$\Delta\eta = (\eta_{0.3T}^{3.15} - \eta^{Si}) / \eta^{Si} \quad (4.5)$$

Where  $\Delta\eta$  is the change in loss factor,  $\eta_{0.3T}^{3.15}$  is the loss factor of 3.15  $\mu\text{m}$  MRE at 0.3T and  $\eta^{Si}$  is the loss factor of Pure- Si sample. The loss factor values and the respective percentage enhancements are listed in Table 4.1 below.

**Table 4.1:** Loss factor values calculated from the transmissibility plots.

Sample	Loss factor		% increase	
	0 Tesla	0.3 Tesla	Absolute	Relative
Pure Silicone	0.129	0.129	NA	
3.15 $\mu\text{m}$ MRE	0.175	0.279	116.27	59.42
6.25 $\mu\text{m}$ MRE	0.155	0.1934	49.92	24.77

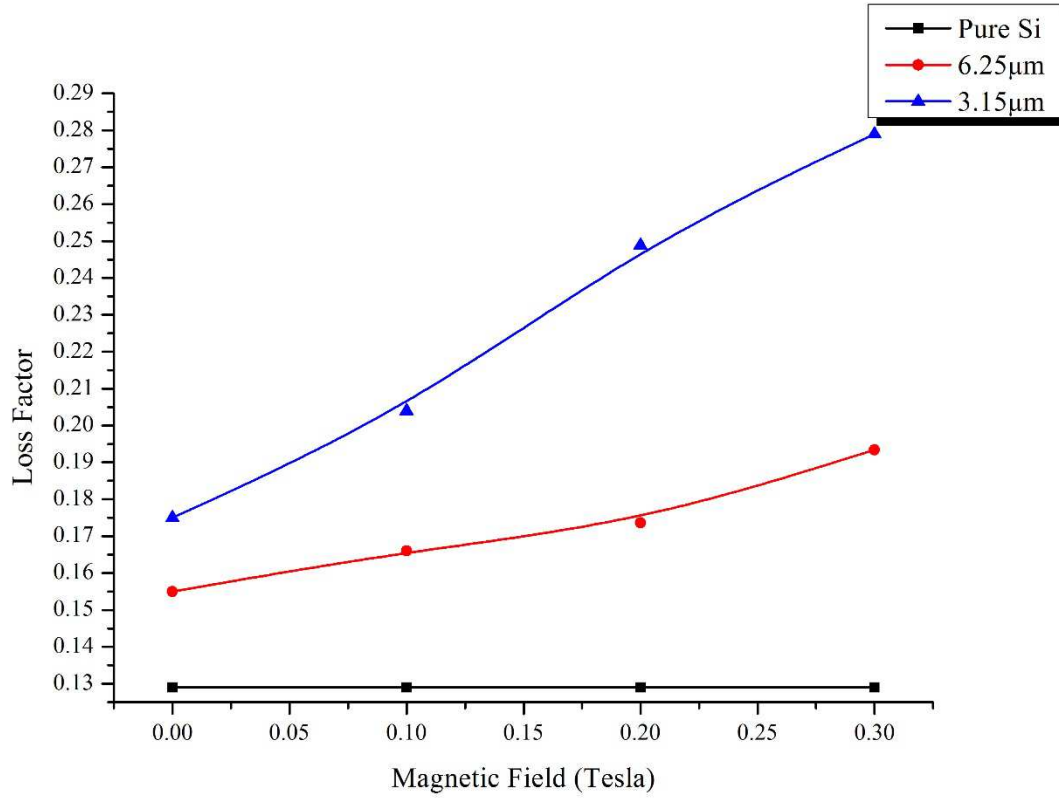


**Figure 4.6.** Loss factor variation with magnetic field

The 3.15 µm MRE showed an improvement of about 115% when compared to Pure-Si sample and 6.25 µm MRE showed about 50% enhancements in loss factor. The loss factor variation of the samples with magnetic field is shown Figure 4.6. The 3.15 µm MRE showed better MR effect than other samples in the current set of experiments. The property enhancement of MRE with the magnetic field is because of the alignment of CIP particles along the flux lines. During the process, there will be interfacial-friction between the iron particles and the elastomer matrix resulting in an improvement in damping property. From the microstructure images, the 3.15 µm MRE had more agglomeration which results in an increased effective diameter of the particles. Increase in effective diameter increases the interfacial friction resulting in higher damping ratio. Under the influence of magnetic field, there is a dipole moment formation between adjacent particles given by the relation below ( Gong 2005).

$$m_a = 4\pi\mu_m\mu_0R\beta H \quad (4.6)$$

Where,  $\mu_0$  is the vacuum permeability,  $\mu_p$  is the relative permeability of the particles,  $R$  is the radius of the particles and

$$\beta = (\mu_p - \mu_m) / \mu_p + 2\mu_m \quad (4.7)$$

From the relation (4.6) with increase in the effective radius due to agglomeration, the dipole moment is increased which in turn improves the damping properties. It is demonstrated by a simple diagram (figure 4.7).

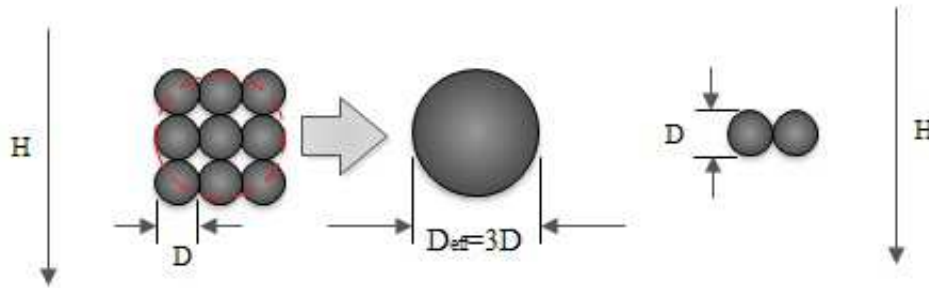


**Figure 4.7.** Increase in effective diameter due to agglomeration

Consider a simple assumed agglomeration of particles and the direction of the field and the directions of the magnetic field are represented by the arrow mark. In the first case, the effective diameter is  $3D$ , which is three times that of the second case. This causes higher dipole moment resulting in better performance. From the microstructure images (Figure 4.3), in particle size of  $3.15 \mu\text{m}$  MRE, the agglomeration in the direction of magnetic field is more than that of  $6.25 \mu\text{m}$  MRE which is evident in the transmissibility ratio plots. In the present research, the smaller diameter particles have shown better performance. Even though it can be concluded that the particle ingredient size does affect the performance of the MRE, the current experiments are not sufficient to conclude that smaller size particles produce more agglomeration resulting in better performance. More studies are necessary to come to concrete conclusions regarding the extent of influence of the size of particles on the MRE performance by employing different-sized particles.

### 4.3 INFLUENCE OF DIMENSIONS OF THE MRE

The geometry of the MRE resilient element is an important factor which needs to be addressed while designing the isolator. The variation in geometry may affect the magnetic-field induction inside MRE which in turn influences the smart characteristics. This section explores the influence of the dimensions of the MRE on the damping performance. The photographs of the tests specimens are depicted in figure 4.8. The shear area is maintained constant, and the thickness of the MRE was varied. The dynamic tests were performed in a force vibration test set up at varying magnetic fields. Since the thickness of the samples is different, the way each sample magnetizes and demagnetizes is different. Carbonyl iron powders have excellent magnetic properties, and it has a very

low or zero remnant magnetic field. But in order to ensure there is no hysteresis in the samples, sufficient time is provided for relaxation between each set of experiment. Before beginning the next set of experiments, it was made sure that the samples have no hysteresis by measuring the magnetic field with gauss meter across the thickness of the sample.

The force vibration tests were conducted for all samples as explained earlier by varying the input frequency from 30 Hz to 400 Hz. The transmissibility corresponding to the tested samples is shown below. The transmissibility ratios versus frequency graphs were plotted for all the samples, which are shown in figures below. Figure 4.9 to 4.11 shows the transmissibility ratio plots pure silicone, 15% MRE and 25% MRE respectively. From the TR plots, dependency of TR on thickness is visualized from the shift in peak amplitude. The thickness dependent variation on TR is attributed to the dependency of stiffness on sample thickness.

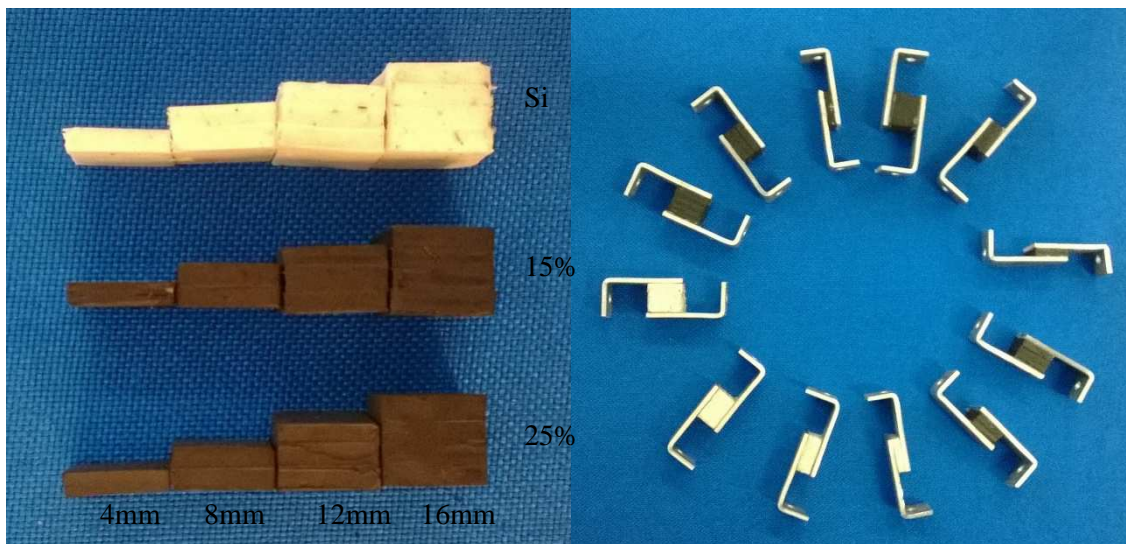


**Figure 4.8**MRE Test samples

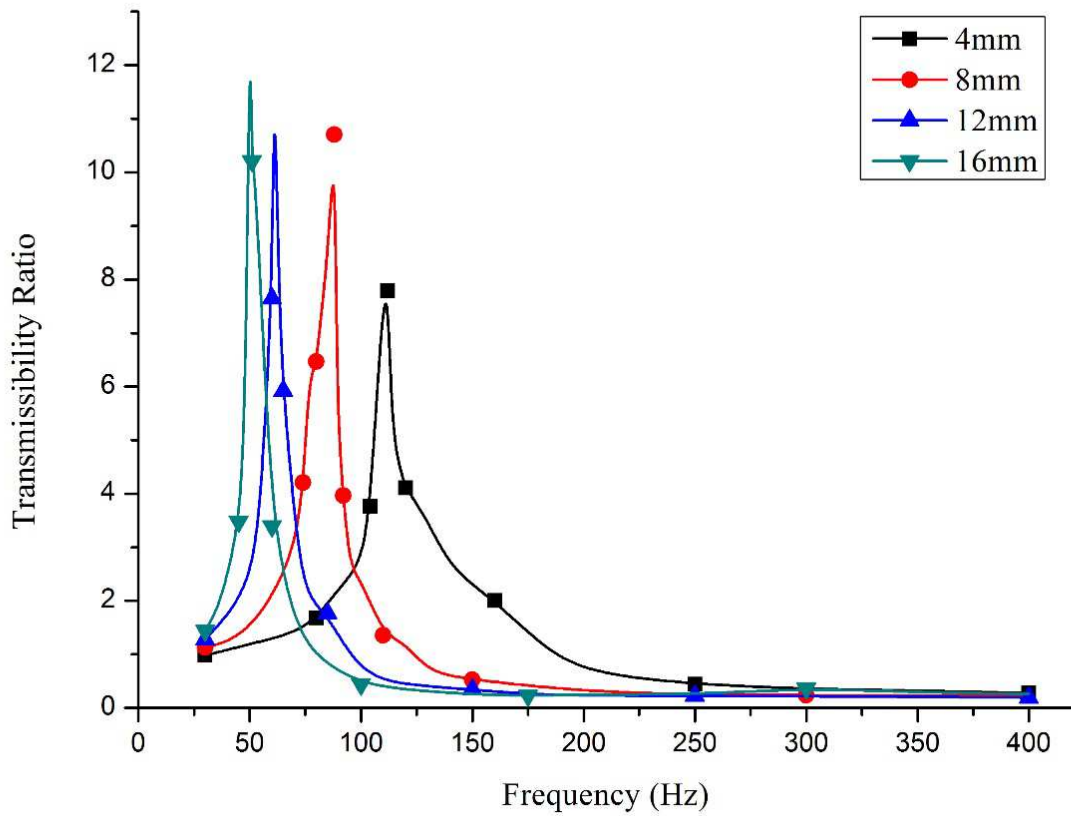


**Figure 4.9.** Transmissibility plot of Pure Silicone

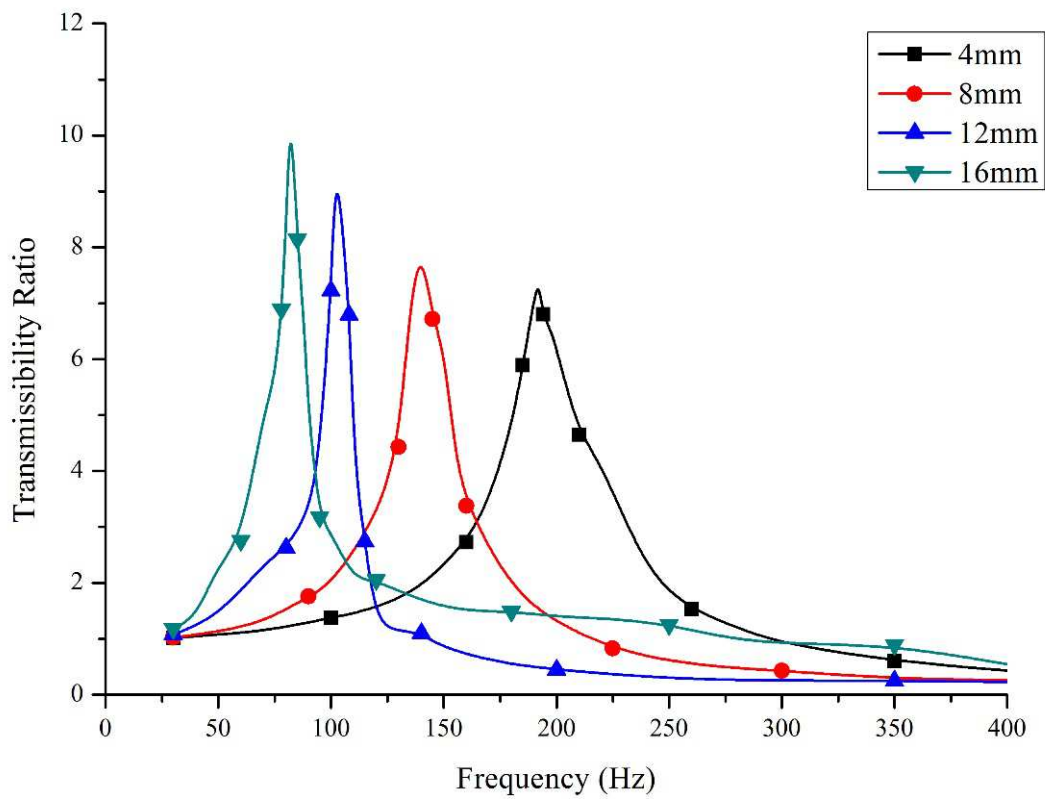


**Figure 4.10.** Transmissibility plot of 15% MRE



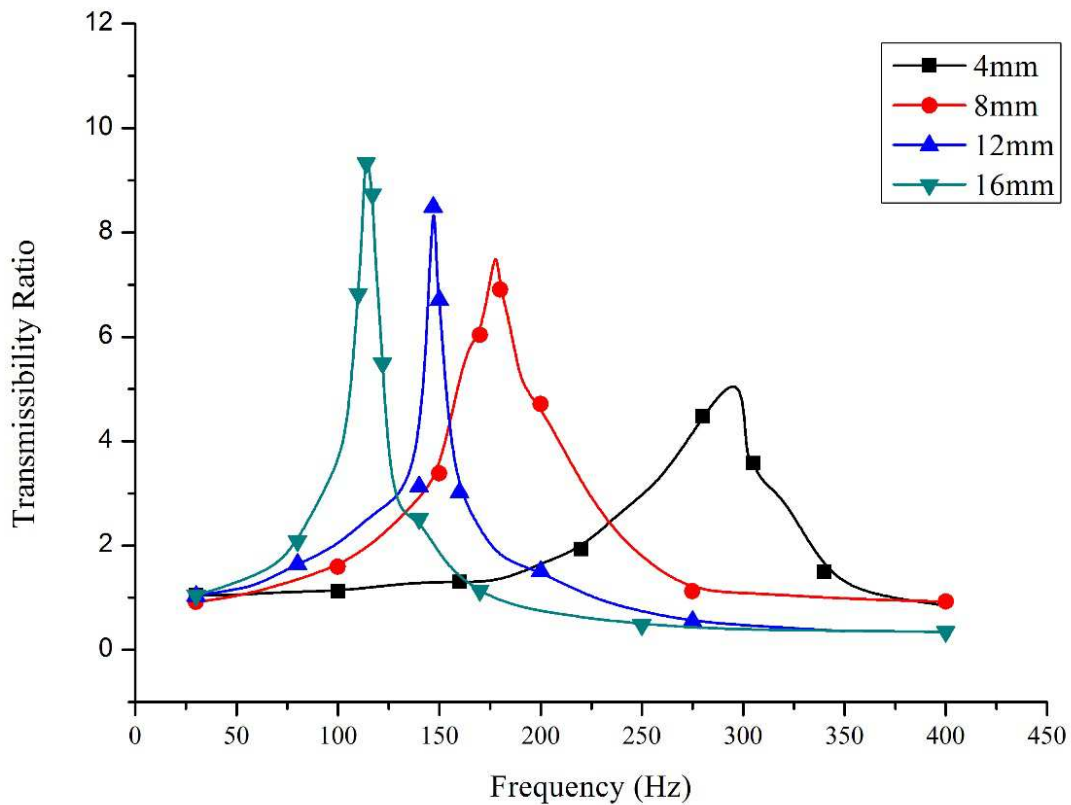


**Figure 4.11.** Transmissibility plot 25% MRE

The loss factors estimated from the TR are plotted in Figure 4.12 and 4.13 respectively. These figures show the influence of thickness on the loss factor variation. As the thickness is reduced, the stiffness is increased, which is evident from increase in natural frequency as well as a reduction in transmissibility peak. The loss factor of 16 mm sample was found to be 0.07604, and it increased to 0.12935 for 4 mm thick sample, an improvement of 70%. The MRE samples showed similar trends of loss factor reduction with the decrease in thickness. The loss factor of 15% MRE changed from 0.0942 for 16mm sample to 0.13698 for 4 mm sample showing 45% increase. For the 25% MRE, the loss factor changed from 0.1073 for 16 mm sample to 0.1853, showing 72% increase.

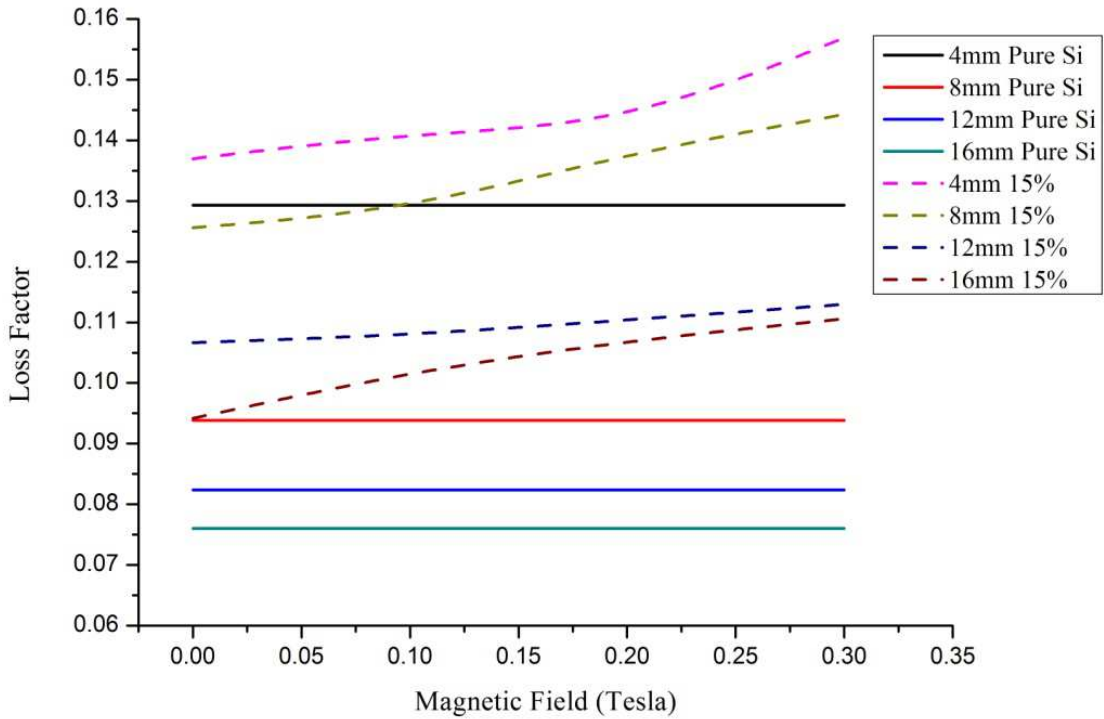


**Figure 4.12.** Loss factor variation of 15% MRE

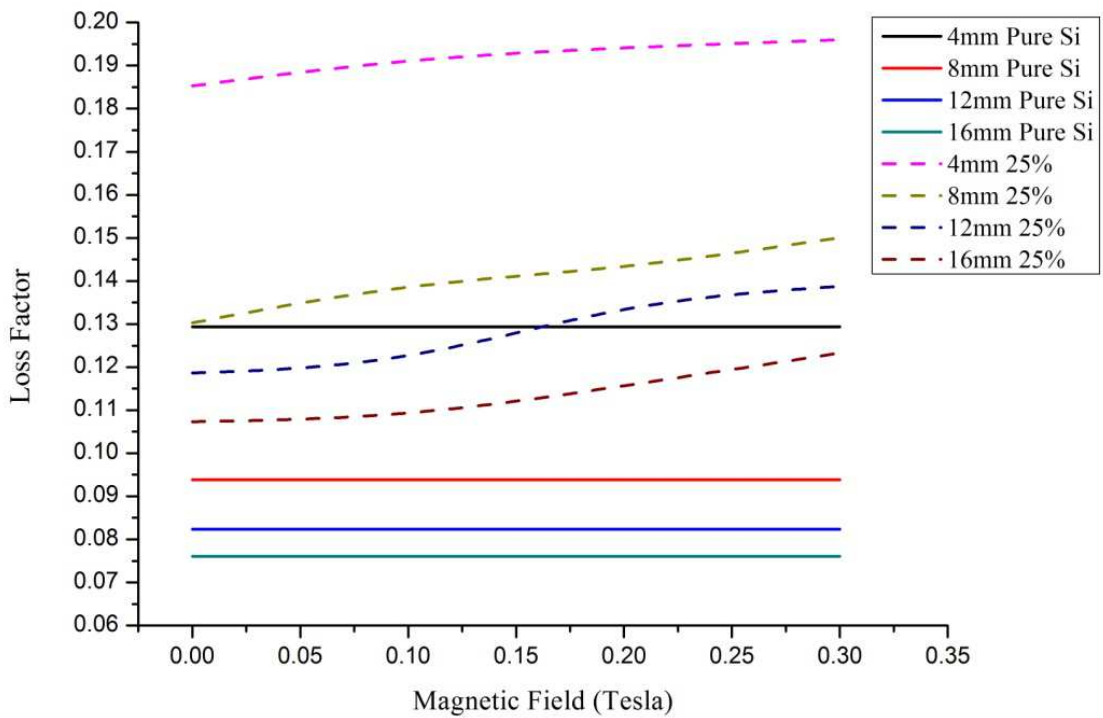


**Figure 4.13.** Loss factor variation of 25% MRE

The loss factor is higher for the thinner samples and it reduced with the increase in sample thickness. Similar behaviour was observed under the influence of magnetic field. The analysis of the loss factor shows that the thickness influences the property and lesser thickness samples showed better damping properties which are evident from the plots.

The thickness effect on the field-induced loss factor variation in MRE is attributed to the magnetic-field induction inside the matrix. The intensity of magnetic field varies with the distance between the magnetic dipoles. With thin MRE samples, the magnetic dipole distance can be maintained closer, which results in homogenous field distribution. As the thickness is increased, the distance between the dipoles increases due to which the field in the center of thicker MRE will be less than that of thinner samples. In other words, the magnetic-field penetration is easier in thinner samples. It is analyzed using FEMM simulation of magnetic-field distribution across the thickness of the MRE samples for different thickness. The graph (Figure 4.14) shows the variation of magnetic field across MRE samples of different thickness. It can be observed that thinner samples experienced higher magnetic-field intensity than thicker samples. The field variation across thicker samples namely, 12 mm and 16 mm were more non-linear and thinner samples showed better linearity. This proves that thinner samples will enable better magnetic-field distribution resulting in improved loss factor values. Overall it can be concluded that it is more practical to employ MREs with lesser thickness since it is stiffer and provides better damping properties.

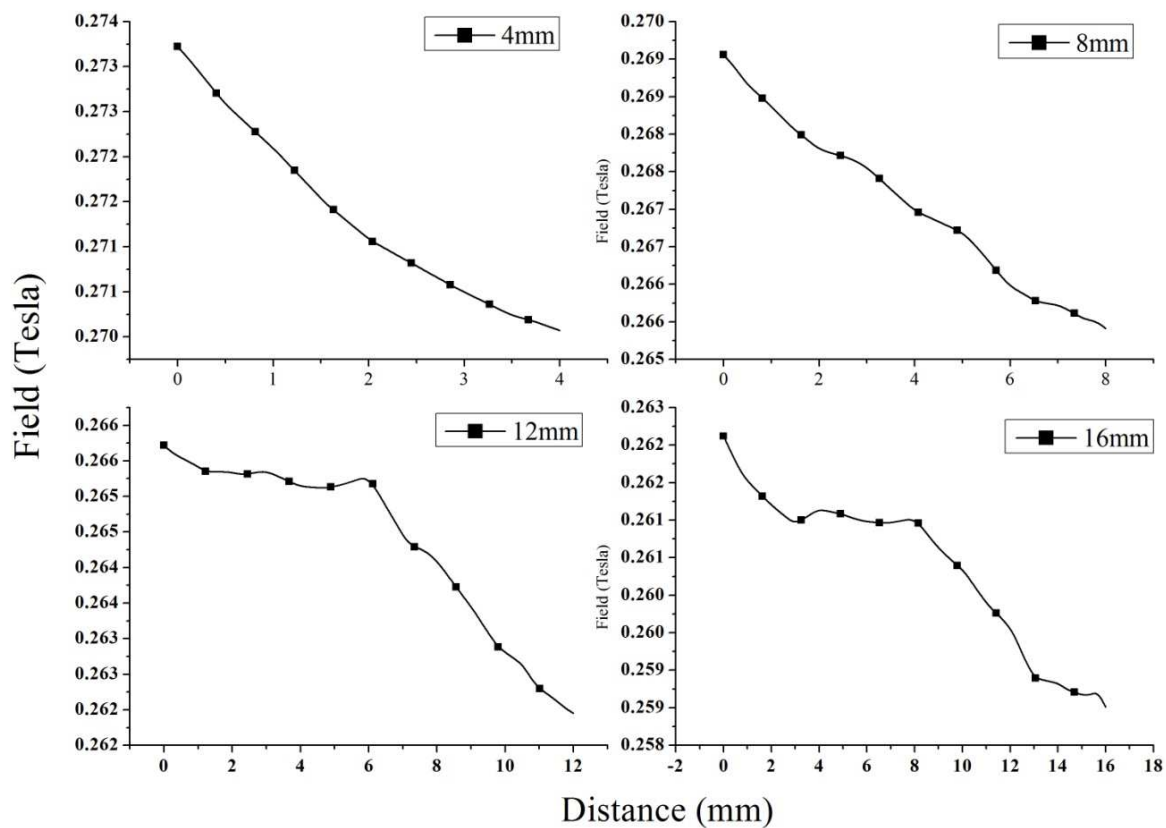


**Figure 4.14.** Magnetic field variation across the thickness

#### **4.4 INVESTIGATION OF HYBRID MRE**

Conventional MREs are usually made of HTV matrices, which are quite complicated to prepare. Silicone RTV is a soft matrix which is not suited for high-strength applications. To achieve better property and use the advantage of a hard matrix, a hybrid MRE by mixing silicone RTV and Polyurethane harder matrix is explored. Mixing two polymers utilizes the properties of both the materials. The behaviour of this novel type of MRE was studied by performing force transmissibility tests. The performance was investigated by subjecting MRE samples to frequencies below 45 Hz and at two different strain amplitudes.

##### **4.4.1 MATERIAL PREPARATION**

Polyurethane (PU) and RTV silicone were mixed in proper proportions, and its damping properties were experimentally analyzed. The RTV silicone is a very soft material with low shore A hardness. To improve its mechanical properties, Polyurethane 7545 A/C was mixed and a different type of composite was prepared. Polyurethane A/C is a two-part system consisting of resin and a curing agent to be mixed with 1:0.87 by weight. By mixing these two polymers, four different types of MRE sample were prepared i.e. Pure Si, 80% Silicone: 20% PU, 70% Silicone: 30% PU and 60% Silicone: 40% PU. In total eight, samples were prepared for experimental analysis. Further increase of PU was not possible because the working time of PU was 6 minutes and that of the silicone was 45 minutes. The difference in curing time made it difficult to mix when the percentage of PU was higher. MREs were prepared by adding 5 grams of carbonyl iron powder to each percentage of composite. The sample size was 20 mm x 20 mm x 6 mm in dimensions. The test samples were prepared by sticking the samples to Aluminum strips of width 20 mm and thickness 3mm bent in the form of an "L." Cyanoacrylate quick glue was used as adhesive.

The samples were analyzed using confocal microscope at CMTI, Bangalore to understand the distribution of CIP. The images are shown below from Figure 4.15 to 4.18. The silicone MRE shows uniform distribution of CIP throughout the matrix. As the percentage of PU was increased, the agglomeration was noticed even though the distribution of CIP was uniform. The pure samples of higher percentage show the formation of air bubbles which are difficult to avoid as the mixing process cannot be accomplished within the working time of polyurethane.

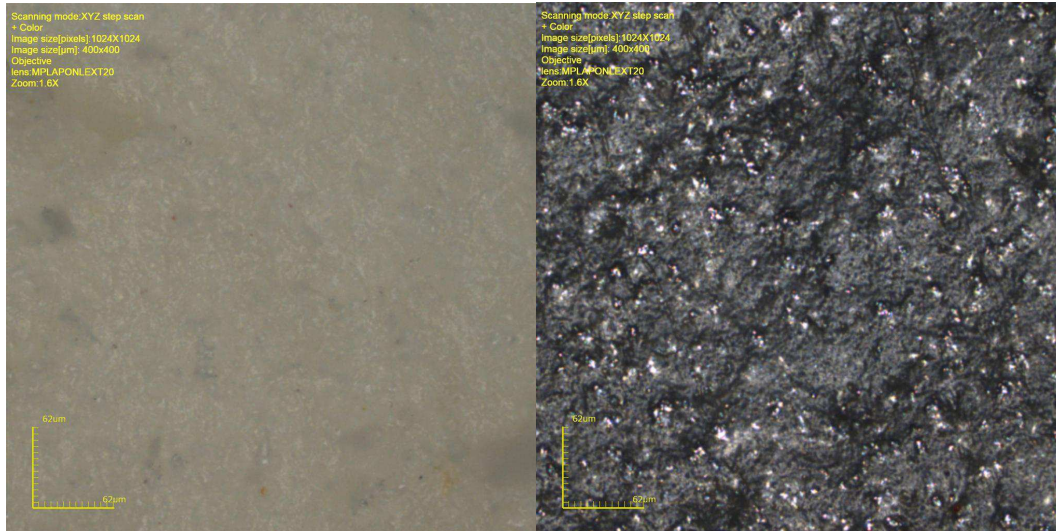


**Figure 4.15.** Pure silicone and Silicone MRE

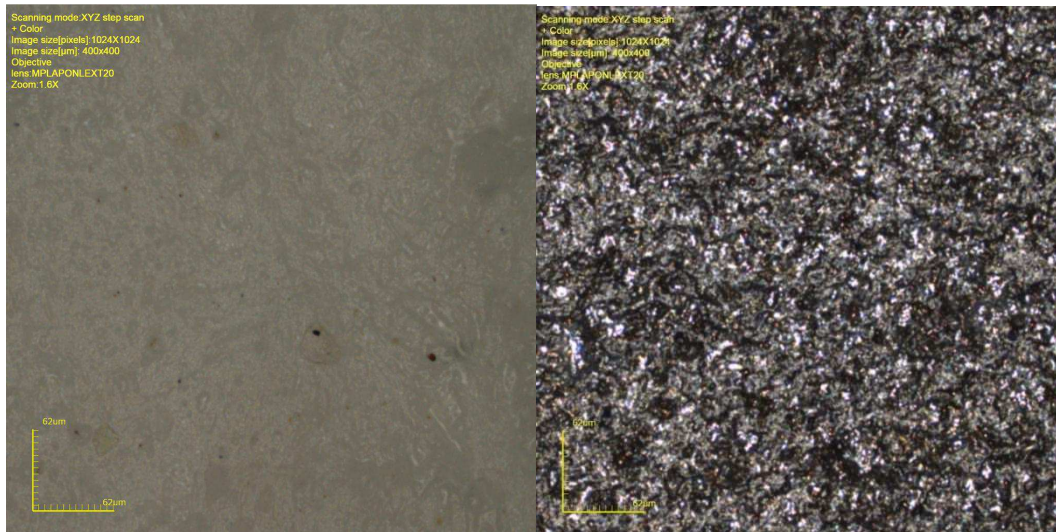


**Figure 4.16.** Pure 80-20 and 80-20+Fe MRE

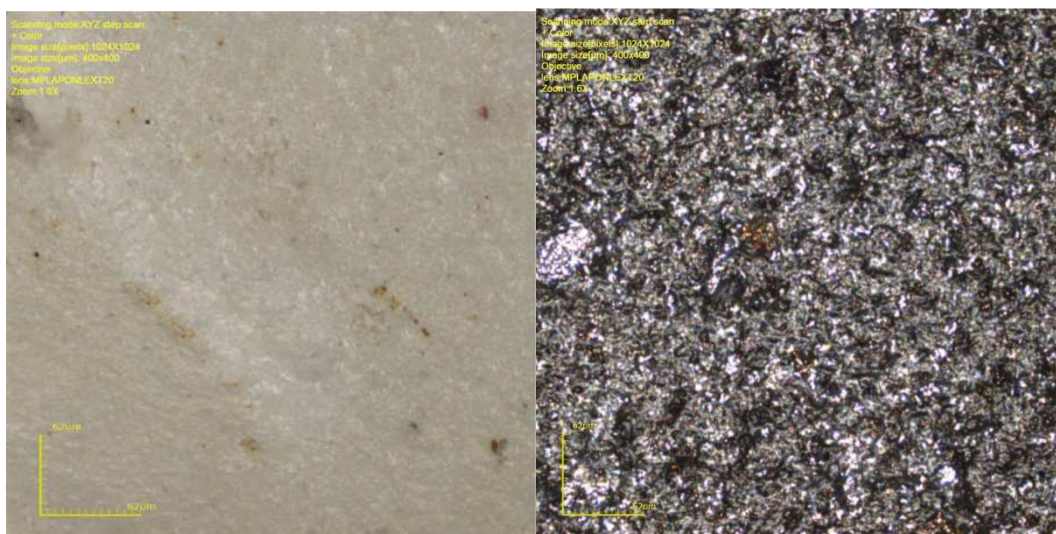


**Figure 4.17.** Pure 70-30 and 70-30+Fe MRE

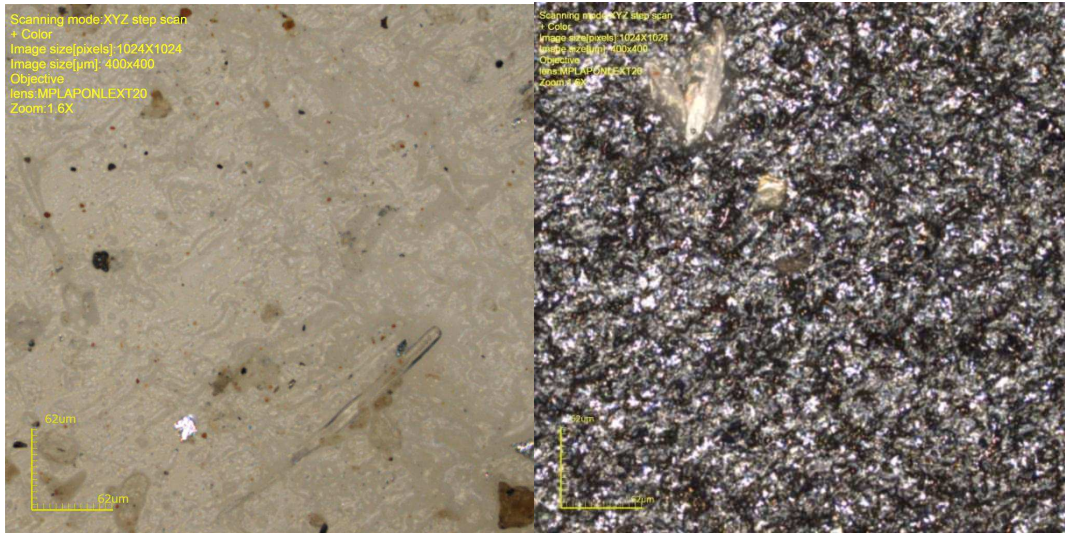


**Figure 4.18.** Pure 60-40 and 60-40+Fe MRE

#### 4.4.2 EXPERIMENTAL ANALYSIS

Forced vibration tests were conducted for all the samples as by varying the frequency from 40 Hz to 400 Hz by varying the magnetic field from 0 Tesla to 0.3 Tesla. The Transmissibility Ratio plots obtained from the force vibration tests are listed in Figure 4.19 to 4.22.

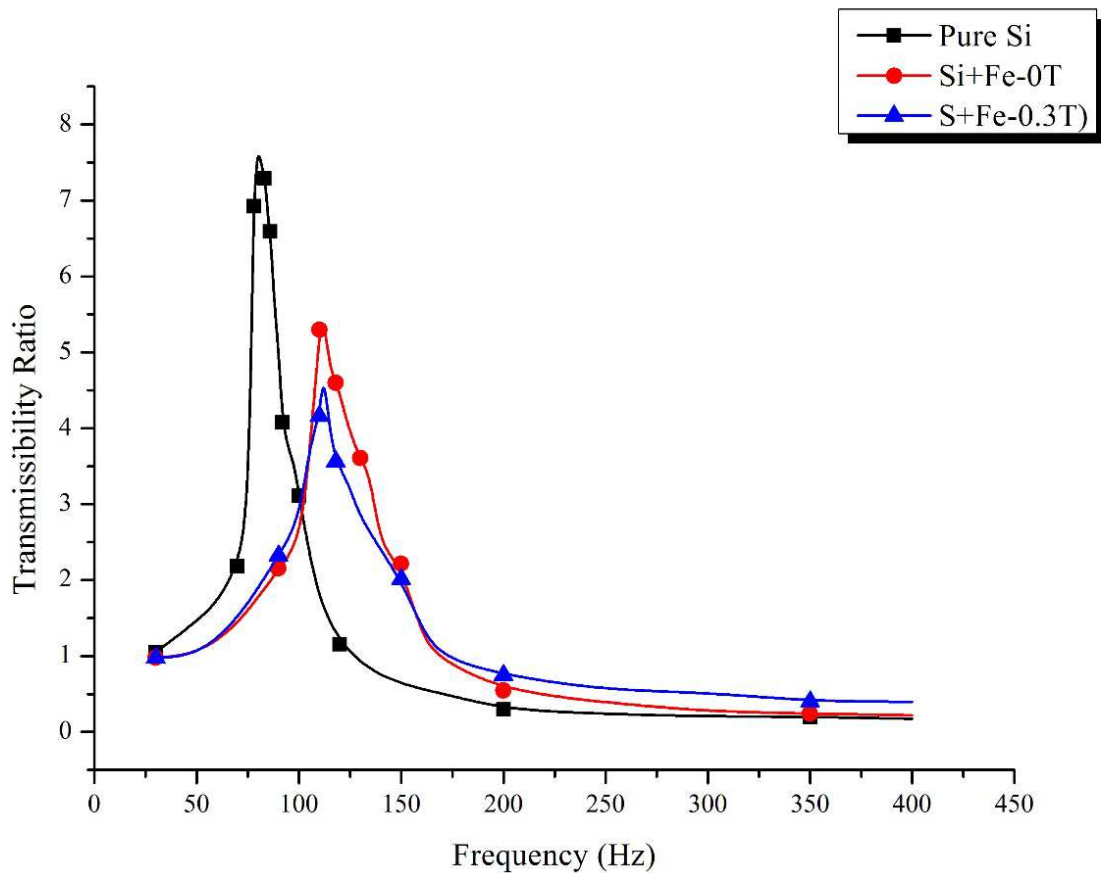


**Figure 4.19.** Transmissibility Silicone MRE samples

The Figure 4.19 shows the response of pure silicone and silicone MRE sample. The transmissibility ratio of silicone at resonance is about 7.8 and by adding MRE it reduced to 5.48 showing approximately 29% reduction at 0 Tesla. As the magnetic field was increased from 0 to 0.3 Tesla the transmissibility ratio further reduced to 4.75 showing about 39% reduction. When the transmissibility ratio of the MRE alone was compared at 0 and 0.3 Tesla, the field induced reduction was about 13%. The loss factor of the sample was about 0.1296 and it increased to 0.1824 at 0 Tesla and 0.2102 at 0.3 Tesla showing a 62% improvement.

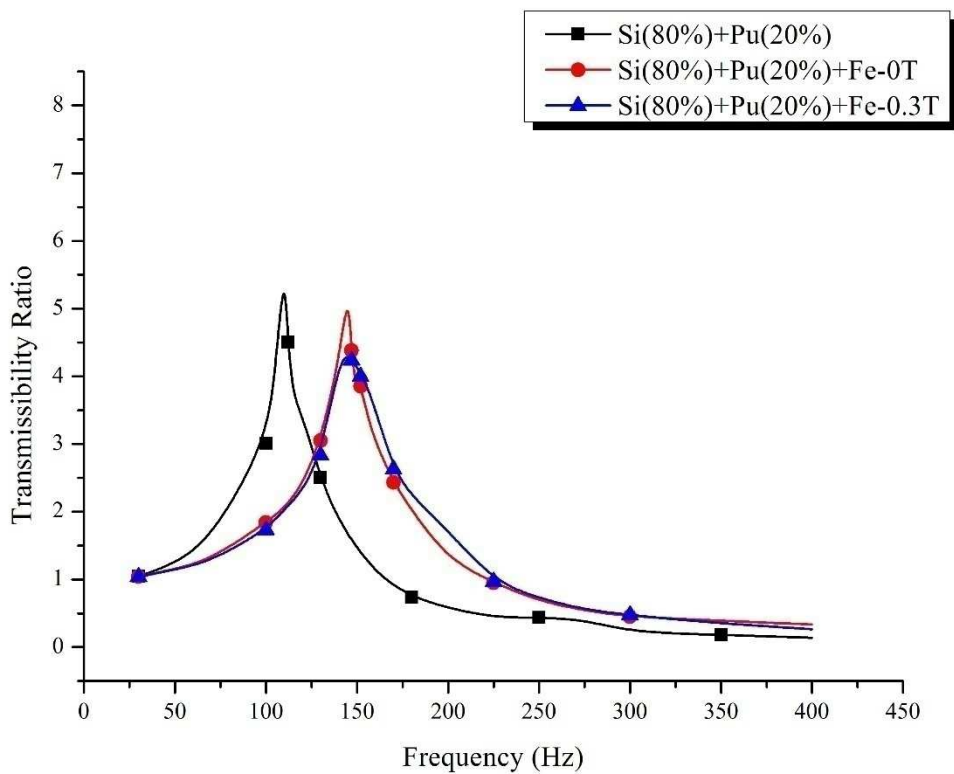


**Figure 4.20.** Transmissibility 80-20 (Si+PU) MRE samples

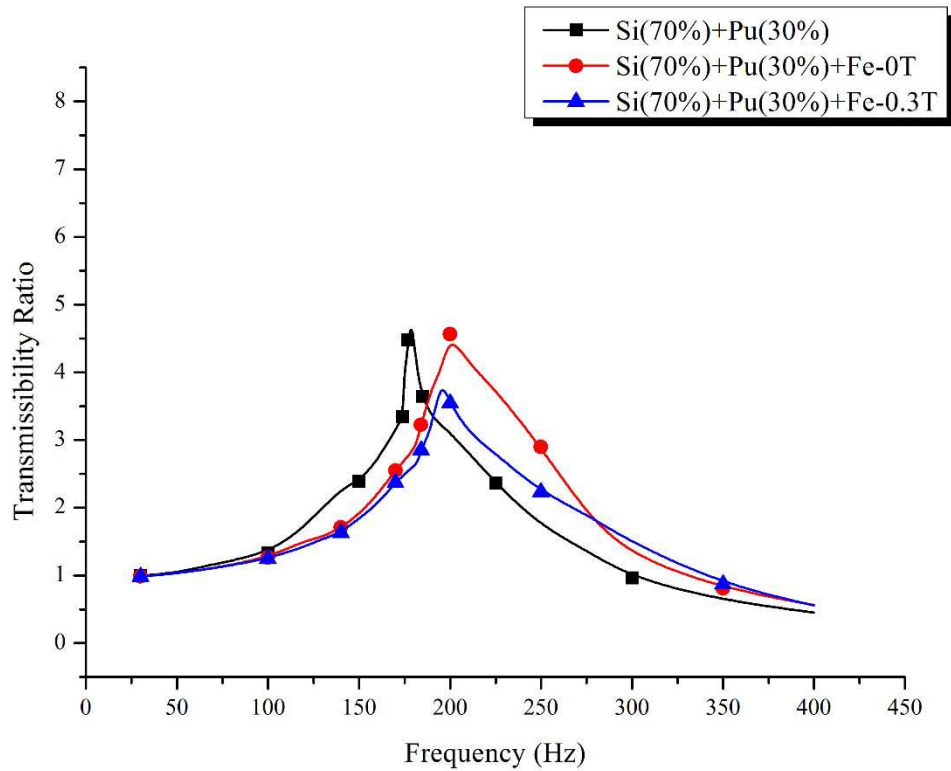


**Figure 4.21.** Transmissibility 70-30 (Si+PU) MRE samples

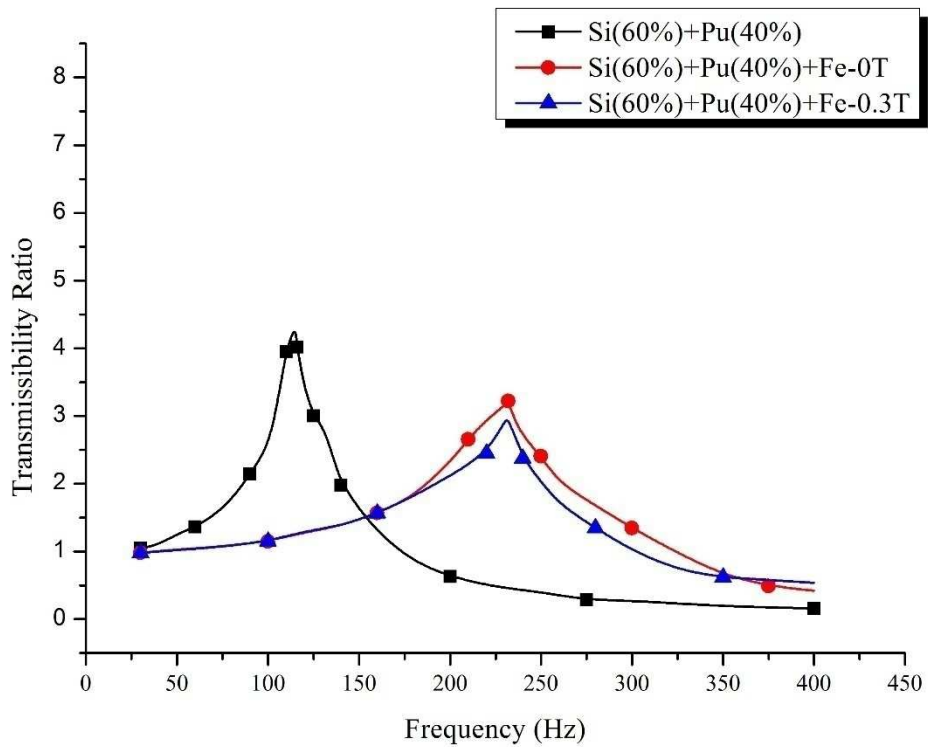


**Figure 4.22.** Transmissibility 60-40 (Si+PU) MRE samples

The behaviour of 80-20 pure sample and 80-20 MRE is depicted in figure 4.20. Loss factor improvement of 80-20 MRE when compared with pure silicone was about



78% which shows that by adding PU to silicone matrix, the loss factor can be enhanced. In a conventional MRE, the damping of the MRE can be assumed to be a factor of the damping present in the matrix material, the damping of the CIP and the interfacial contact friction between the polymer matrix and the CIP. In hybrid samples, there exists an additional friction between the two types of matrices since they do not mix chemically. The effect is visible in the form of improvement in damping by mixing. The transmissibility ratio of 80-20 sample without iron powder was about 5.67 which is 26% less than the pure silicone sample proving that there exists an additional damping introduced because of two immiscible matrices.

The behaviour of 80-20 pure sample and 80-20 MRE is depicted in Figure 4.20. Loss factor improvement of 80-20 MRE when compared with pure silicone was about 78%, which shows that by adding PU to silicone matrix, the loss factor can be enhanced. In a conventional MRE, the damping of the MRE can be assumed to be a factor of the damping of the matrix material, the damping of the CIP and the interfacial contact friction between the polymer matrix and the CIP. In hybrid samples, there exists an additional friction between the two types of matrices since they do not mix chemically. The effect is visible in the form of improvement in damping by mixing. The transmissibility ratio of 80-20 sample without iron powder was about 5.67, which are 26% less than the pure silicone sample proving that there exists an additional damping introduced because of two immiscible matrices.

The response of 60-40 sample is shown in Figure 4.22. The 60-40 MRE sample showed the best performance among all the samples. The transmissibility ratio reduced to 4.33 for the pure sample, a 45% reduction when compared with pure silicone sample. Transmissibility reduction of MRE sample when magnetic field was varied from 0 Tesla to 0.3 Tesla was least among all the samples about 5% only. This indicates that as the PU percentage in the sample was increased, the stiffness of the sample also increased resulting in more resistance for the interfacial action between the particles and the matrix. Hence even though there was an overall improvement in damping properties, the relative improvement with the magnetic field was compromised. The loss factor of this sample showed 158% enhancement at 0.3 Tesla when compared with pure silicone sample. But the relative improvement of loss factor with the magnetic field was the least for 60-40 MRE sample of about 8%.

The loss factor variation with magnetic field of all the samples are shown in Figure 4.23. The field induced improvement of samples reduced with the increase in the polyurethane percentage, but the overall loss factor improved.

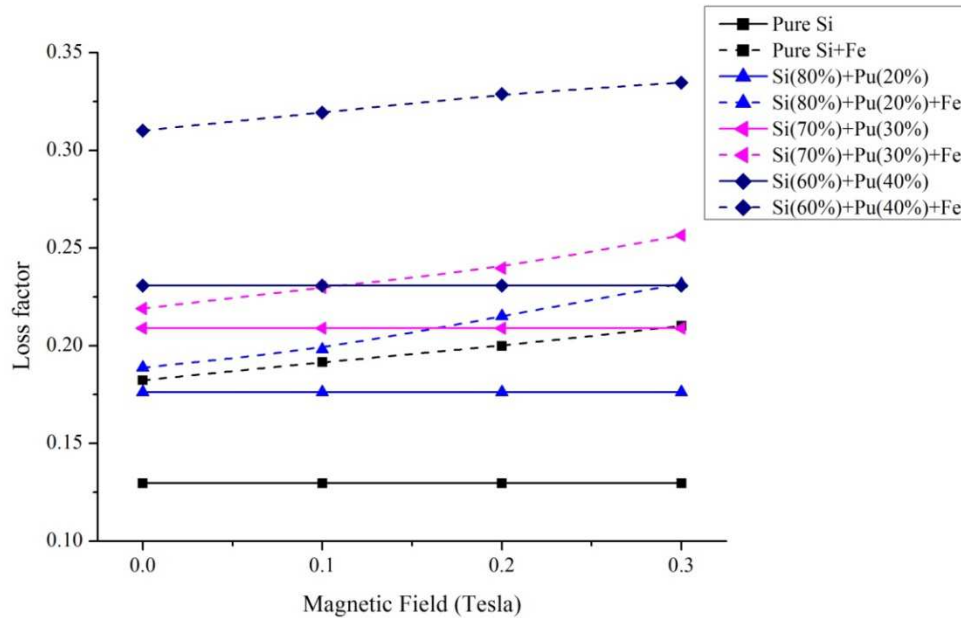


**Figure 4.23.** Loss factor variation of the MRE samples

From the above analysis, it can be deduced that hybrid MREs can be a potential isolator material. If the mixing issues are addressed, this can serve as an excellent material as the experiments have shown that it can produce results equivalent to that of nitrile rubber.

#### 4.4.3 INFLUENCE OF STRAIN AND FREQUENCY

In this section, the effect of strain amplitude and frequency is presented. Like conventional viscoelastic materials, MRE also exhibits frequency, strain amplitude and temperature dependency on dynamic properties. These properties are evaluated using direct stiffness method focusing on frequency range between 5 to 45 Hz. Experiments were conducted at lower strain amplitudes of 0.075 mm and 0.15 mm to ensure linear viscoelastic behaviour. Polymers in general are made of cross linked chains of molecules and molecular level interactions happen during deformation of polymers. These interactions give rise to its inherent properties like stiffness and energy dissipation in response to a cyclic deformation which is referred to as damping. In homogeneous and isotropic polymers like the samples tested in the present work, the stiffness and damping characteristics vary with the temperature and to a lesser degree with operating frequency.

The frequency and strain dependent viscoelastic properties are studied by adapting direct stiffness method generally used to characterize the isolators. In this method, the stiffness of MRE is assessed with respect to the drive point or blocked transfer stiffness (Pan Jie et.al. 2005).

Measuring input strain with respect to input force is called driving point stiffness and input strain to the transmitted force called dynamic transfer stiffness. Both the methods can be employed to measure the dynamic properties of elastomers. But, dynamic transfer stiffness method is said to be more efficient since inertial effects do not influence it. In this test, both the stiffness value is measured at two different strains and different operating frequencies at varying magnetic fields up to 0.3 Tesla.

Force at the input and blocked side are measured by two Kistler force transducers and strain measurement was done using the micro epsilon laser pick up. The photograph of the experimental set-up is shown in Figure 4.24 below. When a sinusoidal input force is applied to a viscoelastic material, the resulting displacement is also sinusoidal with a phase difference or lag. The plots corresponding to input force versus measured displacement shows a hysteresis behaviour which is elliptical in nature. This behaviour can be employed to compute the dynamic properties of the MRE viscoelastic properties. The slope of the major axis gives the stiffness of the material and the ratio of minor axis to major axis (aspect ratio) is a measure of damping. (Lakes 2009) The dynamic properties can be computed from the response curve as shown in Figure 4.25 below.

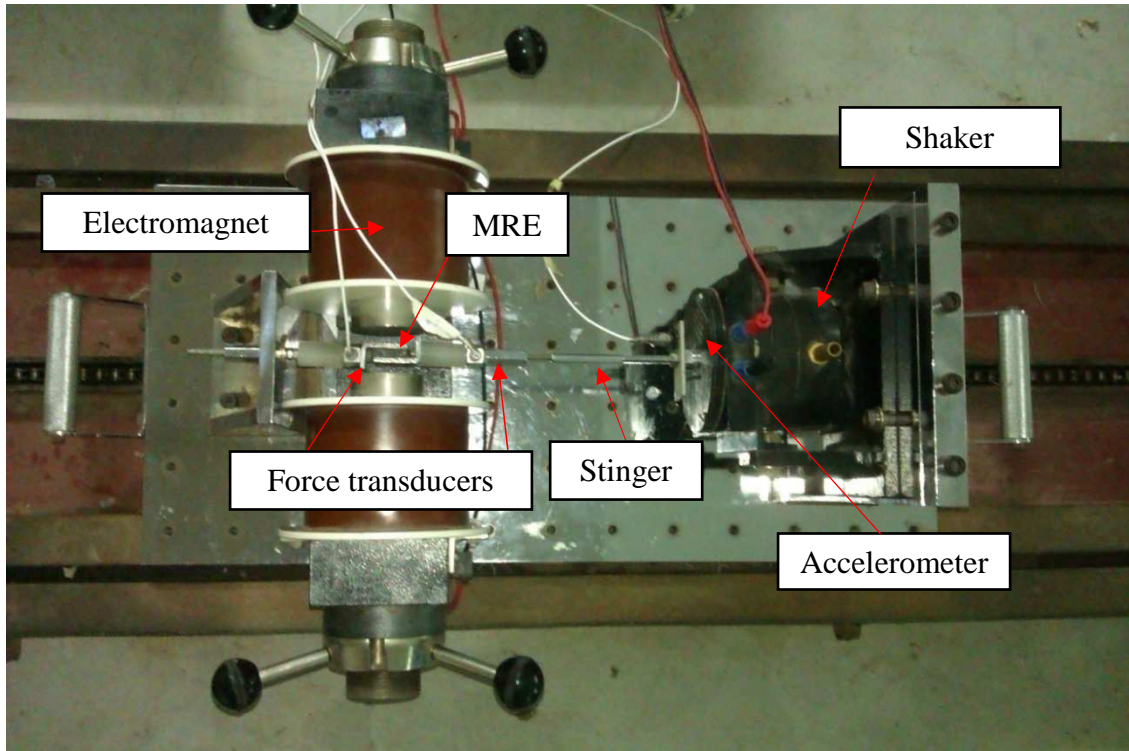


**Figure 4.24.** Experimental setup

The force versus displacement graph of all the samples at an input frequency of 5 Hz is shown in the figure below. Because of the sheer number of graphs, only one graph is shown. At the same operating conditions, the 60-40 sample showed better results i.e. the area under the curve was found to be maximum and the slope of the curve which is a measure of the stiffness of the material was highest for the 60-40 sample indicating its superior properties. With the increase in magnetic field, increase in slope of the loop is noticed which is an indication of the stiffness enhancement under the magnetic field.

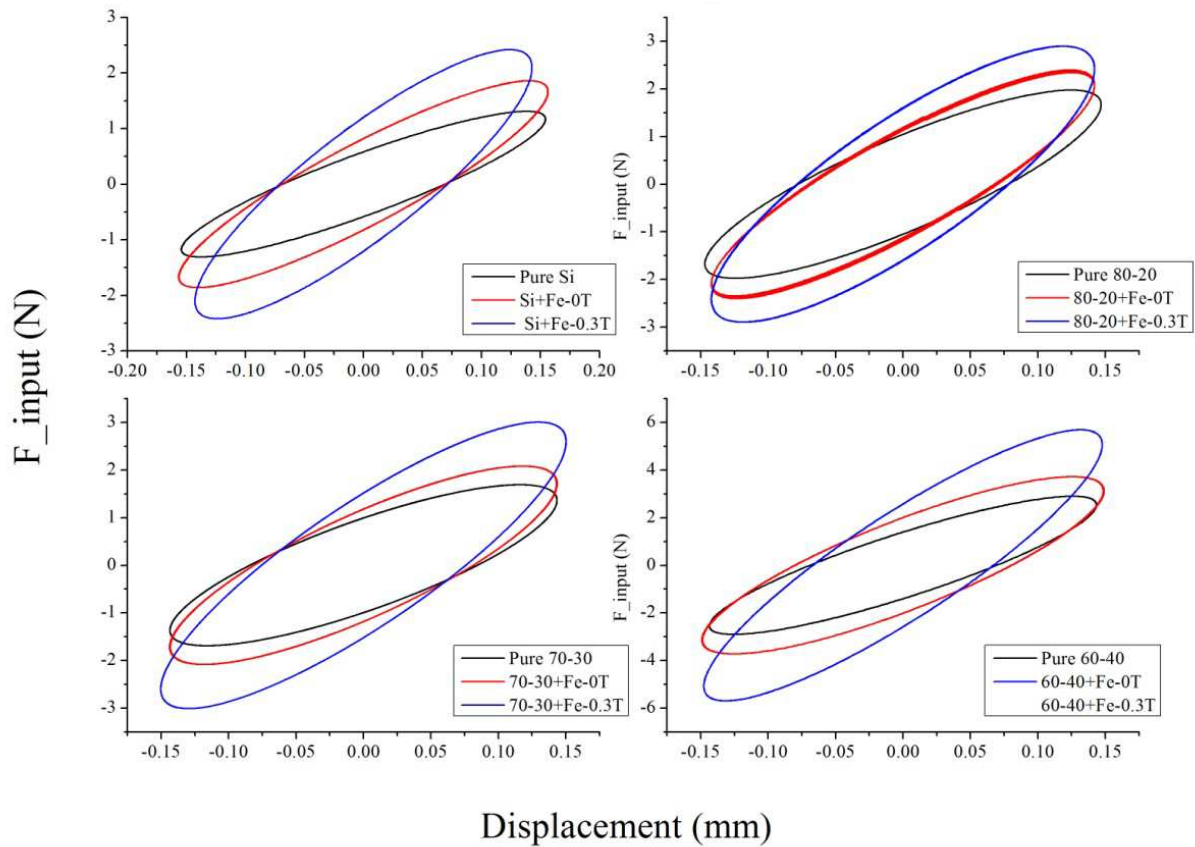


**Figure 4.25.** Force v/s Displacement plots at 5 Hz

Viscoelastic materials are a type of materials whose dynamic properties are dependent, to some extent, on input strain and operating frequency. Since in most applications, viscoelastic materials are mostly employed in lower frequencies, the operating frequency was limited up to 45Hz in the current work. The input frequency was increased from 5 Hz to 40 Hz in steps of 5 Hz. Two input strains of 0.15 mm and 0.075 mm were input to the MRE samples at frequencies varying from 5 Hz to 45 Hz. The variation of blocked transfer stiffness with the frequency was plotted. The dynamic stiffness extracted from the hysteresis loop is shown in the Figures 4.26 to 4.29.

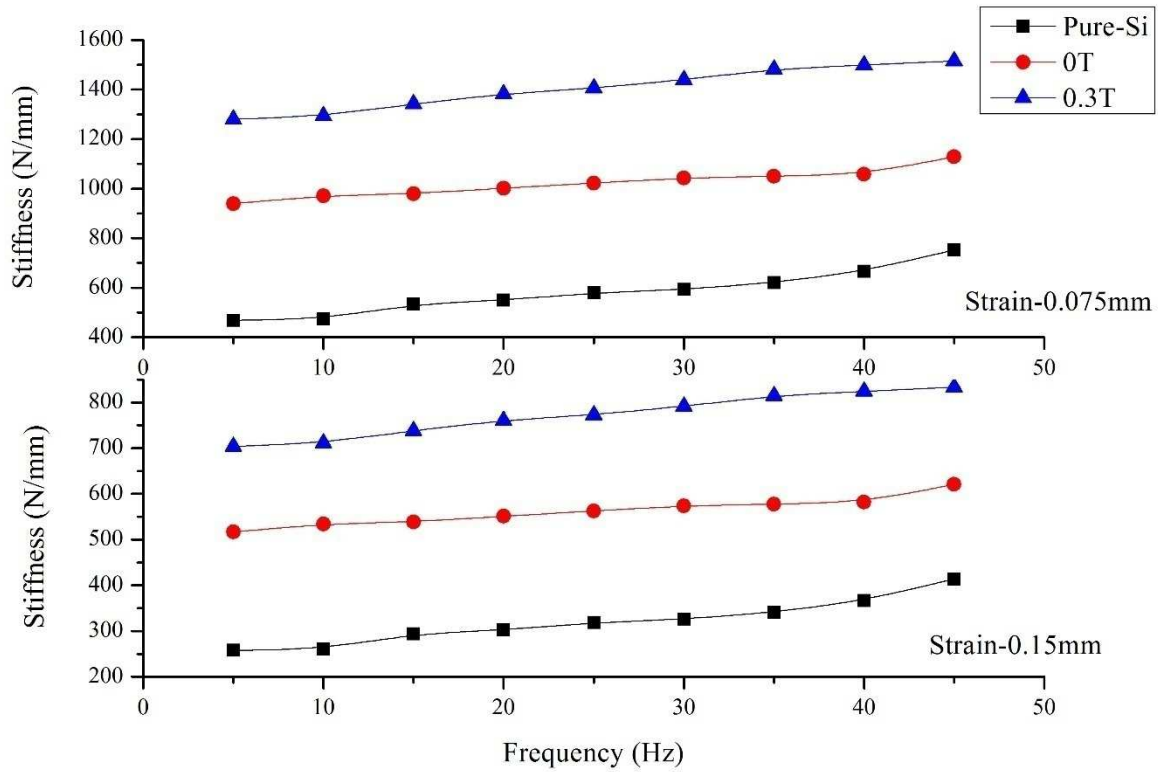


**Figure 4.26.** Stiffness variation of Si-MRE with frequency

The behavior of silicone samples is depicted in Figure 4.26. In this case, it can be observed that the stiffness increase with addition of iron powder and with the magnetic field. At both the strain amplitudes, the stiffness increased with the increase in concentration. The stiffness increase with respect to frequency is linear in this range. The Figure 4.27 shows the stiffness variation of 80-20 mixed MRE samples. This sample showed better performance than silicone MREs at a higher magnetic field as it is evident from the graph. The stiffness increase with the frequency was more for this sample when compared to the silicone sample. Figure 4.28 shows the plots of 70-30 MRE samples. As the strain was increased from 0.075 mm to 0.15 mm, the sample showed a decrease in stiffness, which was more than the silicone and 80-20 MRE samples. For both the strain amplitudes, there was an increase in stiffness with the frequency for the tested range.

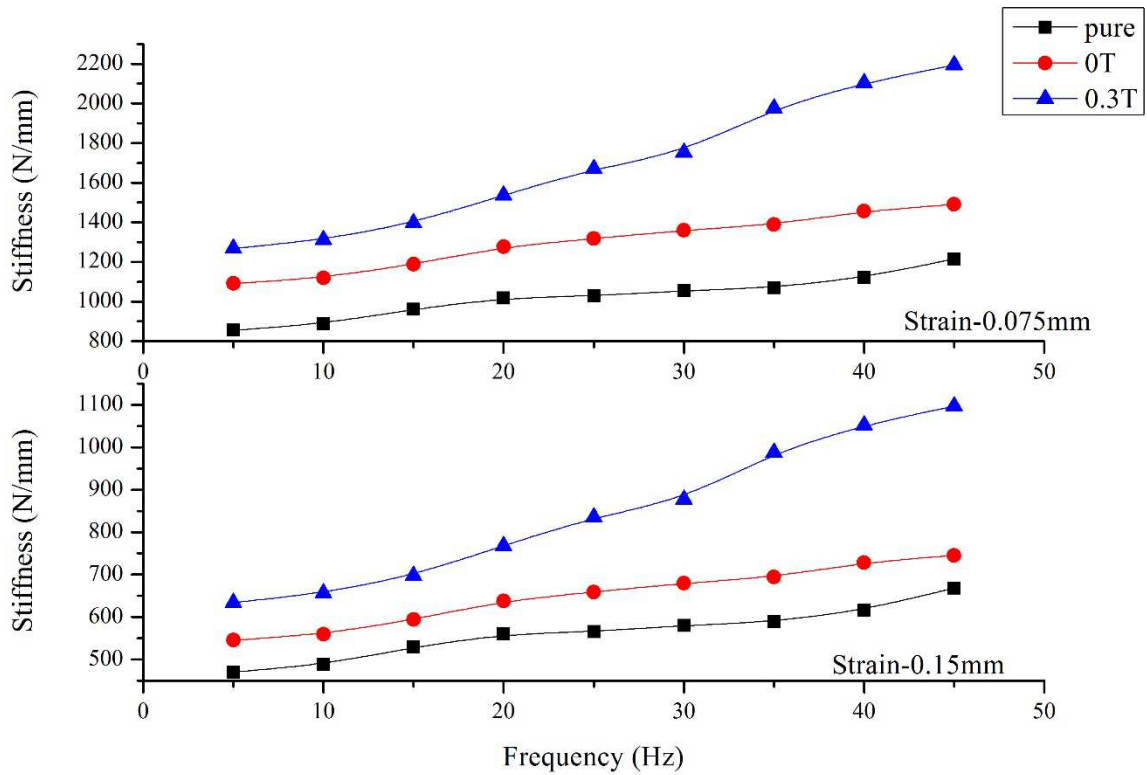


**Figure 4.27.** Stiffness variation of 80-20-MRE with frequency

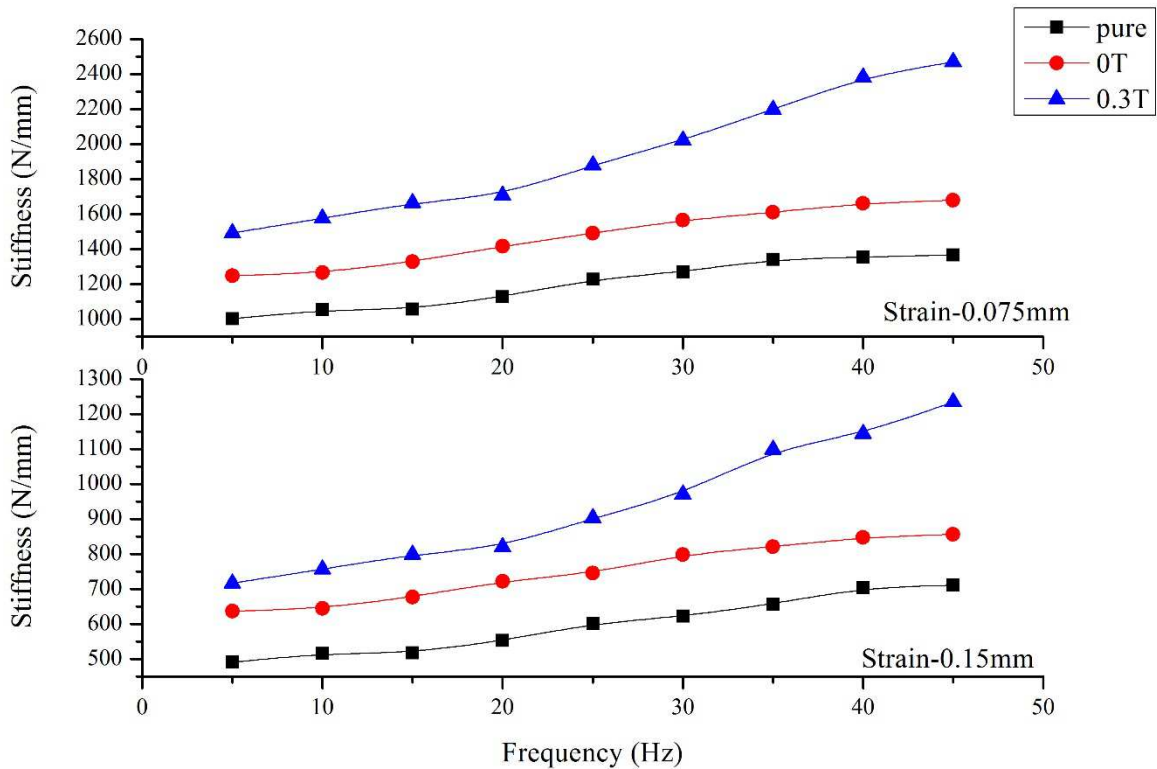


**Figure 4.28.** Stiffness variation of 70-30-MRE with frequency

The Figure 4.29 below shows the behavior of 60-40 MRE samples. This sample also shows similar behavior like other samples. All the four types of samples have shown linear behavior in this lower frequency range of 45 Hz.

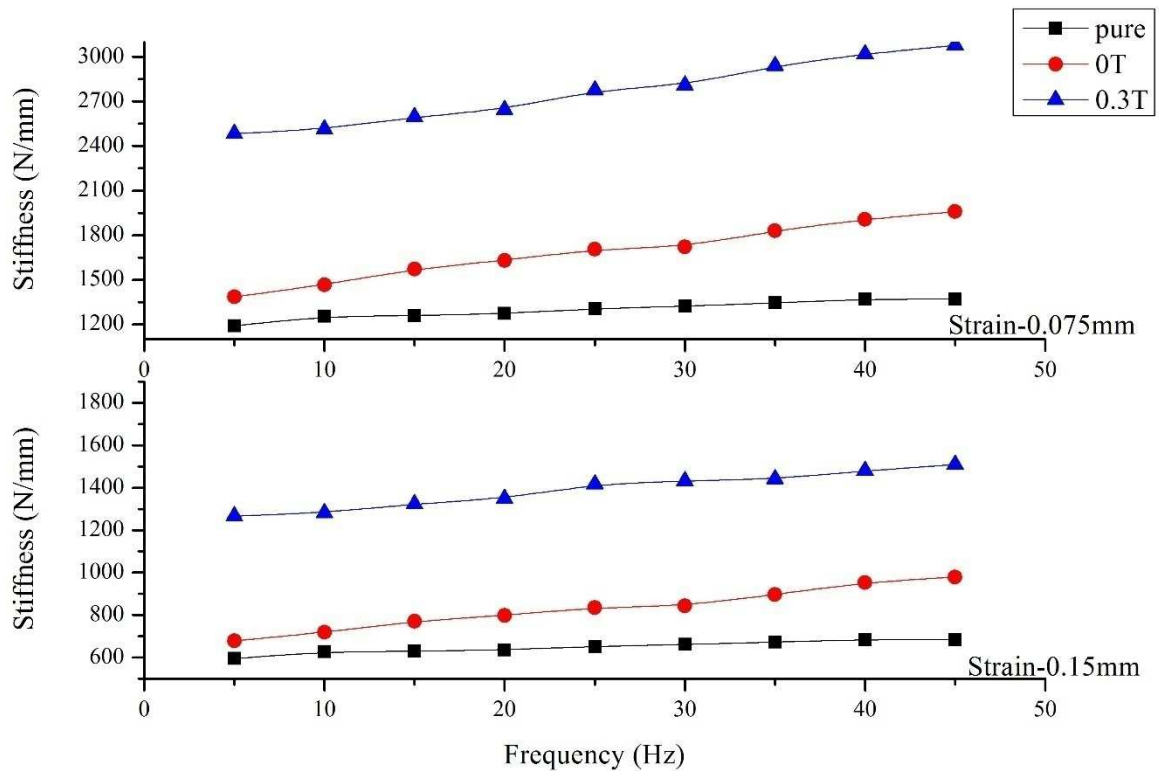


**Figure 4.29.** Stiffness variation of 60-40-MRE with frequency

The figure shows that the behavior of MRE is dependent on frequency. With the increase in frequency, the stiffness of the MRE is increased as generally observed in viscoelastic materials. The frequency-dependent increase in stiffness is attributed to the increased stiffness of bulk polymer chains. From the figures, it is also observed that with the increase in strain amplitude, the stiffness of MRE showed a decreasing trend which can be attributed to the matrix bond breakage effect generally found in rubber (Funt, 1987). The amplitude dependent behaviour is consistent with the increase in the magnetic field. Compared to unfilled rubber, the influence of strain on property variation is more pronounced in MRE samples consisting of CIP. Addition of fillers creates weak interface friction between the filler and the matrix which varies with the frequency as well as strain amplitude. Experiments conducted verify that the magnetic field and strain amplitude are the key operating parameters which define the property enhancements.





## CHAPTER 5

### PARAMETER IDENTIFICATION BY VISCOELASTIC MODELING

Magnetorheological elastomers consist of viscoelastic polymer matrix and ferromagnetic filler ingredient, which possess magnetic field-induced behaviour. The overall dynamic performance of MRE is a combination of viscoelastic characteristics of matrix and the magnetic dipole interactions of CIP fillers (Guojiang Liao et al. 2013, Lin Chen et al. 2013). The presence of CIP in MRE produce reinforcing effect, enhances the dynamic modulus, and alters the energy dissipation resulting from the interfacial friction between the ferromagnetic filler particle and the polymer matrix. An effective model of MRE should consider the contributions all parameters.

The modeling approach of MRE involves the constitutive relations based on linear viscoelastic theory combined with the effect of dipole interactions. Past studies have reported the parametric modeling using Maxwell, Kelvin Voigt, and fractional viscoelastic relations. The models are formulated upon the basis of experimental results where the parameters are extracted from the error minimization function. In the present work, a four-parameter model based on Kelvin-Voigt standard linear model is modified to depict the smart behaviour of MRE. The detailed description of the element of the model and the extraction procedure is illustrated below.

Most materials which are solid in nature follow Hooke's law of elasticity under small strains.

$$\sigma = E\varepsilon \quad (5.1)$$

Where,  $E$  is the Young's modulus of elasticity and  $\sigma$  and  $\varepsilon$  are the stress and strain respectively. Viscous fluids behave very differently and a typical Newtonian fluid under stress follows,

$$\sigma = \eta \frac{d\varepsilon}{dt} \quad (5.2)$$

Where,  $\eta$  is the Dynamic viscosity in  $\text{Ns/m}^2$ . Most polymers exhibit a viscoelastic property under smaller strains or in other words, the response is elastic as well as viscous when the operating strain is controlled within the linear range. This class of material which exhibits both viscous as well as elastic behaviour and are classified as viscoelastic materials. The stress-strain behaviour of these materials is hysteretic in nature and when operated in the linear range, the shape of the hysteresis curve is symmetric. To study the

viscoelastic behaviour, mathematical formulation of viscoelastic theory is necessary. This will enable to predict the material response to arbitrary loading conditions. MRE also has an elastomer matrix which exhibits viscoelastic behaviour. Popular linear viscoelastic models can be fitted to the experimental data. The following section briefs about some of the most widely applied linear models and the development of the model used in the current work by modifying the existing ones. In the current work, model is developed by modifying the three-parameter classical solid Zener model.

## 5.1 FORMULATION OF THE MODEL

The Maxwell model (Figure 5.1) describes a material as a dashpot which represents the viscous behavior in series with spring describing elastic behavior.

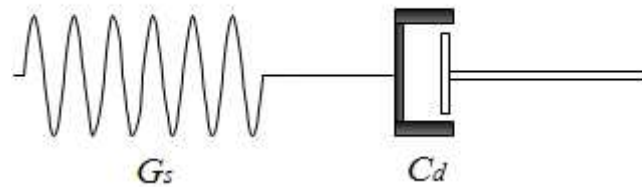


**Figure 5.1.** Maxwell Model

When a shear stress is applied, it is uniform through the element and the total strain of the viscoelastic element can be expressed as

$$\varepsilon = \varepsilon_s + \varepsilon_d \quad (5.3)$$

The governing equation can be written as,

$$\frac{d\varepsilon}{dt} = \frac{1}{G} \frac{d\sigma}{dt} + \frac{\sigma}{C_d} \quad (5.4)$$

Where,  $\varepsilon$  is the strain in the element,  $G_s$  is the Shear modulus in Pascal,  $\sigma$  is the shear stress in N/m<sup>2</sup> and  $C_d$  is the damping coefficient in N-s/m. Suppose that a cyclic strain is input to a viscoelastic material, the stress induced also will be cyclic with a phase difference.

$$\varepsilon = \varepsilon_o e^{i\omega t} \quad (5.5)$$

Where  $\omega$  is the frequency of excitation in Radians and  $\varepsilon_o$  is the strain amplitude.

The induced stress is,

$$\sigma = \sigma_o e^{i(\omega t + \delta)} \quad (5.6)$$

$$i\omega\varepsilon = \sigma \left( \frac{i}{G} \omega + \frac{1}{C_d} \right) \quad (5.7)$$

By rearranging the terms, we obtain the following expression for stress induced in Maxwell spring element.

$$\sigma_1 = \left( \frac{iG_1 C_d \omega}{iC_d \omega + G_1} \right) \varepsilon \quad (5.8)$$

Consider an additional spring element (Figure 5.2) in parallel with the Maxwell spring, in which the total stress can be expressed as depicted in equation 5.9.

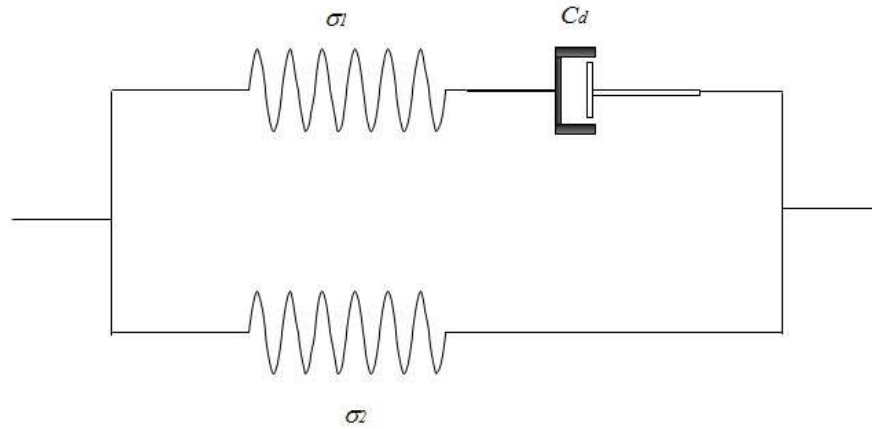


**Figure 5.2.**Zener Model

In this case, the stress is distributed to two elements and both the elements will strain equally which is mathematically expressed as,

$$\sigma = \sigma_1 + \sigma_2 \quad (5.9)$$

Where  $\sigma_2$  is the stress induced in the additional spring element. By substituting for  $\sigma_1$  from equation 5.8, we get,

$$G^* = \left( \frac{iG_1 C_d \omega}{iC_d \omega + G_1} \right) + G_2 \quad (5.10)$$

Where  $G^*$  is the complex shear modulus since the material under consideration is a viscoelastic material.

$$G' + iG'' = \left( \frac{iG_1 C_d \omega + G_2 (iC_d \omega + G_1)}{(iC_d \omega + G_1)} \right) \quad (5.11)$$

By rearranging the above equation,

$$G' + iG'' = \left( \frac{G_1 G_2 + iC_d \omega_2 (G_1 + G_2)}{(iC_d \omega + G_1)} \right) \quad (5.12)$$

By eliminating complex term in denominator, the equation 5.12 can be modified to,

$$G' + iG'' = \left( \frac{G_1^2 G_2 + C_d^2 \omega^2 (G_1 + G_2) + i(C_d \omega (G_1 + G_2) - C_d \omega G_1 G_2)}{C_d^2 \omega^2 + G_1^2} \right) \quad (5.13)$$

By rearranging the above equation and separating the real and imaginary parts, equation 5.13 can be re-written as,

$$G^* = G' + iG'' = \left( \frac{G_1^2 G_2 + \omega^2 C_d^2 (G_1 + G_2)}{G_1^2 + \omega^2 C_d^2} \right) + i \left( \frac{\omega C_d G_1^2}{G_1^2 + \omega^2 C_d^2} \right) \quad (5.14)$$

By comparing the real and imaginary parts, we obtain the expressions for storage modulus ( $G'$ ) and loss modulus ( $G''$ ).

$$G' = \frac{G_1^2 G_2 + \omega^2 C_d^2 (G_1 + G_2)}{G_1^2 + \omega^2 C_d^2} \quad (5.15)$$

$$G'' = \frac{\omega C_d G_1^2}{G_1^2 + \omega^2 C_d^2} \quad (5.16)$$

However, both these models do not account for the magnetic-field induced changes. To compensate for the magnetic-field induced changes, another element  $\sigma_m$  is introduced, which is field-induced stress. This is assumed to be in parallel with the existing Zener model. The schematic of the modified model with the element accounting for the field-induced changes is depicted in Figure 5.3. This has been developed by extending the three-parameter linear viscoelastic model.

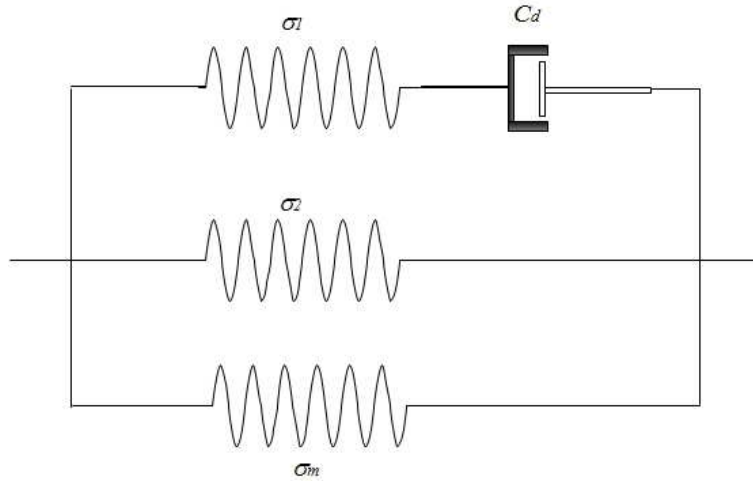


**Figure 5.3.** Modified Model

The total stress induced can be written as,

$$\sigma = \sigma_1 + \sigma_2 + \sigma_m \quad (5.17)$$

The magnetic field induced stress can be expressed as a function of field induced stiffness,

$$\sigma_m = k_m \varepsilon \quad (5.18)$$

$$\text{Where, } k_m = K_m B \quad (5.19)$$

B is in Tesla. By substituting these modifications, the equations developed can be written as,

$$G' = \frac{G_1^2 G_2 + \omega^2 C_d^2 (G_1 + G_2) + K_m B}{G_1^2 + \omega^2 C_d^2} \quad (5.20)$$

$$G'' = \frac{\omega C_d G_1^2}{G_1^2 + \omega^2 C_d^2} \quad (5.21)$$

## 5.2 PARAMETER IDENTIFICATION

The model proposed in the study consists of four parameters-  $G_1$ ,  $G_2$  and  $C_d$  deals with the damping capabilities and  $K_m$  the field induced stiffness. The equations 5.15 and 5.16 can be used to identify the parameters using the method of least squares to minimize error between the stress predicted by the model “ $f_{\text{stress}}$ ” and the experimental stress “ $s_{\text{stress}}$ ”. The parameters were identified for different experimental data using MATLAB optimization tool. The MATLAB code is shown in the appendix of the thesis for reference. The force-displacement experimental results of the silicone-RTV samples are considered for parameter identification. Stress is calculated by dividing the force by shear area and strain by dividing the displacement by the original height of the MRE sample. The sample in consideration is Silicone RTV. The silicone MRE contained 5 grams of carbonyl iron powder. The parameters were identified for different experiments and the Table 5.1 shows the parameters identified for strain input of 0.15 mm and 0.075 mm at 15 Hz frequency for a magnetic field up to 0.3 Tesla.

**Table 5.1** Parameters Identified for Silicone samples at 15Hz

Material	Strain	$K_m$	$G_1$	$G_2$	$C_d$	Error
Pure Si		-0.0065	187.751	124.564	11.9211	1.91E-06
Si+Fe-0T	0.15 mm	100.51	194.786	130.421	14.4091	2.18E-06
Si+Fe-0.3T		109.861	204.632	135.758	23.0573	1.32E-06
Pure Si		-0.004	175.6498	91.1756	17.778	1.04E-06
Si+Fe-0T	0.075 mm	92.62366	218.431	145.584	16.4410	3.84E-06
Si+Fe-0.3T		102.8303	206.9081	146.287	11.8778	1.15E-04

Similarly, this model can be extended for different frequencies and different materials to predict the four parameters. The plot below (Figure 5.4) shows the comparison of experimental and predicted for 0.15mm strain. The comparison of stress-

strain relationship at 0.075mm strain is shown in Figure 5.5. Comparison between the experimental results and the developed model shows good consistency. At both the strain amplitudes, the parameter values increased with the magnetic field.

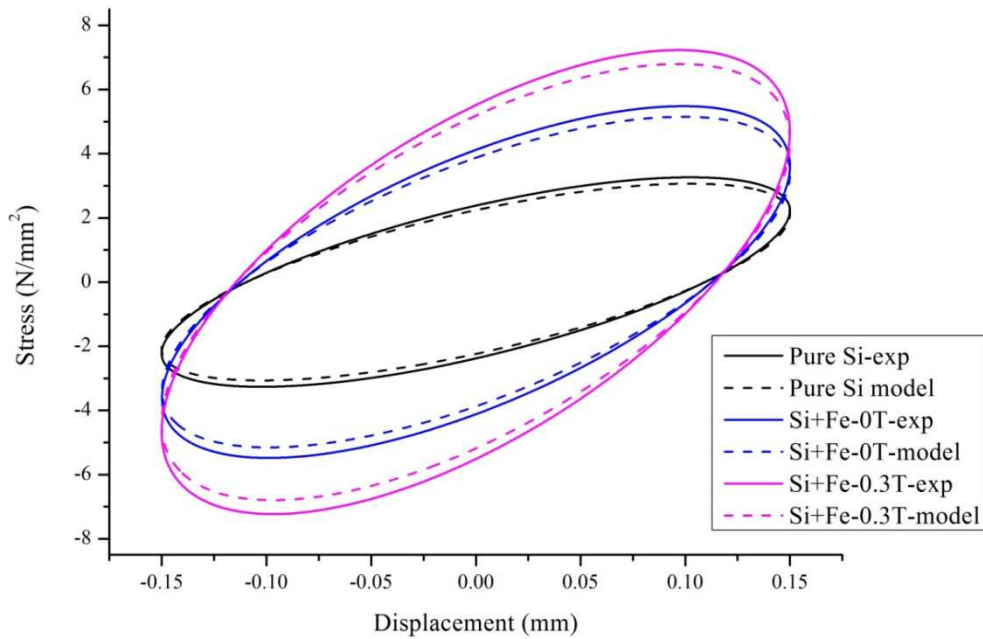


**Figure 5.4.** Silicone MRE sample behavior at 0.15mm strain

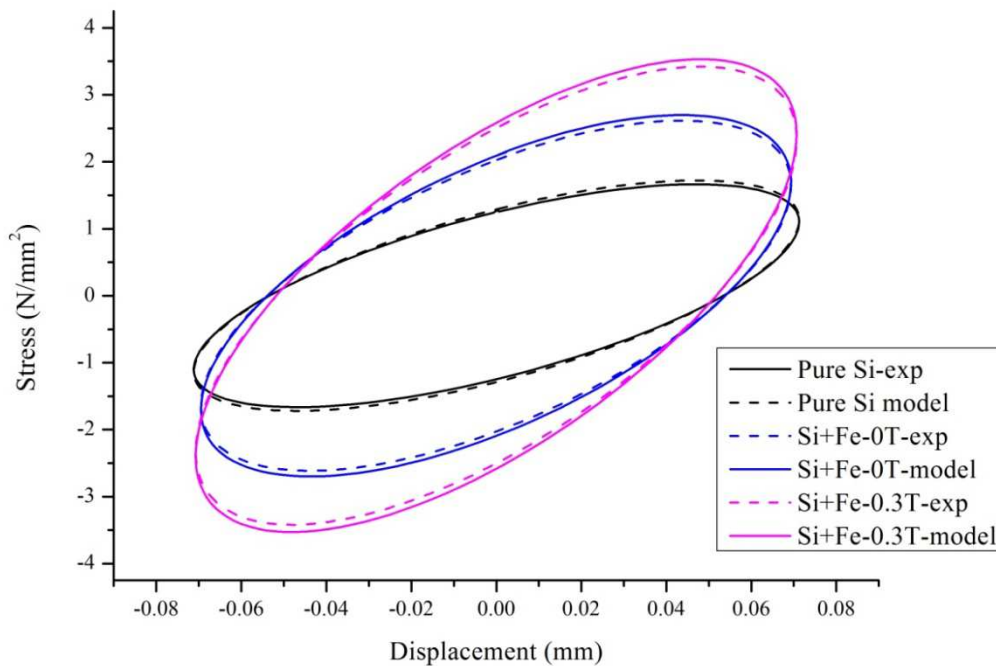


**Figure 5.5.** Silicone MRE sample behavior at 0.075mm strain

The errors between the simulated and the experimental values are very low, which show the credibility of the model. This model can be extended for other samples and at various other frequencies, which will be useful in describing the performance of Magnetorheological elastomers.

## CHAPTER 6

### MRE AS A MATERIAL FOR CONSTRAINED LAYER DAMPING

Focus of the current research so far has been on the preparation and characterization of magnetorheological elastomers. The factors which influence the zero field as well field-induced properties were discussed. This chapter involves the application of MRE samples in constrained layer damping treatment. The ability of MRE in modifying the characteristics of a base beam is evaluated by adapting the ASTM-E756-05 standard. The response of the MRE sandwich beam is assessed by obtaining the frequency response function by impulse excitation in the presence of a non-homogeneous field. The studies are extended to understand the influence of matrix material and percentage concentration of CIP on the loss factor and shear modulus of sandwich structure.

#### 6.1 MATERIAL PROCESSING

The preparation of the samples is explained in detail in chapter 3. This method also involved the use of the same type of matrices employed for force transmissibility tests. The sample dimensions are strips of size 200mm x 20mm x 6mm. Five samples of these strips were produced by varying the percentage by volume of Carbonyl iron powder. The prepared samples were of 0%, 10%, 15% and 20 and 25% by volume.

The strips using RTV silicone samples with similar dimensions as the HTV samples were prepared in the lab at NITK, Surathkal as explained in the previous chapters. Five samples were prepared with 0%, 10%, 15%, 20% and 25% by volume of CIP in each type of material. In total 20 samples were employed for experiments.

#### 6.2 EXPERIMENTAL TECHNIQUE

Sandwich beam configuration is a very reliable technique to measure the mechanical properties of viscoelastic materials. MRE sandwich beams were prepared by making use of the strips prepared as mentioned in the previous section and ASTM standard E-756-05-2010 was employed to evaluate the shear modulus ( $G$ ) and loss factor ( $\eta$ ). The force vibration tests discussed in previous section were performed using permanent magnets, which could produce a magnetic field up to 0.3 Tesla. In sandwich beam configuration, electromagnet with a maximum capacity of 0.75 Tesla field was employed, which allows the tests to be conducted at higher fields. Experiments conducted by Guoliang Hu et. al. (2011) proved that the magnetic-field induced changes are more if the field is applied



near the fixed end and the strain is more near the fixed end. In the current research, the magnetic field was applied over a length of 50mm near the fixed end of the beam. Comparison of performance is made at the end, and possible sources of errors are also listed.

### 6.2.1 SUMMARY OF THE METHOD

The configuration for the cantilever beam test specimen is selected based on the type of damping material to be investigated and the damping properties that are desired. Fig. 6.1a to 6.1d shows the four different test specimens which are recommended to investigate tensile and shear damping properties of different types of materials over a wide range of modulus values.

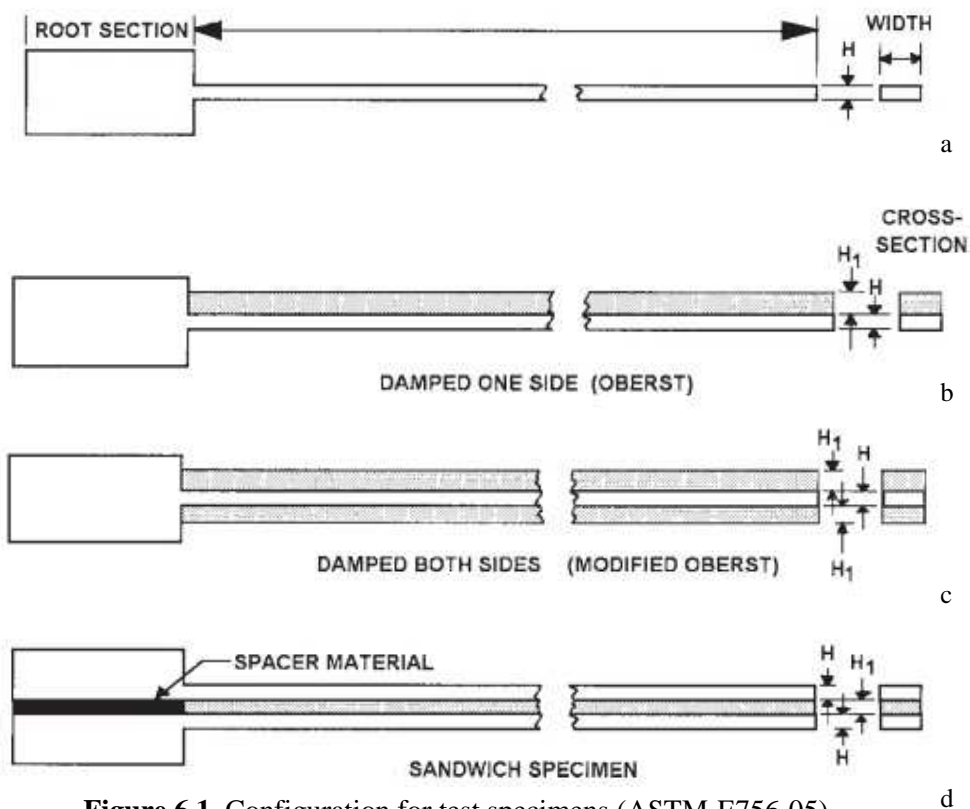


**Figure 6.1.** Configuration for test specimens (ASTM-E756-05)

Self-supporting damping materials are characterized by making a single, uniform test beam (Fig. 6.1a) from the material to be tested.

Non-self-supporting damping materials are characterized for by a two-step process. In the first step, a self-supporting metal beam which is called the base beam or bare beam should be tested to find its natural frequencies. In the second stage, the damping material is bonded to the base beam, and a damped composite beam is prepared by employing one of two test specimen configurations as shown above (Fig. 6.1b or 6.

1c). The damped composite beam is used for experiments to find its natural frequencies and corresponding composite loss factors. The damping properties of the material are computed using the stiffness of the base beam which is calculated from the results from the base beam experiments and the results of the composite beam tests.

The method to ascertain the shear modulus of non-self-supporting damping materials is like the two-step method explained above but needs two identical base beams to be tested and the composite beam to be made by the sandwich specimen configuration as shown above (Fig. 6. 1d).

Once the test beam configuration has been finalized, and the test sample has been prepared, it is clamped in a fixture. Two transducers are used in the measurement, one to apply an excitation force to cause the test beam to vibrate, and one to measure the response of the test beam to the applied force. By measuring several resonances of the vibrating beam, the effect of frequency on the material's damping properties can be established.

## 6.2.2 SANDWICH BEAM PREPARATION

Sandwich beam specimens were prepared as per the standard E 756-05, which specifies that the length sandwich core should vary from 180 to 240 millimeters. Aluminum was selected as the base beam for the sandwich beam. Base beam dimensions are 240mm x 20mm x 1.2mm. The root section of the beam is critical since any inaccuracies, here can alter the fixed-free boundary condition of the beam. As it was recommended by the standard, a spacer of thickness equal to the core material, and of same material as the base beam was used. The spacer dimensions were 40 mm x 20 mm x 6 mm. The MRE sandwich beams were prepared by gluing the viscoelastic material in between the aluminum base beams by using synthetic rubber based adhesive. The schematic of the sandwich beam with appropriate dimensions is shown in Figure 6.2.

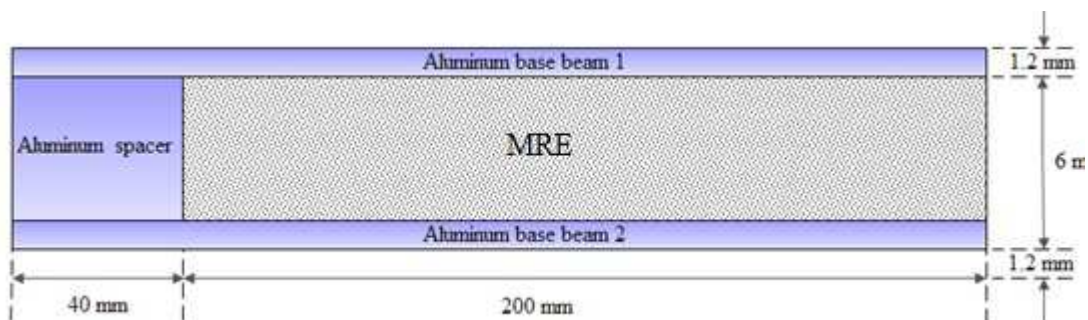


**Figure 6.2.** A sandwich beam used in experiment

The standard specifies that both the base beams should be of same dimensions and their natural frequencies should match. One end of the beam was clamped using a table vice to create the fixed-free boundary condition. The schematic of the experimental setup is shown in figure below (Figure 6.3).

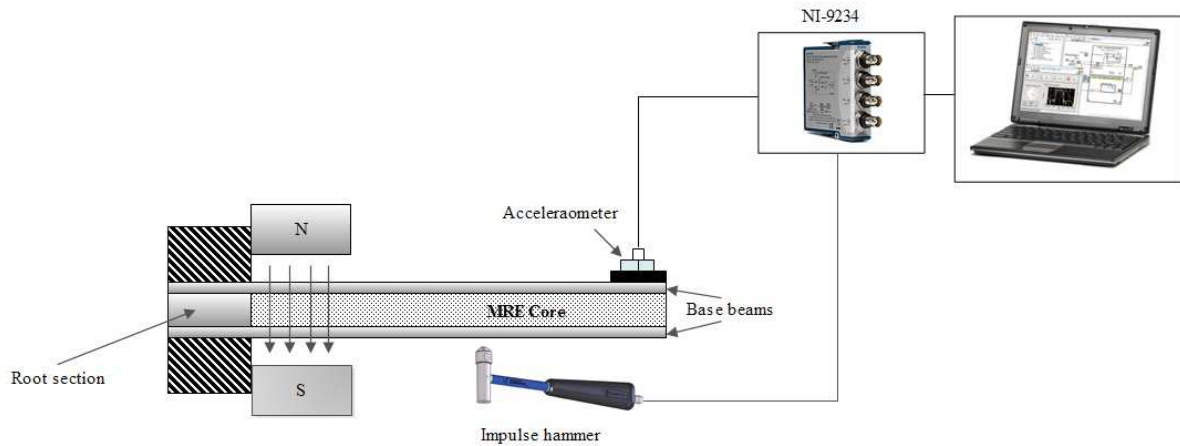


**Figure 6.3.** Schematic top view of the experimental setup

In the current work, modal analysis is done through impact excitation technique through an impact hammer of sensitivity 2.25 mV/N. As per the standard; two transducers are required- one to give input excitation and other acquires the response. Impact hammer provides the impulse, and response will be gathered by the output signal of the accelerometer. A Kistler accelerometer of sensitivity 101.9mV/g was used for measuring acceleration of the beam and acceleration data was acquired by NI-9234 data-acquisition module through NI-LabVIEW 2010 graphical programming. The FRF of the acquired signal gives the natural frequency spectrum of the beams. The first two dominant modes are considered for analysis since the higher modes are less likely to occur in reality, and moreover, viscoelastic materials more often operated in the lower frequency range.

The tests were conducted at different magnetic-field levels starting from 0 Tesla to 0.6 Tesla in steps of 0.1 Tesla. Magnetic field was applied using an electromagnet with a pole diameter of 50 mm and can produce a field of up to 0.75 Tesla. As explained earlier, the magnetic field was applied over a length of about 50 mm near the fixed end of the beam.

The force amplitude must be kept constant for accurate measurement of the response. In the current experiment, to assure the consistency in the readings, the response of the beam was divided by the force amplitude as suggested by the standard. The transfer function (in this case  $\ddot{X} / F$  or accelerance) as a function of frequency was considered for the measurement. 15 averages were considered so that there is consistency

in measurement. Even though the accelerometer is in contact with the beam, the impact on the reading is not much because of the low weight of the accelerometer, and the impact time of the hammer is also for a fraction of a second. To verify the results, the experiments were repeated three times in the same conditions and the average of the results was considered for analysis. A plot of the acceleration against the frequency is shown in the figure 6.4 for the Nitrile rubber sample. To acquire sensible data; the tests should be conducted in the linear range as the standard assumes that damping material behaviour is in accordance with the linear viscoelastic theory. If the force amplitude excites the beam beyond the linear range, the results obtained will not be correct. To ensure the linearity, as suggested by the standard, the maximum displacement of the beam should not be more than the thickness of the supporting beams. To satisfy this condition, the displacement was maintained below 1.2mm (thickness of the supporting beam) this was monitored by integrating the acceleration signal.

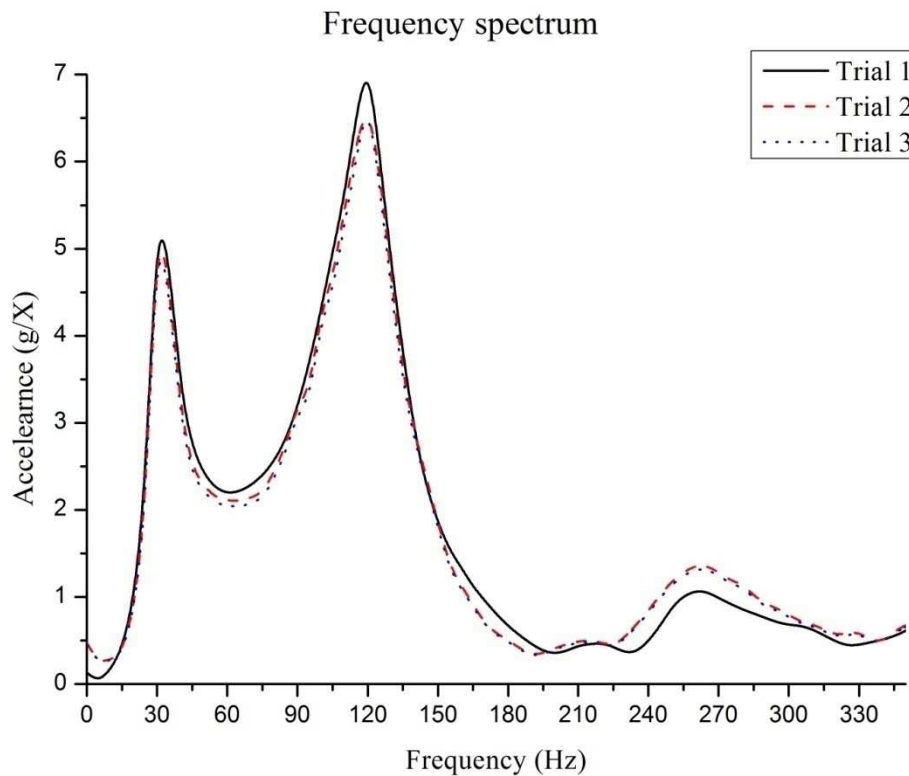


**Figure 6.4.** Snapshot of the impact test

The tests were conducted at different magnetic-field levels starting from 0 Tesla to 0.6 Tesla in steps of 0.1 Tesla. Magnetic field was applied using an electromagnet with a pole diameter of 50mm and can produce a field of up to 0.75 Tesla. As explained earlier, the magnetic field was applied over a length of about 50 mm near the fixed end of the beam. Using the half power bandwidth technique, the

shear modulus  $G_1$  and loss factor  $\eta_1$  Values can be calculated from the response curves with the aid of the formulas given by the standard. The shear modulus of the damping material is given by the following formula (ASTM-E756-05),

$$G_1 = \left[ A - B - 2(A - B)^2 - 2(A\eta_s)^2 \right] \left[ \frac{\left( \frac{2\pi C_n E H H_1}{l^2} \right)}{\left\{ (1 - 2A + 2B^2) + 4(A\eta_s)^2 \right\}} \right] \quad (6.1)$$

And, the loss factor of the damping material is given by,

$$\eta_1 = \frac{(A\eta_s)}{\left[ A - B - 2(A - B)^2 - 2(A\eta_s)^2 \right]} \quad (6.2)$$

Where,

$$A = (f_s / f_n)^2 (2 + DT)(B / 2)$$

$$B = 1 / \left[ 6(1 + T^2) \right]$$

$C_n$  = coefficient for mode n, of clamped-free (uniform) beam,

$D = \rho_1 / \rho$ , density ratio,

$E$  = Young's modulus of base beam, Pa,

$f_n$  = resonance frequency for mode n of Base beam, Hz,

$f_s$  = resonance frequency for mode s of composite beam, Hz,

$\Delta f_s$  = half-power bandwidth of mode s of composite beam, Hz,

$G_1$  = shear modulus of damping material, Pa,

$H$  = thickness of base beam, m,

$H_1$  = thickness of damping material, m,

$l$  = length of beam, m,

$s$  = index number: 1, 2, 3, . . . ( $s=n$ ),

$T = H_1 / H$ , thickness ratio,

$\eta_1$  = shear loss factor of damping material, dimensionless,

$\eta_s = \Delta f_s / f_s$ , loss factor of sandwiched specimen, dimensionless,

$\rho_1$  = density of damping material,  $\text{kg/m}^3$ ,

$\rho$  = density of base beam,  $\text{kg/m}^3$ ,

### 6.3 RESULTS AND DISCUSSIONS

The field induced loss factor and shear modulus variation MRE samples evaluated as per ASTM standard. First two dominant modes of the force response function are considered for analysis. The field induced property enhancements are compared for CIP as well as the matrix material variation. This test will also enable to investigate the effect of frequency on the properties of MRE samples. The variation in damping property and shear modulus in different modes of vibration can be investigated.

#### 6.3.1 LOSS FACTOR VARIATION

The loss factor is a basic measure of damping present in the system. It is a measure of how fast the oscillations of the system decay. Higher the loss factor values, better is the damping capability of a material. The loss factor is generally approximated as the twice that of the damping ratio for the materials for viscoelastic materials. The damping ratio is a dimensionless property of the material which is the ratio of the damping coefficient to the critical damping coefficient of the material. To implement MRE as smart vibration isolation system, it is necessary to investigate the extent to which the loss factor can be improved with respect to the magnetic field so that it can be used in vibration control applications. The loss factor variation with respect to magnetic field, CIP percentage and the type of matrix material are plotted and shown in the Figures 6.5 to 6.8 below.

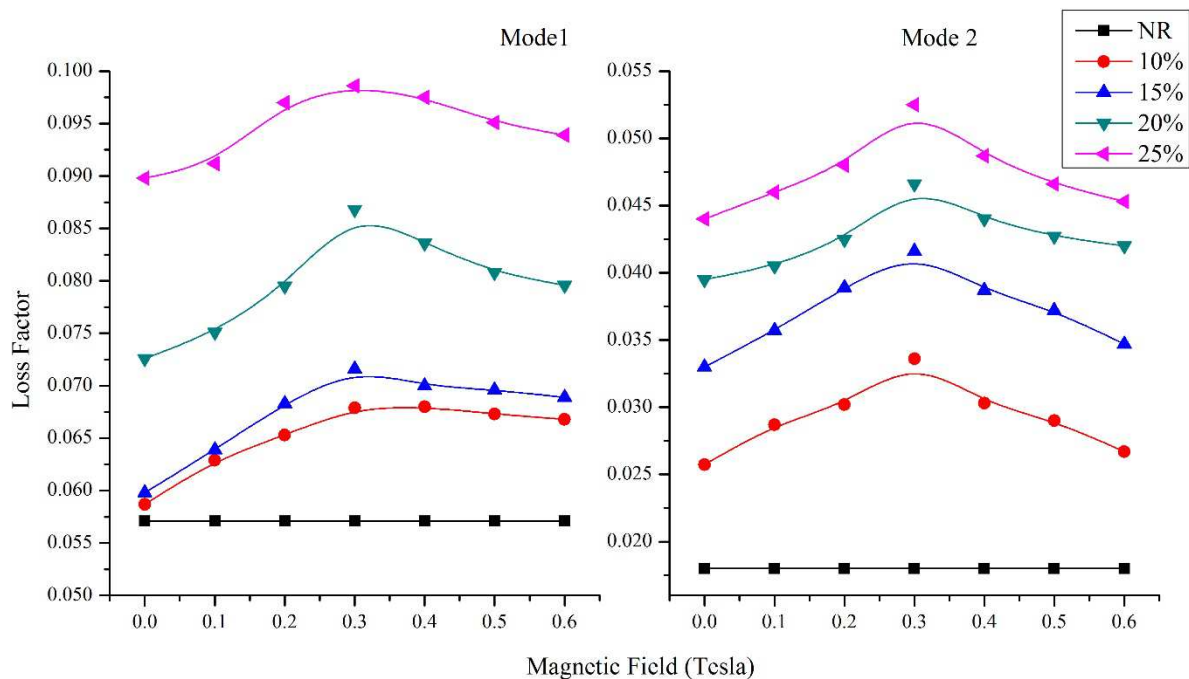
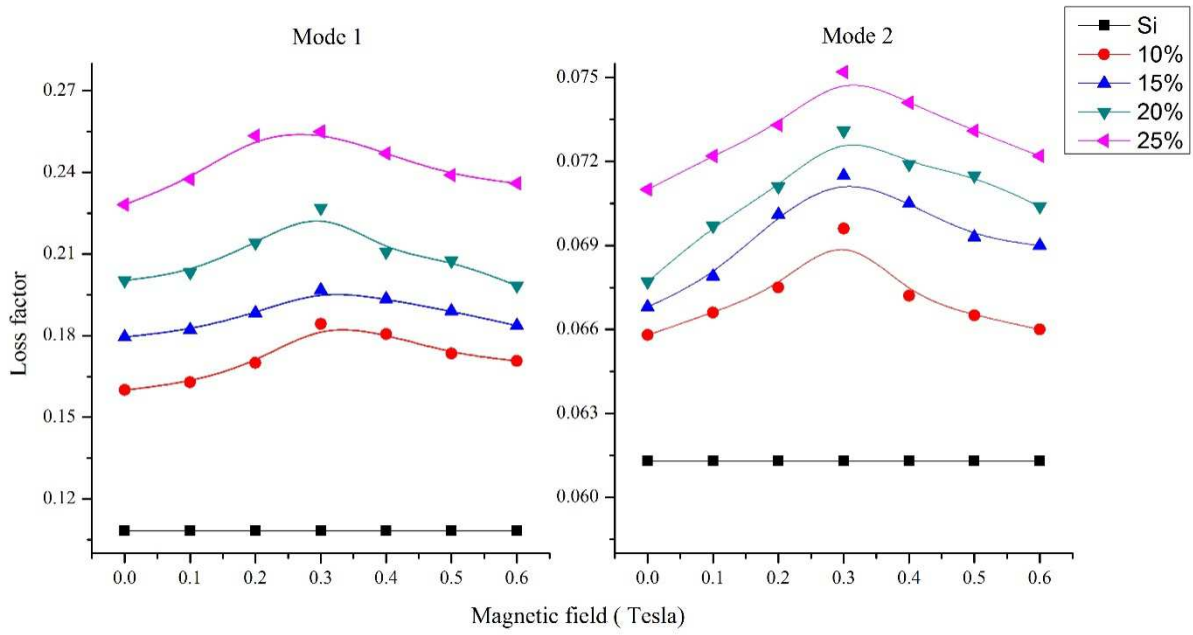
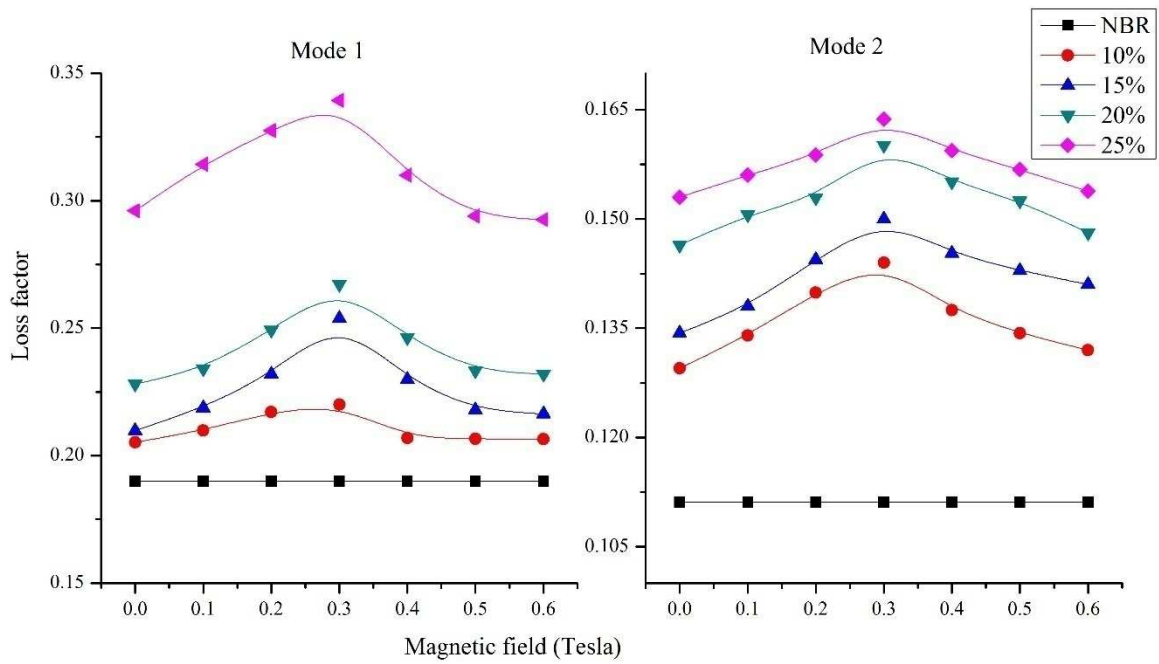


Figure 6.5. Loss factor variation of Natural rubber samples



**Figure 6.6.** Loss factor variation of Silicone-HTV rubber samples



**Figure 6.7.** Loss factor variation of Nitrile rubber samples

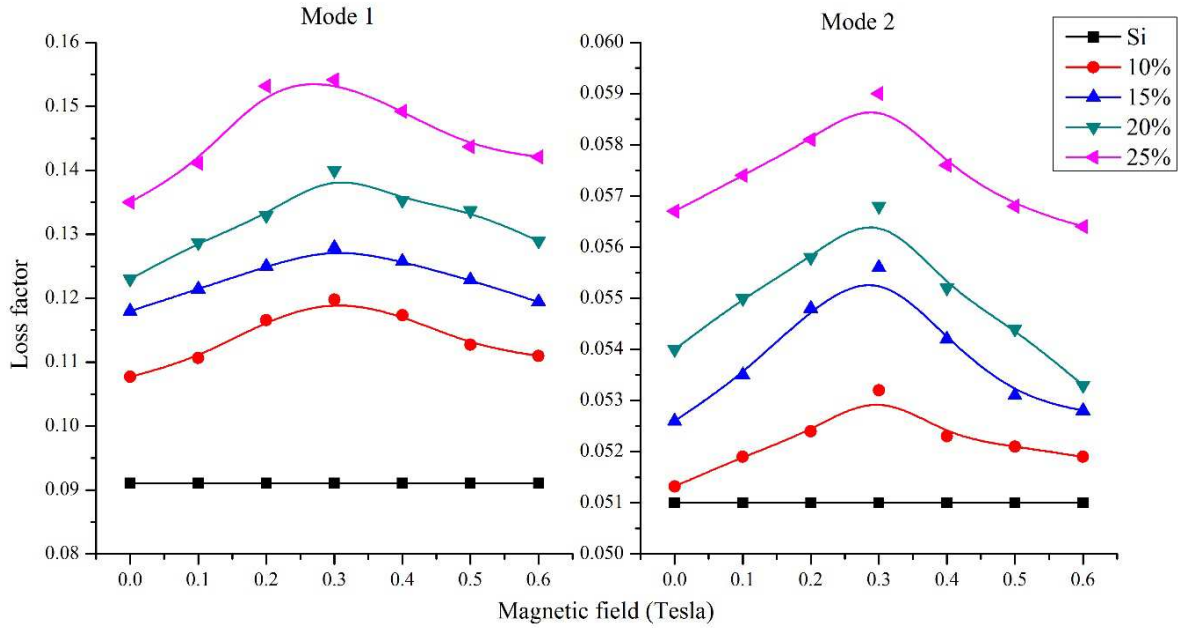


**Figure 6.8.** Loss factor variation of Silicone-RTV rubber samples

From the graph, it was observed that the properties of unfilled rubber are unaffected by the presence of magnetic field. This verifies that the experimental set-up is qualified to perform the field-induced property variations of MRE. As the particle content of the filler is increased the loss factor of the MRE is enhanced, but the loss factor registered for first mode is higher than the second mode. Under the magnetic field, the loss factor variation showed a unique trend. The loss factor initially increased with the increase in the magnetic field but further increase in the magnetic field beyond 0.3 Tesla reduced the loss factor. The field dependent variation in loss factor is observed to be consistent with the second mode which gives the indication that the field-induced enhancement does not vary with the higher modes. In other words, the field dependent loss factor increase is consistent with the increase in frequency, but the frequency increase is accompanied by the reduction in loss factor as generally observed in viscoelastic materials. The variation in field-induced change in the loss factor of all samples under all tested magnetic field and percentage CIP variation is listed in Table 6.1a and 6.1b.



**Table 6.1a:** Structural Loss factor values of the MRE samples

Percentage content /Applied field	Natural Rubber				Nitrile Rubber			
	$\eta_1$	% change	$\eta_2$	% change	$\eta_1$	% change	$\eta_2$	% change
0% / 0T	0.057	N/A	0.018	N/A	0.190	N/A	0.111	N/A
10% / 0T	0.059	2.98	0.026	42.94	0.205	8.053	0.130	16.67
10% / 0.1T	0.063	10.35	0.029	59.44	0.210	10.474	0.134	20.72
10% / 0.2T	0.065	14.56	0.030	67.78	0.217	14.263	0.140	26.04
10% / 0.3T	0.068	19.12	0.034	86.67	0.220	15.789	0.144	29.73
10% / 0.4T	0.068	19.30	0.030	68.33	0.207	8.947	0.138	23.87
10% / 0.5T	0.067	18.07	0.029	61.11	0.207	8.737	0.134	20.99
10% / 0.6T	0.067	17.19	0.027	48.33	0.207	8.684	0.132	18.92
15% / 0T	0.060	4.91	0.033	83.33	0.210	10.44	0.134	21.02
15% / 0.1T	0.064	12.11	0.036	98.33	0.219	15.16	0.138	24.32
15% / 0.2T	0.068	19.82	0.039	116.11	0.232	22.11	0.144	30.09
15% / 0.3T	0.072	25.61	0.042	131.11	0.254	33.63	0.150	35.14
15% / 0.4T	0.070	22.81	0.039	115.00	0.230	21.00	0.145	30.90
15% / 0.5T	0.070	22.11	0.037	106.67	0.218	14.68	0.143	28.74
15% / 0.6T	0.069	20.88	0.03	92.78	0.216	13.89	0.141	27.03
20% / 0T	0.073	27.37	0.040	119.44	0.228	20.05	0.146	31.89
20% / 0.1T	0.075	31.75	0.041	125.00	0.234	23.21	0.151	35.68
20% / 0.2T	0.080	39.47	0.043	136.11	0.249	31.16	0.153	37.75
20% / 0.3T	0.087	52.28	0.047	158.89	0.267	40.63	0.160	44.23
20% / 0.4T	0.084	46.67	0.044	144.44	0.246	29.63	0.155	39.73
20% / 0.5T	0.081	41.75	0.043	137.22	0.233	22.79	0.153	37.39
20% / 0.6T	0.080	39.649	0.04	133.33	0.232	22.11	0.148	33.42
25% / 0T	0.090	57.544	0.044	144.44	0.296	55.84	0.153	37.84
25% / 0.1T	0.091	60.000	0.046	155.56	0.314	65.42	0.156	40.54
25% / 0.2T	0.097	70.175	0.048	166.67	0.328	72.37	0.159	43.06
25% / 0.3T	0.099	72.982	0.053	191.67	0.339	78.63	0.164	47.48
25% / 0.4T	0.098	71.053	0.049	170.56	0.310	63.16	0.159	43.60
25% / 0.5T	0.095	66.842	0.047	158.89	0.294	54.74	0.157	41.26
25% / 0.6T	0.094	64.737	0.05	151.67	0.293	54.00	0.154	38.56

**Table 6.1b:** Structural Loss factor values of the MRE samples

Percentage content /Applied field	Silicone Rubber(RTV)				Silicone Rubber(HTV)			
	$\eta_1$	% change	$\eta_2$	% change	$\eta_1$	% change	$\eta_2$	% change
0% / 0T	0.108	N/A	0.061	N/A	0.091	N/A	0.051	N/A
10% / 0T	0.160	48.15	0.066	7.87	0.108	18.35	0.051	0.63
10% / 0.1T	0.163	50.79	0.067	9.18	0.111	21.57	0.052	1.76
10% / 0.2T	0.170	57.41	0.068	10.66	0.117	28.08	0.052	2.75
10% / 0.3T	0.184	70.65	0.070	14.10	0.120	31.63	0.053	4.31
10% / 0.4T	0.181	67.13	0.067	10.16	0.117	28.95	0.052	2.55
10% / 0.5T	0.173	60.56	0.067	9.02	0.113	23.86	0.052	2.16
10% / 0.6T	0.171	58.06	0.066	8.20	0.111	21.93	0.052	1.76
15% / 0T	0.180	66.20	0.067	9.51	0.118	29.67	0.053	3.14
15% / 0.1T	0.182	68.61	0.068	11.31	0.121	33.41	0.054	4.90
15% / 0.2T	0.188	74.35	0.070	14.92	0.125	37.36	0.055	7.45
15% / 0.3T	0.197	82.22	0.072	17.21	0.128	40.57	0.056	9.02
15% / 0.4T	0.194	79.17	0.071	15.57	0.126	38.18	0.054	6.27
15% / 0.5T	0.189	75.00	0.069	13.61	0.123	35.01	0.053	4.12
15% / 0.6T	0.184	70.09	0.069	13.11	0.119	31.23	0.053	3.53
20% / 0T	0.200	85.46	0.068	10.98	0.123	35.16	0.054	5.88
20% / 0.1T	0.203	88.24	0.070	14.26	0.129	41.43	0.055	7.84
20% / 0.2T	0.214	98.24	0.071	16.56	0.133	46.11	0.056	9.41
20% / 0.3T	0.227	110.09	0.073	19.84	0.140	53.85	0.057	11.37
20% / 0.4T	0.211	95.19	0.072	17.87	0.135	48.73	0.055	8.24
20% / 0.5T	0.208	92.16	0.072	17.21	0.134	46.91	0.054	6.67
20% / 0.6T	0.198	83.70	0.070	15.41	0.129	41.71	0.053	4.51
25% / 0T	0.228	111.29	0.071	16.39	0.135	48.35	0.057	11.18
25% / 0.1T	0.238	119.91	0.072	18.36	0.141	55.05	0.057	12.55
25% / 0.2T	0.254	134.72	0.073	20.16	0.153	68.32	0.058	13.92
25% / 0.3T	0.255	136.11	0.075	23.28	0.154	69.38	0.059	15.69
25% / 0.4T	0.247	128.70	0.074	21.48	0.149	63.99	0.058	12.94
25% / 0.5T	0.239	121.30	0.073	19.84	0.144	57.91	0.057	11.37
25% / 0.6T	0.236	118.52	0.072	18.36	0.142	56.15	0.056	10.59

From the table, it is deduced that the loss factor of MRE is a function of CIP filler content, matrix material and the magnetic field. The interfacial friction is the major contributor for damping in case of particle reinforced composites. As the particle content is increased the number of interfaces are also increased which in turn increases the friction. This improves the loss factor as evident from the increase in loss factor with increase in particle content. The field dependant loss factor is imparted to the MRE due to the magnetic force of attraction developed between them under the action of magnetic field. When the magnetic field is applied, the iron particles get aligned with the magnetic flux line which results force of attraction between the adjacent dipoles. The force of

attraction resists the interfacial friction which further increases the friction under magnetic field. At lower magnetic fields, the force of attraction between the adjacent particles is less, but it is enough to create a relative motion between the matrix and the iron particles. It results in interfacial friction amounting to energy dissipation which manifests as an overall enhancement in damping property. However, as the field is increased, the attraction between the adjacent iron particles is high enough to cease the relative motion between the iron particles and matrix. Under this condition, the particles are arrested as friction cannot overcome the magnetic force of attraction and results in decrease of loss factor as the field is increased beyond 0.3 Tesla. Similar results were observed by S.K. Dwivedy et.al (2013) and Xin-long Gong et.al. (2008).

From the graph, it is also observed that the loss factor registered for unfilled NBR is the highest and for NR it is the least. This trend was consistent even after adding CIP at different percentages. Addition of ferromagnetic fillers does not alter the trend in which the loss factor is varied. This indicates that the loss factor variation of MRE under zero fields is the function of damping property of the matrix under unfilled state. However, the variation depends on the type of matrix material. With the magnetic field, the variation rate was different even though every matrix material showed enhancements when subject to magnetic field. The Si-RTV sample showed better percentage improvement of about 135% at 0.3 Tesla field than other samples. Natural rubber at 0.3 Tesla showed an improvement of 93%. But the Si-HTV and NBR showed lesser improvement which indicates that the influence of matrix material is predominant on the relative changes in properties. The trend observed for the second mode was similar to the first mode, but the loss factor values were lesser than the first mode.

### **6.3.2 SHEAR MODULUS VARIATION**

Shear modulus of resilient element is a critical parameter which reflects the isolation performance of an isolator. In the current work, the shear modulus of MRE samples is evaluated by sandwich beam tests. The property variations are studied at different magnetic fields to analyze the extent to which the shear property can be controlled. The Figures 6.9 to 6.12 show the shear modulus variation of the samples at different magnetic fields.

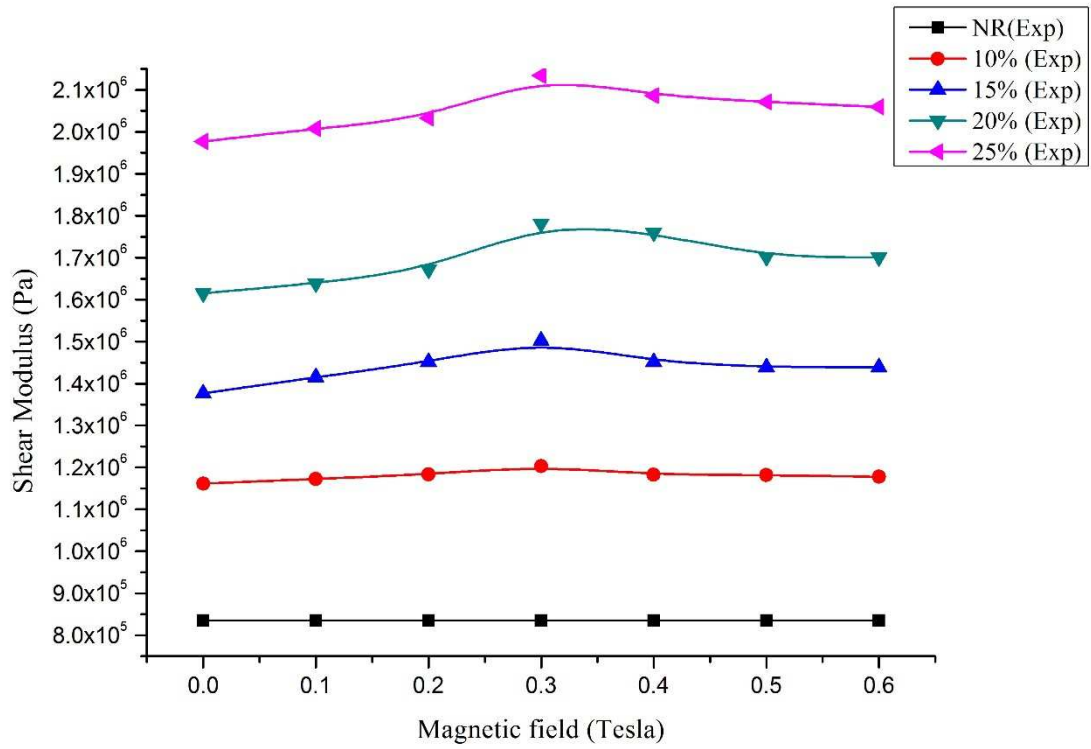


**Figure 6.9.** Shear modulus variation of Natural rubber samples

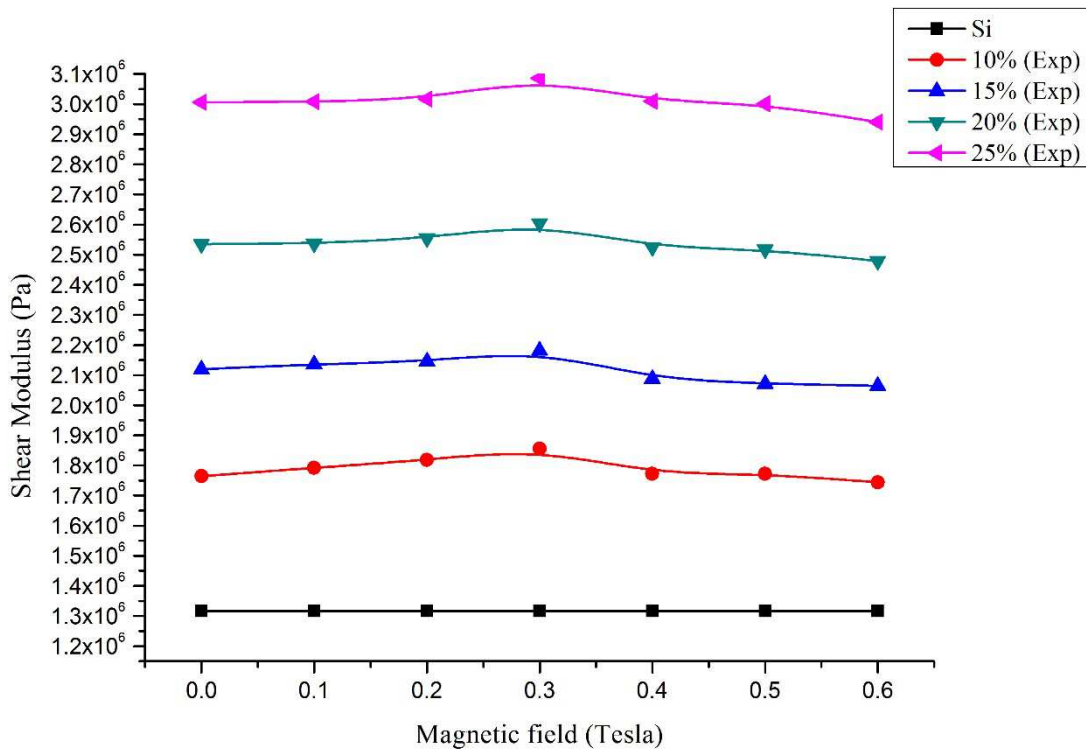


**Figure 6.10.** Shear modulus variation of Silicone-HTV rubber samples

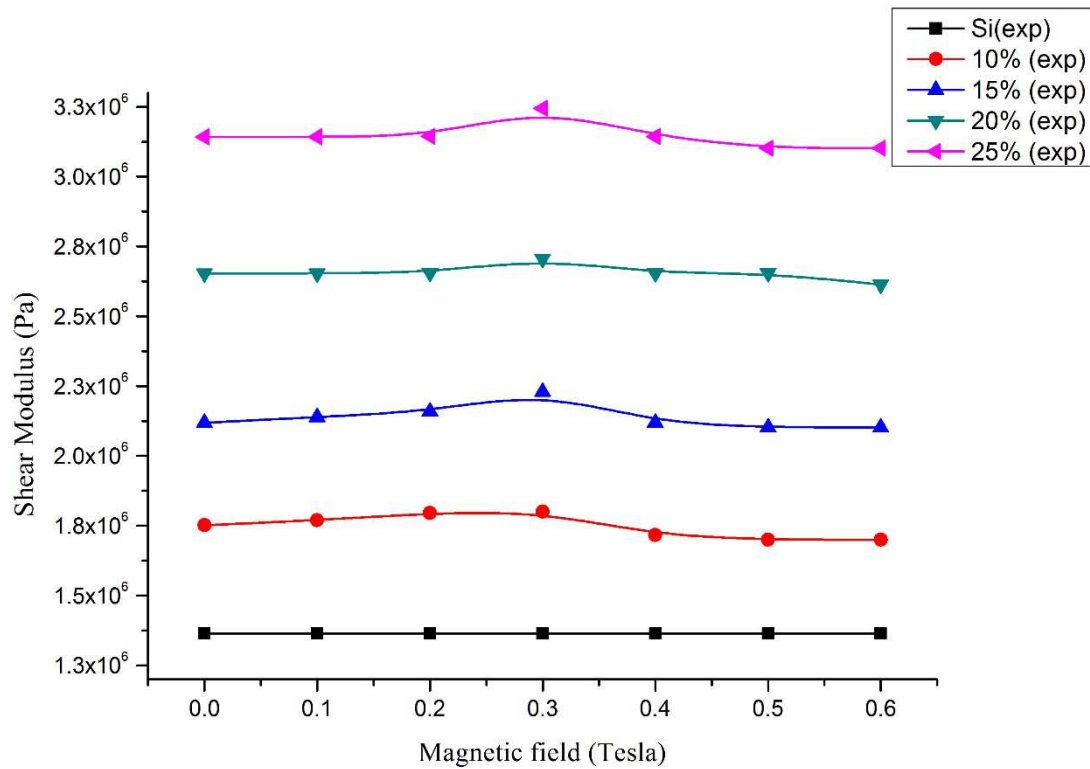


**Figure 6.11.** Shear modulus variation of Silicone-RTV rubber samples

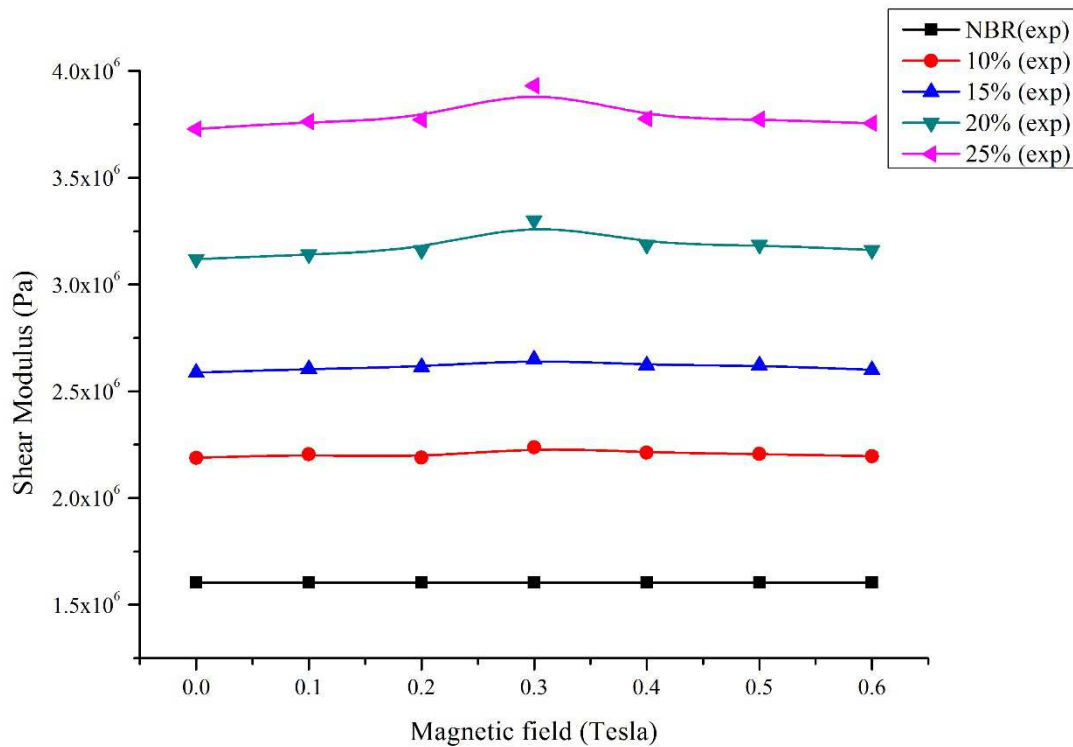


**Figure 6.12.** Shear modulus variation of Nitrile rubber samples

The graphs show that the trend of shear modulus variation is similar to the loss factor, i.e. even the zero-field modulus of the matrix is influenced by the addition of CIP.

The application of magnetic field did not affect the unfilled samples. The plots were like that of the loss factor i.e. initially it increased and after 0.3 Tesla, it did not show any improvement. The field-induced changes depend on the type of matrix material. The relative change of shear modulus of Si-RTV was about 14% and natural rubber was about 10% for the 25% sample. But the relative improvements of NBR and Si-HTV were lesser at 5% and 6.5% respectively. The following Table 6. 2a shows the comparison of natural rubber and nitrile rubber samples and 6.2 b shows the experimental results of Silicone HTV and RTV samples.

**Table 6.2a:** Shear modulus values

Percentage content /Applied field	Natural Rubber	Nitrile Rubber
	G (Pa)	G(Pa)
0% / 0T	8.35E+05	1.60E+06
10% / 0T	1.16E+06	2.19E+06
10% / 0.1T	1.17E+06	2.20E+06
10% / 0.2T	1.18E+06	2.19E+06
10% / 0.3T	1.20E+06	2.24E+06
10% / 0.4T	1.18E+06	2.21E+06
10% / 0.5T	1.18E+06	2.21E+06
10% / 0.6T	1.18E+06	2.20E+06
15% / 0T	1.38E+06	2.59E+06
15% / 0.1T	1.42E+06	2.61E+06
15% / 0.2T	1.45E+06	2.62E+06
15% / 0.3T	1.50E+06	2.65E+06
15% / 0.4T	1.45E+06	2.62E+06
15% / 0.5T	1.44E+06	2.62E+06
15% / 0.6T	1.44E+06	2.60E+06
20% / 0T	1.62E+06	3.12E+06
20% / 0.1T	1.64E+06	3.14E+06
20% / 0.2T	1.67E+06	3.16E+06
20% / 0.3T	1.78E+06	3.30E+06
20% / 0.4T	1.76E+06	3.19E+06
20% / 0.5T	1.70E+06	3.19E+06
20% / 0.6T	1.70E+06	3.16E+06
25% / 0T	1.98E+06	3.73E+06
25% / 0.1T	2.01E+06	3.76E+06
25% / 0.2T	2.03E+06	3.77E+06
25% / 0.3T	2.13E+06	3.93E+06
25% / 0.4T	2.09E+06	3.78E+06
25% / 0.5T	2.07E+06	3.77E+06
25% / 0.6T	2.06E+06	3.76E+06

**Table 6.2b: Shear modulus values**

Percentage content /Applied field	Silicone Rubber(HTV)	Silicone Rubber(RTV)
	G(Pa)	G(Pa)
0% / 0T	1.32E+06	1.36E+06
10% 0T	1.76E+06	1.75E+06
10% / 0.1T	1.79E+06	1.77E+06
10% / 0.2T	1.82E+06	1.80E+06
10% / 0.3T	1.86E+06	1.80E+06
10% / 0.4T	1.77E+06	1.72E+06
10% / 0.5T	1.77E+06	1.70E+06
10% / 0.6T	1.77E+06	1.70E+06
15% / 0T	2.12E+06	2.12E+06
15% / 0.1T	2.14E+06	2.14E+06
15% / 0.2T	2.15E+06	2.16E+06
15% / 0.3T	2.19E+06	2.23E+06
15% / 0.4T	2.14E+06	2.12E+06
15% / 0.5T	2.12E+06	2.10E+06
15% / 0.6T	2.12E+06	2.10E+06
20% / 0T	2.54E+06	2.65E+06
20% / 0.1T	2.54E+06	2.65E+06
20% / 0.2T	2.55E+06	2.66E+06
20% / 0.3T	2.60E+06	2.71E+06
20% / 0.4T	2.58E+06	2.65E+06
20% / 0.5T	2.56E+06	2.65E+06
20% / 0.6T	2.55E+06	2.61E+06
25% / 0T	3.01E+06	3.14E+06
25% / 0.1T	3.01E+06	3.14E+06
25% / 0.2T	3.02E+06	3.14E+06
25% / 0.3T	3.09E+06	3.24E+06
25% / 0.4T	3.03E+06	3.14E+06
25% / 0.5T	3.01E+06	3.10E+06
25% / 0.6T	3.01E+06	3.10E+06

To analyze the field induced property variations, the beam is assumed as a SDOF system. The variation in shear modulus is associated with the natural frequency change of MRE under the magnetic field. The natural frequency of a beam in fixed-free condition is given by,

$$\omega_n = \frac{1}{2\pi} \sqrt{\frac{k}{m}} \text{ Hz} \quad (6.10)$$

Where  $k$  is the stiffness of the system in N/m and  $m$  is the modal mass in kilograms. For a fixed-free condition beam, the stiffness can be calculated by,

$$k = \frac{3EI}{l^3} \quad (6.11)$$

Where,  $E$  is the young's modulus of the material in Pascal,  $I$  is the second moment of inertia in  $m^4$  and  $l$  is the length of the beam in meters. The young's modulus and shear modulus are related by the Poisson's ratio by,

$$G = \frac{E}{2(1+\nu)} \quad (6.12)$$

From the equations 6.10 to 6.12, it is clear that the magnetic field results in an improvement of the shear modulus of the MRE. Under magnetic field, the carbonyl iron particle in the matrix tries to get aligned in the system thereby increasing the stiffness in the flux direction. Increased stiffness enhances the shear modulus without altering the system parameters. It was also observed that the increase in loss factor as well as shear modulus was only up to a field of 0.3 Tesla and then it reduced. This can be attributed to the fact that the property enhancement is due to the relative motion between the iron particles and the polymer matrix. At relatively lower magnetic field, the relative motion is higher because of the lower force of attraction between the adjacent particles. At higher field strengths, the force attraction is strong enough to arrest the relative motion. This results in a downward trend in field induced property changes. However, it was also observed that the samples showed better zero field properties as the percentage concentration of iron powders was increased. This is attributed to the reinforcing effect by the addition of iron particles. Comparing the performance of the MRE samples prepared from different types of matrices, it is clear that more the modulus of the matrix material, more is the modulus of the respective MRE sample. The Figure 6.14 shows the comparison of the shear modulus of the pure samples.



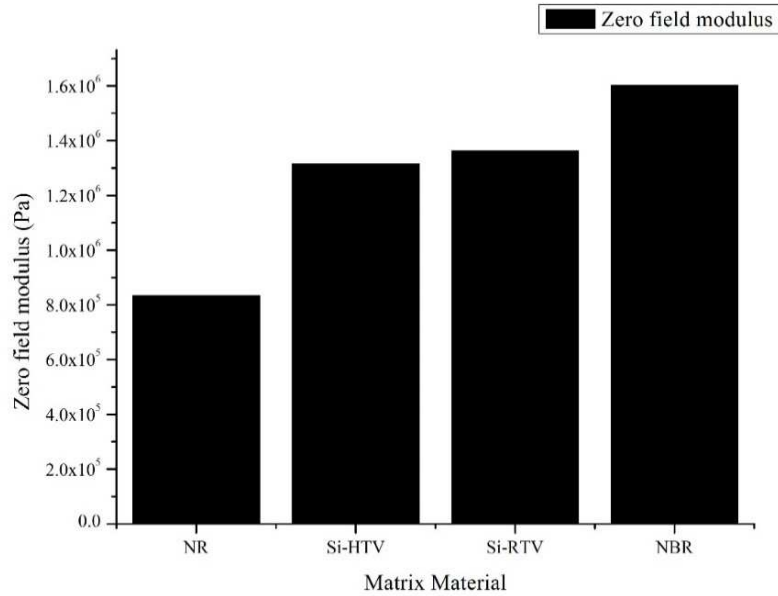


**Figure 6.13.** Modulus values of pure samples

The relative improvement of Nitrile rubber was less compared to other matrix materials, which can be attributed to a higher initial modulus. The sample with softer matrix, i.e. natural rubber and silicone-RTV showed a higher relative change in the properties even though modulus or the loss factor values are less than silicone and nitrile rubber. For the HTV matrix materials which have higher pre-cure viscosity, mixing iron powder is also difficult and mixing losses may be more, which is evident from the higher percentage of error in theoretical calculations. The error was more for the MRE samples with higher percentage concentration for all the matrices. The difference is attributed to the loss of CIP particle during mixing using the mastication process.

## CHAPTER 7

### CONCLUSIONS AND SCOPE FOR FUTURE WORK

The current research was focused on experimentally characterizing MRE to realize it as a vibration mitigating device. The influence of the matrix and the particle concentration on the field-induced enhancement in damping is studied. Basic studies on the understanding the influence of filler particle size and the dimension of the MRE are carried out. These studies have been extended to understand the frequency and strain dependent viscoelastic properties of MRE. A four-parameter viscoelastic model is presented to simulate the field-induced viscoelastic properties. As an application problem, the damping capability of MRE was studied by employing it as material for constrained layer treatment. The experimental investigation yielded the following conclusions.

1. The damping characteristics of MRE depend on the intrinsic damping of the parent matrix material. The addition of fillers relatively enhances the damping of MRE. The enhancement in damping of MRE with lower damping matrix is comparatively less than the matrix with higher damping. The zero-field enhancement of Si-RTV for 25% fillers is about 86% but for Nitrile, it is 78% and for Si-HTV it was only 21%. The field-induced enhancement of damping characteristics is a function of the matrix material. Reduced restrictions to the motion of the fillers within the matrix promote better interactions among the fillers. Increased interactions result in increased interfacial friction and enhance the field induced damping of the MRE with the softer matrix. The Si-RTV which is the softest among the tested samples showed a 26% relative improvement in damping at 0.3 Tesla for the 25% sample. Whereas, the 60%-40% Si-PU hybrid which higher damping showed only 5% relative improvement.
2. Increased reinforcing effect resulted by the fillers enhanced the damping as the number of interfaces are increased. Further increase in the filler content imparts brittle nature to the MRE. The optimum damping characteristics are obtained for a concentration of 25% volume fraction of the fillers. This includes the cumulative contribution of intrinsic damping of the matrix and the matrix-filler interactions.
3. The intensity of magnetic field has a significant influence on the damping characteristics of MRE. The interaction between the fillers and the matrix is pronounced up to a magnetic field of 0.3 Tesla. Increase in the magnetic field

above 0.3 Tesla results in domination of the filler-filler interaction which results in reduced damping characteristics of MRE.

4. The basic studies on the filler particle size revealed its influence on the characteristics of MRE. The MRE with smaller size particle is beneficial in enhancing the damping as the number of interfaces is increased due to higher surface area. The smaller-sized fillers result in agglomerations, which function as larger size dipoles resulting in enhanced magnetic-field induced effect. The loss factor improvement of the smaller sized-MRE is about 116%, and the larger sized MRE is about 50% for a magnetic field of 0.3 Tesla.
5. The hybrid MRE is beneficial in enhancing the intrinsic damping characteristics of MRE. The damping of hybrid MRE includes the additional contribution arising from the interface between the two matrices. The friction at the matrix -matrix interface imparts additional frictional energy dissipation resulting better damping compared to regular matrices. The preparation of hybrid MRE is complicated since it depends on the working time of both the matrices. This results in difficulty in mixing the two polymers as the percentage of the matrix with the lower working time increases.
6. The stiffness of the test sample is a function of the geometry. For the same cross section, increasing the thickness reduces the stiffness and alters the damping characteristics. The thinner MRE samples exhibit better damping characteristics. The loss factor of 4 mm thick MRE is about 70% more than the 16 mm thick MRE. The magnetic field induced damping of MRE depends on the thickness. Uniform filed distribution within thinner MRE samples result better filed induced damping compared to thicker ones.
7. The viscoelastic properties of the MRE depended on the operating conditions like frequency and strain amplitude. Increased frequency results in a stiffness increase due to the reduced time available for the relaxation of polymer chains. Increased strain reduces the stiffness of the MRE associated with the Payne effect seen in rubbers. The stiffness reduction is almost 50% when the strain amplitude was increased from 0.075 mm to 0.15 mm.
8. An application of MRE as a constrained layer damping was experimentally carried out by following the ASTM E-756-05 standard. The damping properties of all the samples were observed to be increasing up to 0.3 Tesla, and any more

increase in the magnetic field resulted in deterioration of the damping properties. Shear modulus also showed a similar trend since expression for finding the modulus is a function of the loss factor. It can be concluded that non-homogeneous magnetic fields are not an efficient way of conducting experiments. The size of the pole of the magnet should be at least equal to the cross-section of the test sample.

9. A modified four parameter mathematical model was developed based on the existing linear viscoelastic model to simulate the behaviour. The MATLAB optimization tool box was employed for the modeling process. Stress-strain experimental data of silicone sample at 15 Hz operating frequency was employed for parameter identification. The parameter identification was done for 25% RTV-Si at zero field and 0.3 Tesla field. The developed model successfully simulated the experimental results.

## **7.1 SCOPE FOR FUTURE WORK**

The current study mainly focused on the experimental characterization of MRE prepared by making use of different matrix materials by varying the percentage content of carbonyl iron powders.

- The main focus of the current study was on the resonant region of the frequency response curves. Since many applications of viscoelastic materials involve frequency of operation less than 100 Hz, the behaviour of the MRE at lower frequency needs to be addressed. Samples with lower natural frequency need to be prepared to understand the magnetic-field induced frequency changes of the MRE samples.
- Even though a small comparison work on the influence of CIP average diameter on the damping properties was done, it is not conclusive. To properly investigate the influence of particle size, more experiments with different particle size need to be conducted. Since CIP is not available in different sizes, soft iron particles could be used as an alternative. Different-sized particles could be prepared using the ball milling process, and the products could be used for preparing MRE with different-sized particles.
- The influence of strain on the damping of MRE needs to be carefully investigated. The current work focused on only two values of strain amplitudes in the linear viscoelastic range. The behaviour of MRE in the non-

linear region also needs to be investigated thoroughly. The influence of magnetic field on the non-linearity also needs to be addressed.

- The hybrid MRE showed better damping properties than conventional in the current investigation. Due to the difference in the working time of the polymers, mixing was difficult. The tested samples contained same weight percentages and higher percentages were not performed due to difficulty in mixing. By employing samples with lower pre-cure viscosity and higher working time, the influence of different volume concentration on the performance can be done.
- Constrained layer damping can be carefully applied by making use of a mechanism to apply magnetic field uniformly across the whole length of the beam. Non-contact type data acquisition could be used for better accuracy in displacement measurement. Finite-element studies can be performed by making use beam theories.
- MRE isolator/damper can be designed by incorporating an electromagnetic coil. The characterization of the damper needs to be done by subjecting it to different types of input conditions. Different control strategies need to be applied to investigate its feasibility as a tuned vibration damper.

## REFERENCES

- Alam M.S. et al., (2007a). "Utilizing the shape memory alloys to enhance the performance and safety of civil infrastructure: a review." *Can. J. Civ. Eng.* 34: 1075-1087 (2007).
- Alam M.S. et al., (2008b). "Experimental investigation on the seismic behavior of beam column joints reinforced with super-elastic shape memory alloys." *Journal of Earthquake Engineering*, 12:1205–1222, 2008.
- ASTM-E756-05 (2013). "Standard Test Method for Measuring Vibration-Damping Properties of Materials." *ASTM standard*.
- Basdogan Cagatay et.al. (2010). "Characterization of frequency-dependent material properties of human liver and its pathologies using an impact hammer." *Medical Image Analysis*, 15:45–52.
- Bellan.C, and Bossis. G (2002). "Field dependence of viscoelastic properties of MR Elastomers." *International Journal of Modern Physics B*, Vol. 16, Nos. 17 & 18 (2002) 2447-2453.
- Bohdana Marvalova (2008). "Modelling of Magnetosensitive Elastomers." *Recent Advances in Modelling and Simulation*, Giuseppe Petrone and Giuliano Cammarata (Ed.), ISBN: 978-3-9 02613-25-7.
- Boltežar M. and Koblar D. (2013). "Evaluation of the Frequency-Dependent Young's Modulus and Damping Factor of rubber from Experiment and Their Implementation in a Finite-Element Analysis." *Experimental Techniques*, Society for Experimental Mechanics.
- Bose Holger, Rabindranath R. and Ehrlich J. (2012). "Soft magnetorheological elastomers as new actuators for valves." *Journal of Intelligent Material Systems and Structures* ,23: 989.
- Bossis G. et.al. (2006). "Micromechanical analysis of an elastomer filled with particles organized in chain-like structure." *J Mater Sci*, 41:5941–5953.
- Carlson David, Jolly R (2000b). "MR fluid, foam and elastomer devices." *Mechatronics* 10:555-569.
- Chen Lin and Jerrams Steve (2011). "A Rheological Model of the Dynamic Behaviour of Magnetorheological Elastomers". *Articles.Paper 9*. <http://arrow.dit.ie/cerart/9>.

- Chung D.D.L. (2001). "Review Materials for vibration damping." *Journal of materials science*, 36(2001) 5733 – 5737.
- Claeysen. F. and Lhermet N. (2002). "Actuators based on giant magnetostrictive materials." *Actuator 2002*, 8th International Conference on New Actuators, 10 – 12 June 2002, Bremen, Germany
- Cunefare K.A. and Lerner A. (2007). "Performance of MRE-based Vibration Absorbers." *Journal of Intelligent Material Systems and Structures* ,19: 551.
- David Meeker (2009). "Finite Element Method Magnetics.", 2005:1-155.
- Davis L.C. (1999). "Model of magnetorheological elastomers." *Journal of applied physics*, 85, 3348.
- DemchukS. A. and Kuz'minV. A.(2002) . "Viscoelastic properties of magnetorheological Elastomers in the regime of dynamic deformation." *Journal of Engineering Physics and Thermophysics*, Vol. 75, No. 2.
- DongX. et.al. (2013). "Predicating magnetorheological effect of magnetorheological elastomers under normal pressure." *Journal of Physics: Conference Series*, 412:012035.
- DwivedyS.K., NayakB., and Murthy K.S.R.K. (2011a). "Dynamic analysis of magnetorheological elastomer-based sandwich beam with conductive skins under various boundary conditions." *Journal of Sound and Vibration* 330: 1837–1859.
- DwivedyS.K., NayakB., and Murthy K.S.R.K. (2011b). "Dynamic stability of magnetorheological elastomer based adaptive sandwich beam with conductive skins using FEM and the harmonic balance method." *International Journal of Mechanical Sciences*, 77:205–216.
- ElejabarrietaJ , Agirre-OlabideIker, Berasategui J, and Bou-Ali M. (2014). "Characterization of the linear viscoelastic region of magnetorheological elastomers." *Journal of Intelligent Material Systems and Structures*,
- Farjoud A. et.al. (2011). "Experimental Investigation of MR Squeeze Mounts." *Journal of Intelligent Material Systems and Structures* , 22: 1645.
- Funt J.M. (1987). "Dynamic testing and reinforcement of rubber." Rubber Division, American chemical society.

- George Lucaet al. (2005). "Passive, active and semi-active systems in Civil engineering." *The bulletin of the polytechnic institute from IASI*, 3-4, 2005.
- Ginder J. M, Peter J R, and J Klingenberg D (1998a)." Electro-and Magneto-rheology." *Current Opinion in Colloid & Interface Science*, 3:373-381.
- Ginder J. Met.al. (1999b). "Magnetorheological Elastomers: Properties and Applications." *SPIE Conference on Smart Materials Technologies*, 3675:131-138.
- Giurgiutiu et al., (2000). "Energy-Based Comparison of Solid-State Actuators." Report # *USC-ME-LAMSS-2000-102*, March 1, 2000.
- Goddard, Kemp and Lane(1997). "An overview of Smart TechnologyPackaging Technology and Science, Volume 10, pp 129 – 143.
- Gong X.L., Chen L; Li W (2008a)"Damping of Magnetorheological Elastomers." *Chinese journal of Chemical Physics*, Vol. 21:581-585.
- Gong X.L ,Jian-feng Li (2008b)"Dynamic damping property of magnetorheological elastomer." *J. Cent. South Univ. Technol.* 15(s1): 261–265.
- Gong X.L et.al. (2012c)."Investigation on the mechanism of damping behavior of magnetorheological elastomers." *Smart Mater. Struct.* 21 :125015 (11pp).
- GongX L et.al. (2010d)."Investigation of the durability of anisotropic magnetorheological elastomers based on mixed rubber." *Smart Mater. Struct.* 19: 085008 (10pp).
- Gong X.L et.al (2006e). "Effects of rubber/magnetic particle interactions on the performance of magnetorheological elastomers." *Polymer Testing*, 25:262–267.
- GongX.L., ZhangX.Z. and Zhang P.Q.(2005f)."Fabrication and characterization of isotropic magnetorheological elastomers." *Polymer Testing*, 24:669–676.
- Gong X.L et.al (2005g)."New magnetorheological elastomers based on polyurethane/Si-rubber hybrid." *Polymer Testing*, 24: 324–329.
- Gong X.L. et.al. (2011h). "Interfacial friction damping properties in magnetorheological elastomers." *Smart Mater. Struct.*, 20 035007 (8pp).
- Gong X.L et.al. (2007i)"Investigation on magnetorheological elastomers based on natural rubber." *J Mater Sci*, 42:5483–5489.



- Gong X.L., Chen L. and Li W.H. (2007j). "Microstructures and viscoelastic properties of anisotropic magnetorheological elastomers." *Smart Mater. Struct.* 16 : 1–6.
- Gong X.L. et al. (2012k). "The investigation on the nonlinearity of plasticine-like magnetorheological material under oscillatory shear rheometry." *J. Rheol.*, 56(6), 1375-1391.
- Gong X.L. et al. (2009l) "Radiation Vulcanization of Magnetorheological Elastomers Based on Silicone Rubber." *Chinese journal of chemical physics*, volume 22, number 5.
- Gong X.L. and Deng (2007m). "Adaptive Tuned Vibration Absorber based on Magnetorheological Elastomer." *Journal of intelligent material systems and structures*, Vol. 18:1205-1210.
- Gong X.L. and Deng (2008n). "Application of magnetorheological elastomer to vibration absorber." *Communications in Nonlinear Science and Numerical Simulation*, 13:1938–1947.
- Sun T.L. and Gong X.L. et al. (2008). "Study on the damping properties of magnetorheological elastomers based on cis-polybutadiene rubber." *Polymer Testing*, 27: 520–526.
- Gordaninejad F., Wang X. and Mysore Praveen (2012a). "Behavior of thick magnetorheological elastomers." *Journal of Intelligent Material Systems and Structures*, 23(9) 1033–1039.
- Gordaninejad F., David Y. and Wang X. (2011b). "A New Magnetorheological Mount for Vibration Control." *Journal of Vibration and Acoustics*, Vol. 133 / 031003-1.
- Hu Wei (2005). "Development of magnetorheological fluid elastomeric dampers for helicopter stability augmentation." PhD thesis, Faculty of the Graduate School of the University of Maryland.
- J. P. Rich and P. S. Doyle et al., (2012). "Magneto rheology in an aging, yield stress matrix fluid." *Rheol Acta* (2012) 51:579–593.
- John R. Brauer (2008). "Magnetic actuators and sensors." *John Wiley Publications*, 2005:7-28.
- Jolly M.R., Carlson J.D. and Muñoz B.C. (1996a). "A model of the behaviour of magnetorheological materials." *Smart Mater. Struct.*, 5 : 607–614.

Jones (2001). "Handbook of Viscoelastic Vibration Damping." *John Wiley Publications*; 2001:1-410.

Juan de Vicente, Daniel J. Klingenberg and Roque Hidalgo-Alvarez (2010). "Magnetorheological fluids: a review." *Soft Matter*, 2011, 7, 3701.

Jung H.J., Eem S.H. and Koo J.H. (2012). "Modeling of Magneto-Rheological Elastomers for Harmonic Shear Deformation." *IEEE Transactions on Magnetics*, Vol. 48, No. 11.

Kaleta J., Królewicz M. and Lewandowski D. (2011). "Magneto mechanical properties of anisotropic and isotropic magnetorheological composites with thermoplastic elastomer matrices." *Smart Mater. Struct.*, 20: 085006 (12pp).

Ke-xiang W. et al. (2008). "Experimental investigation on vibration characteristics of sandwich beams with magnetorheological elastomers cores." *J. Cent. South Univ. Technol.*, 15(s1): 239–242.

Kim Y.K. et al. (2010). "Vibration Isolation Strategies using Magneto-Rheological Elastomer for a Miniature Cryogenic Cooler in Space Application." *IEEE/ASME International Conference on Advanced Intelligent Mechatronics*, 978-1-4244-8030-2/10.

Kramarenko E.Yu. et al. (2007a). "Effect of a homogeneous magnetic field on the viscoelastic behavior of magnetic elastomers." *Polymer*, 48: 488-495.

Kramarenko E. Y. et al. (2011b). "Low Frequency Rheology of Magnetically Controlled Elastomers with Isotropic Structure." *Polymer Science, Ser. A*, Vol. 52, No. 12, pp. 1344–1354.

Lakes R. (2009). "Viscoelastic Materials.", *Cambridge University Press*. 1-480.

Li W and Zhang (2008a). "Research and Applications of MR Elastomers." *Recent Patents on Mechanical Engineering*, 1161-166.

Li W et al. (2011b) "Experimental investigation of the vibration characteristics of a magnetorheological elastomer sandwich beam under non-homogeneous small magnetic fields." *Smart Mater. Struct.* 20:127001 (7pp).

Li W. et al. (2008c). "Analysis and fabrication of patterned magnetorheological elastomers." *Smart Mater. Struct.* 17: 045001 (5pp).

Li W et al. (2010d). "Creep and recovery behaviors of magnetorheological elastomers." *Front. Mech. Eng. China*, 5(3): 341–346.

- Li W. H., Zhou Y. and Tian T. F. (2010e). “Viscoelastic properties of MR elastomers under harmonic loading.” *Rheol Acta*, 49:733–740.
- Li W., Zhang X. and Gong X. L. (2008f). “An effective permeability model to predict field-dependent modulus of magnetorheological elastomers.” *Communications in Nonlinear Science and Numerical Simulation*, 13:1910–1916.
- Li W. H. and Zhang X. Z. (2009g). “A study of the magnetorheological effect of bimodal particle based magnetorheological elastomers.” *Smart Mater. Struct.*, 19:035002 (8pp).
- Li W. H., Zhang X. Z. and Du H. (2012h). “Development and simulation evaluation of a magnetorheological elastomer isolator for seat vibration control.” *Journal of Intelligent Material Systems and Structures*, 23(9) 1041–1048.
- Lu X. et al. (2011). “Mechanical and structural investigation of isotropic and anisotropic thermoplastic magnetorheological elastomer composites based on poly (styrene-b-ethyleneco-butylene-b-styrene) (SEBS).” *Rheol Acta*, 10.1007/s00397-011-0582-x.
- Luca G. S. et al. (2005). “Passive, active and semi-active control systems in Civil engineering.” *Buletinul Institutului Politehnic din IASI, Tomul LI(LV)*, Fasc. 2-4.
- Melenev P. et al. (2011). “Modeling of the Field-Induced Plasticity of Soft Magnetic Elastomers.” *Journal of intelligent material systems and structures*, Vol. 22:531.
- Monner H. P. (2005). “Smart materials for active noise and vibration reduction.” Keynote Paper Novem – *Noise and Vibration: Emerging Methods*, Saint-Raphaël, France, 18-21 April 2005.
- Naimzad M. et al. (2011). “MREs Development and Its Application on Miniature Gripper.” *International Conference on Advanced Materials Engineering*, vol. 15:75-79.
- Ni Y. Q., Ying Z. G. and Chen Z. H. (2011). “Micro-vibration suppression of equipment supported on a floor incorporating magnetorheological elastomer core.” *Journal of Sound and Vibration*, 330:4369–4383.
- Ogden R. W., A. Dorfmann and Saccoccia G. (2004). “Universal relations for non-linear magnetoelastic solids.” *International Journal of Non-Linear Mechanics*, 39:1699 – 1708.
- Opie S. and Yim W. (2010). “Design and Control of a Real-Time Variable Modulus Vibration Isolator.” *Journal of Intelligent Material Systems and Structures*, 22: 113.

- Pagel.K et al. (2015). “Smart-smart materials for smart applications.”*Procedia CIRP*:36 (2015 ) 211 – 216.
- PanJie, LinT. R., Farag N H. (2005). “Evaluation of frequency dependent rubbermount stiffness and damping by impact test.” *Applied Acoustics*,66 : 829–844.
- Popp K.M.and, LiW.H. et.al. (2009).“MRE properties under shear and squeeze modes and applications.” *Journal of Physics: Conference Series*, 149:012095.
- PossingerT. et.al. (2013)“Influence of interfacial adhesion on the mechanical response of magneto-rheological elastomers at high strain.”*Microsyst Technol*, DOI 10.1007/s00542-013-2036-0.
- ReitichF. and Jolly M.R. et.al. (1999)“Estimation of the Effective Permeability in Magnetorheological Fluids.” *Journal of Intelligent Material Systems and Structures*, 10: 872.
- Ripin Z.M. and Ooi L.E. (2010).“Dynamic stiffness and loss factor measurement of engine rubber mountby impact test.” *Materials and Design*, 32: 1880–1887.
- Ruddy .C, Ahearne. E and Byrne .G (2007).”A review of magnetorheological elastomers: properties and applications.”*Proceedings of the International Manufacturing Conference (IMC)* 24 999-1005.
- Shixing et al., (2011). “Experimental Research on Aircraft Landing Gear DropTest Based on MRF Damper.” *Procedia Engineering* 15 (2011) 4712 – 4717.
- StenbergB. and Lokander M. (2003).“Performance of isotropic magnetorheological rubbermaterials.”*Polymer Testing*,22: 245–251.
- SunL. et.al. (2013).Derivation of stiffness matrix in constitutive modeling of magnetorheological elastomer.”*Journal of Physics: Conference Series*,412: 012028.
- Tian T.F. et.al. (2011) “Microstructure and magnetorheology of graphite-based MR elastomers.” *Rheol Acta*,50:825–836.
- Unsal.M. et al. (2004). “Two Semi-Active Approaches for Vibration Isolation: Piezoelectric Friction Damper and Magnetorheological Damper.” *IEEE transactions*:2004.

Wang Yinling et.al. (2006). "Preparation and Properties of Magnetorheological Elastomers Based on Silicon Rubber/Polystyrene Blend Matrix." *Journal of Applied Polymer Science*, Vol. 103, 3143–3149.

Wu Jinkui et.al. (2007). "Preparation and Characterization of Isotropic Polyurethane Magnetorheological Elastomer Through In Situ Polymerization." *Journal of Applied Polymer Science*, Vol. 114, 901–910.

Wang X. et.al. (2009). "Sensing Behavior of Magnetorheological Elastomers." *Journal of Mechanical Design*, Vol. 131 / 091004-1.

Xiao-min D. et.al. (2009). "A new variable stiffness absorber based on magnetorheological elastomer." *Trans. Nonferrous Met. Soc. China*, 19:s611-s615.

Yeh J.Y. (2013). "Vibration analysis of sandwich rectangular plates with magnetorheological elastomer damping treatment." *Smart Mater. Struct.*, 22:035010 (8pp).

Yu M. et.al. (2012). "A novel porous magnetorheological elastomer: preparation and evaluation." *Smart Mater. Struct.*, 21 : 035001 (10pp).

Zhou G. Y. and Li J.R. (2003). "Dynamic behavior of a magnetorheological elastomer under uniaxial deformation: I. Experiment." *Smart Mater. Struct.*, 12: 859–872.

Zhou G. (2003a). "Shear properties of a magnetorheological elastomer." *Smart Mater. Struct.*, 12:139–146.

Zhou G.Y. and Wang Q. (2005b). "Magnetorheological elastomer-based smart sandwich beams with nonconductive skins." *Smart Mater. Struct.*, 14:1001–1009.

Zhou G.Y. and Wang Q (2006c). "Study on the adjustable rigidity of magnetorheological-elastomer-based sandwich beams." *Smart Mater. Struct.*, 15:59–74.

Zhou G.Y., Lin K.C. and Wang Q (2006d). "Finite element studies on field-dependent rigidities of sandwich beams with magnetorheological elastomer cores." *Smart Mater. Struct.*, 15:787–791.

## LIST OF PUBLICATIONS

### International Journal

1. Sriharsha Hegde, K.V. Gangadharan (2014), “ Testing of RTV-Silicone based thick magnetorheological elastomers under harmonic loading conditions”, International Journal of Scientific & Engineering Research, Volume 5, Issue 2, February-2014,ISSN 2229-5518.
2. Sriharsha Hegde, Katari Kiran, K.V Gangadharan(2014),“A Novel approach to investigate the effect of Magnetic field on dynamic properties of natural rubber based isotropic thick Magneto rheological Elastomers in shear mode”. **J. Cent. South Univ.** (2014) 21: 2612–2619.**DOI:** 10.1007/s11771-015-2791-4.

### International Conference

1. Sriharsha Hegde,Umanath R Poojary,K.V Gangadharan (2013), "Investigation of effect of Magnetic field on the Mechanical properties of Natural rubber based Magnetorheological elastomer sandwich beam", Proceedings IEEE International Conference on Energy Efficient Technologies for Sustainability, 10th to 12th April 2013 Kanyakumari, Tamilnadu, India (IEEE Catalog Number: CFP1375U-PRT ISBN: 978-1-4673-6147-7).
2. Sriharsha Hegde,Umanath R Poojary,K.V Gangadharan (2014), “Experimental investigation of effect of ingredient particle size on dynamic damping of RTV Silicone base Magnetorheological elastomers”. *International Conference on Advances in Manufacturing and Materials Engineering (ICAMME-2014)* held at NITK from March 27-29<sup>th</sup> 2014.

### National Conference

1. Sriharsha Hegde, Katari Kiran, K.V Gangadharan (2012) “Design and analysis of an array of rare-earth magnets using FEMM for testing magneto-sensitive Smart materials”, **3<sup>rd</sup> National conference on Emerging Trends in Materials for Advanced Technology (NETMAT)** 20<sup>th</sup>-21<sup>st</sup> March 2012, KVGCE, Sullia.

## CURRICULUM VITAE

**Sriharsha Hegde**

Assistant Professor

Department of Aeronautical & Automobile Department,  
MIT, Manipal.

**Mobile:** +91-8147756715

**E-Mail:** sriharsha.hegde@manipal.edu  
sriharsha.mangalore@gmail.com

**Address:** “CHAITANYA”, 3-35/15,  
Nekkilagudda, Ashoknagar Post,  
Mangalore-575006

### **Academic Profile:**

**2010 M.Tech** in **Nanotechnolgy** from National Institute of  
Technology, Calicut, Kerala.

**2003 B.E.** (**Mechanical Engineering**) from Sri  
Jayachamarajendra College Of Engineering, Mysore, VTU  
Belagavi, Karnataka.

**Industry Experience:** 3.5 years

**Teaching Experience:** 1.5 years

## APPENDIX

### MATLAB Code for parameter Identification

```
function [estimates, model] = fitcurve(~, ydata)
% Call fminsearch with a random starting point.
start_point = [ 6600.9488 10011.1719 1599.0730 1317.3990];
model = @expfun;
estimates = fminsearch(model, start_point);
% expfun accepts curve parameters as inputs, and outputs sse,
% the sum of squares error for A*exp(-lambda*xdata)-ydata,
% and the FittedCurve. FMINSEARCH only needs sse, but we want
% to plot the FittedCurve at the end.
function [sse, FittedCurve] = expfun(params)
kb = params(1);
k1 = params(2);
k2 = params(3);
c2 = params(4);
w = 2*pi*15;
j = 1;
for(t=0:0.0005:0.0665)
g1a = (k1*kb + k2*kb + k1*k2)*((k1+k2)^2 + (c2*w)^2) + c2^2*w^2*k1^2;
g1b = (k1+k2)*((k1+k2)^2 + (c2*w)^2);
g1 = g1a/g1b;
g2 = (c2*w*k1*k1)/((k1+k2)^2 + c2^2*w^2);
phi = atan(g2/g1);
strain = 0.146947;
b = ((g1^2 + g2^2)^0.5)*strain;
FittedCurve(j) = b.*sin(w*t+phi);
j = j+1;
end
ErrorVector = FittedCurve(1) - ydata ;
sse = sum(ErrorVector.^2);
end
end
```